1-1-2013

Enantioselective Hydrogenation of α-Methylcinnamic Acid Over PD/AL2O3: A Spectroscopic and Kinetic Study

Xiaojing Sun
University of South Carolina

ENANTIOSELECTIVE HYDROGENATION OF α-METHYLCINNAMIC ACID OVER Pd/Al_2O_3: A SPECTROSCOPIC AND KINETIC STUDY

by

Xiaojing Sun

Bachelor of Science
Dalian University of Technology, 2008

Submitted in Partial Fulfillment of the Requirements

For the Degree of Doctor of Philosophy in

Chemical Engineering

College of Engineering and Computing

University of South Carolina

2013

Accepted by:

Christopher T. Williams, Major Professor

John R. Monnier, Committee Member

Jochen Lauterbach, Committee Member

Donna A. Chen, Committee Member

John W. Weidner, Committee Member

Lacy Ford, Vice Provost and Dean of Graduate Studies

DEDICATION

For my husband, Long, who has experienced with me for better, for worst, for richer, for poorer, in sickness and health, just as what we vowed.

For my parents, who, spend most of their time and attention to me since I was born. From the beginning of it all, saw more in me than I sometimes saw in myself, and enabled me to succeed.

ACKNOWLEDGEMENTS

I want give my greatest acknowledgment to Dr. Christopher T. Williams, my advisor. I still remember the first time we met in the hallway; his smile and warm greeting blow away all of my uncertain of first time away from motherland. His generous advices and assistances, optimistic characters and understanding make my Ph.D. student life an important, helpful, meaningful and enjoyable journey.

I also want to acknowledge my PhD committee, Dr. John R. Monnier, Dr. Jochen Lauterbach and Dr. Donna A. Chen, for your precious time dedicated to teach me. Thanks Dr. Monnier for guiding me in kinetic study and experimental techniques, also for faciliatating me the instruments and tools necessary to accomplish my Ph.D. experimental work. Thanks Dr. Lauterbach for your delicated explanation in my comprehensive and predefense, your circumspect and serous attitude to science impress me as what a successful scientist should be. Thanks Dr. Chen for teaching me surface science which helps me understands numbers of publications I did not fully understand before. In addition, I want to thank the chemical engineering department staffs, Marcia, Loretta, Diane, Kay, Vernon and Brian, for their assistance and excellent work on providing a friendly and nice working environment. I want also thank Carol for her generous help on experimental work.

I would like to thank my group members, Abe, Weijian, Yunya, Shuai, Yuliana, Youjung, I am happy to work with you and learn to each other. I also want to thank

Yaritza, Jay and Dr. Hu who has already left our group but teach me a lot on experiments setup and data analysis I am working with in my Ph.D. process. I want to express my sincere gratitude to my dearest friends, tingting, jingyi, hong, peng, qiang, shengyang, yunya, weijian, tianyuan, yiling, zhiyong, fan, shuai, suwit, hyunseok, sara, visarn, tong, hyeran, with all of you, I spend one of my happiest time in my life in USC.

ABSTRACT

Synthesis of chemicals containing one or more chiral centers is important for the manufacture of pharmaceuticals, agrochemicals, and fragrances. The move towards enantiopure chemicals has been driven both by performance requirements and environmental concerns. So far, the majority of in-situ spectroscopic studies of these catalysts that have been performed have focused almost entirely on the cinchona alkaloid modifier interaction with the catalyst surface under different conditions. This dissertation reports on semi-batch kinetic and in-situ attenuated total reflection infrared spectroscopic studies of the hydrogenation of α-methylcinnamic acid with a Pd/Al_2O_3 catalyst. It was the aim of this work to begin to elucidate the detailed kinetic and the surface molecular properties that may influence this behavior.

The kinetics of C=C bond hydrogenation in α-methylcinnamic acid over Pd/Al_2O_3 catalyst with and without cinchonidine modifier was carried out in a semi-batch reactor. The hydrogenation reaction exhibits a strong solvent-dependent behavior, with isopropanol showing the best activity performance likely due to its strong polarity and protic nature. Regardless of the absence or presence of modifier, the reaction rate is independent on H_2 pressure and first order in the acid substrate. The TOF on unmodified sites are much faster than modified ones, which results in low enantioselectivity. Apparent activation energies for reaction with and without modifier are similar. Finally, the product has no effect on the reaction rates or enantioselectivity, suggesting that

substrate adsorption and activation may be the rate determining step. ATR-IR studies reveal that most reactant is adsorbed in a bridging carboxylate form on palladium in isopropanol and dioxane, and both bridging carboxylate and molecularly adsorbed species in dichloromethane. Both molecularly and dissociatively adsorbed species are reactive towards hydrogen. Reactant and product adsorption strengths are similar. Cinchonidine modifier is adsorbed in both a parallel and tilted form on the catalyst and is hydrogenated in the present of hydrogen on Pd/Al_2O_3. Cinchonidine interacts with the reactant through H-bonding.

The spectroscopy studies reveal for the first time the adsorption mode of substrate, modifier and product, and their interactions on the surface. The kinetic studies represent the first attempt to detail the kinetic features of this reaction such as reaction orders and activation energy. Together, they provide a much more detailed picture of this important class of heterogeneously catalyzed enantioselective reactions.

TABLE OF CONTENTS

LIST OF TABLES

LIST OF FIGURES

List of Abbreviations

ATR-IR ..... Attenuated total reflection infrared spectroscopy

CD ..... Cinchonidine

DI ..... deionized

DMF ..... N, N- Dimethylformamide

FTIR ..... Fourier transform infrared spectroscopy

MCA ..... α-methylcinnamic acid

MHA ..... α-methylhydrocinnamic acid

CHAPTER 1 INTRODUCTION

1.1 OVERVIEW

The synthesis of chemicals from substrates containing one or more chiral centers has been gaining more and more attention in the field of pharmaceuticals, agrochemicals, and fragrances over time. Specific enantiomers or diastereomers of a given molecule often exhibit very different biological activity, making it desirable (and sometimes mandatory) to deliver a product of high purity. Asymmetric synthesis by chemical catalysis is often carried out in liquid-phase batch processes using homogeneous catalysts such as chiral transition metal complexes or chiral Lewis acids and bases. Take Monsanto L-Dopa synthesis process for example, which achieves highly enantioselective hydrogenation of an enamide using Rh-DIPAMP as a homogeneous catalyst. Though homogeneous asymmetric catalysis is widely used in industry and progresses rapidly, there are several intrinsic drawbacks that need to be considered. For example, several separation steps to meet industry purity standards, resulting in greater complexity and increased waste production in many cases. In addition, the activity and long-term stability of homogeneous catalysts can often be too low for industrial applications [1]. In this respect, the eventual use of heterogeneous catalysts can offer several major advantages, including ease of catalyst separation, reduction of solvent usage, simplification of the synthetic route, and increased selectivity towards desired products.

If optimized, these properties could result in significant economic and environmental benefits.

Compared with excessive studies for enantioselective hydrogenation of α-ketoesters and ketones on cinchona-alkaloid modified metal catalysts [65, 100], there are fewer reports on hydrogenation of substrates containing a C=C bond. Hydrogenation of α-acetamidoacrylic acid and α-acetamidocinnamic acid over 5 wt% Pd on charcoal modified with 1-sparteine and 1-ephedrine was reported in 1971, with a very poor catalytic performance of 0.5%-4.5% e.e. [2]. Different metal catalysts such as Rh [3] and Ni [4] were tried, but they barely work for enantioselective hydrogenation.

To the best of our knowledge, the first report of enantioselective hydrogenation of a C=C bond with cinchona-modified catalyst was in 1985 [5]. Among several works since then, aliphatic and aromatic alkenoic acids are the two main types of probe molecules that have been investigated. Several groups have been working in this area. Nitta et al. mainly focus on the study of (E)-α-phenylcinnamic acid as the substrate, and have investigated reaction variables that affect the activity and enantioselectivity, such as polarity of solvent [10, 13, 19, 20], support texture [6, 14, 16, 20], preparation method of catalyst [14, 20], transition metal loading [11, 14], hydrogen pressure [12, 18], modifier structure [17, 45], substrate structure [7, 9, 46, 47], additives [13, 15], reaction and pretreatment temperature [6, 8] and other factors. The groups of Nitta [6-20, 44, 45], Bartok [21-24, 48-51], and Baiker [25-38] have been the most active with the majority having explored hydrogenation of α, β- unsaturated C=C bonds adjacent to carboxylic acid groups with cinchonidine as modifier. It is suggested that cinchonidine (CD) and reactant acids form a $CD(acid)_2$ complex during the enantioselective hydrogenation [32].

In addition, aromatic acids favor polar solvents, as opposed to aliphatic acids that prefer non-polar environments. These (and other) studies of the cinchonidine-modified metal catalytic system have largely involved kinetics studies, as opposed to probing the surface molecular environment. In addition, the in-situ vibrational spectroscopic studies available have focused almost entirely on the cinchona alkaloid modifier interaction with the catalyst surface under different conditions [21, 25, and 26]. Besides, the kinetic studies available have focused almost entirely on the final conversion and selectivity [7-24], rather than exploring kinetic parameters such as rates, reaction orders, or activation energies.

This dissertation presents kinetic and in-situ attenuated total reflection infrared spectroscopic studies of the hydrogenation of α-methylcinnamic acid (Figure 1.1) with a Pd/Al_2O_3 catalyst. This molecule consists of a prochiral C=C bond located between COOH and phenyl groups, and is a good model compound for the study of C=C hydrogenation in aryl substituted substrates. Overall, the conversion and enantioselectivity of this molecule is reported to be very low over cinchonidine-modified catalysts [21, 22]. It was the aim of this work to begin to elucidate the detailed kinetic and the surface molecular properties that may influence this behavior.

1.2 Background and literature review

1.2.1 Cinchona alkaloid modified metal catalysts

The first paper addressing C=C bond hydrogenation with cinchona-modified transition-metal catalysts was published in 1985, with a study of prochiral cinnamic acid hydrogenation over Pd/C catalysts [5]. Several chiral modifiers including cinchonine and cinchonidine were used then, with a maximum ee of around 72% reported for the

hydrogenation of (E)-α-phenylcinnamic acid with a Pd/TiO_2 catalyst [19]. Largely over the past decade there have been a number of studies [6-51] that followed up on this initial work. However the mechanistic picture is not near complete for this system. In the following sections an overview of what is currently known about this reaction is provided.

Given its well-known effectiveness in hydrogenating C=C bonds, palladium has been the most well studied metal for these reactions. It has been suggested that one reason for the limited enantioselectivity observed is that the hydrogenation rate on unmodified Pd sites is very rapid, while that on modified highly enantioselective sites is hindered. However, a few kinetic studies of other cinchona alkaloid-modified metals (e.g., Pt, Ir, Rh) for C=C reactions also show some promise. For example, Pt was found to exhibit higher enantioselectivity (but lower activity) than Pd for ethyl 2-acetoxyacrylate hydrogenation [23]. Alumina has been the most widely examined support, although titania and carbon are also widely employed [11-20]. Since unmodified Pd sites are extremely active, low surface area supports with large pore volumes are reported to be effective to ensure efficient access of the cinchona alkaloid modifier to all active sites. It is considered that strong metal-support interaction is not favorable for the enantioselective hydrogenation [12].

1.2.2 CINCHONIDINE STRUCTURE AND CONFORMATION

The hydrogenation has no enantioselectivity without modifier, which suggests that the interaction between chiral modifier and substrate is the key part to study in the enantiodifferentiating step. The steric structure of modifier seems important for the

interaction with the substrate, so it is necessary to understand the structure and conformation of modifier adsorption first.

Cinchonidine is one kind of cinchona alkaloid that is present in nature. Cinchona alkaloids are usually isolated from the bark of several species of Cinchona and Remeyia trees [52]. The Wynberg group has made an intensive study of the structure of cinchona alkaloid and the derivatives [52]. Cinchonidine structure and a systematic order of atom numbers and three dihedral angles are shown in Figure 1.2. This order will be used for the rest of dissertation. Cinchonidine has a vinyl group, a quinuclidine moiety and a quinolone moiety. The functions of active sites are summarized in Figure 1.3. Bartok's group tested the modifier effect for hydrogenation of 2-methyl-2-pentenoic acid; cinchonidine-mofidied catalyst has the highest selectivity compared to using 9 other cinchona alkaloids.

Cinchona alkaloids exhibit a very rich conformational behavior, as has been indicated by theoretical modeling [55-59] and experimental studies (NMR, NOESY, X-Ray, etc.) [52, 54, 60, 61]. Through NMR experiments and calculation with Hartree-Fock (HF) level using the 6-31G** basic set, Baiker's group found that conformations of cinchona alkaloids strongly depend on solvent [61]. The most stable (low energy) four cinchonidine conformers, energies, and dihedral angles are shown in Figure 1.4. In general, "Open (3)" is most stable in apolar solvent [54] [57], while "Closed (1)" and "Closed (2)" are more stable in polar solvents [52] due to the greater support provided by their large dipole moment [61]. Here, "Open" indicates that the quinuclidine N points away from quinoline ring, while "Closed" refers to the quinuclidine N pointing toward the quinoline ring.

1.2.3 ADSORPTION OF CINCHONA ALKALOIDS ON METAL SURFACE

The adsorption of cinchona alkaloids was first studied by UHV-based techniques such as X-ray photoelectron spectroscopy (XPS), low-energy electron diffraction (LEED) [67- 69] and mass spectroscopy (MS) [70]. These studies indicated that the quinoline moiety was lying parallel to the metal surface through a π-electron interaction at room temperature, and became tilted at 323K [71]. However, these UHV-based techniques can not reveal any information regarding the surface of chiral-modified metals under actual reaction conditions (i.e. liquid phase, elevated H_2 pressures). Development of in-situ spectroscopic techniques over the past decade made it possible to extract surface information under real reaction conditions. For example, attenuated total reflection infrared (ATR-IR) spectroscopy has been used to detect the adsorption of cinchona alkaloids on supported Pt, Pd and Au under reaction conditions [66, 72-77]. Williams and co-workers used surface enhanced Raman spectroscopy (SERS) to study cinchonidine adsorption in ethanol solvent [78, 101-103] Wang et al. also utilized in-situ STM to study the adsorption of cinchonidine on Cu (111) in an aqueous solution of 0.1M $HClO_4$ and 0.1mM cinchonidine, and showed that the modifier could form a long-range ordered ad-layer on top of Cu surface [79].

In summarize, the quinoline moiety is the responsible function group for the adsorption on the metal surface. The adsorption mode is strongly concentration (i.e. coverage) dependent in the presence of solvent. There are three adsorption modes on Pt [74] depending on the solution concentration: (i) at low concentration (10^{-6}~10^{-7}M), the quinoline moiety is parallel π-bonded to the metal surface; (ii) at higher concentration (~10^{-5}M), the quinoline rings tilt, and two species (α-H abstracted and N lone pair bonded

cinchonidine) were observed. The N lone pair bonded cinchonidine is only weakly bound and in a fast dynamic equilibrium with dissolved cinchonidine. (iii) at high concentration (10^{-4}~10^{-3}M), all three species coexist on the surface, and a slow transition occurs from α-H abstracted cinchonidine to more N lone pair bonded cinchonidine at increasing cinchonidine concentration [74].

The suggested adsorption mechanism of cinchonidine as described above is shown in Figure 1.5. Further study of cinchonidine adsorption on Pd/Al_2O_3 was performed by the same group [98]. The biggest difference of cinchondine adsorption on Pd compared to Pt is that there is no α-H abstracted cinchondine on the former. It adsorbs only as N lone pair bonded at higher concentration (higher than 10^{-5}M). The difference in the diffuseness of the d orbitals of the metal is the likely the reason of different adsorption behavior observed. Species 1, which is strongly adsorbed π-bonded cinchonidine, is proposed to be the species involved in enantiodifferentiation.

1.2.4 CINCHONIDINE (CD)-ACID INTERACTION

After the study of the adsorption of modifier, interaction of modifier and the reactant acid has been examined in the literature, although to a lesser extent. Such interaction of modifier and acid is a key to achieving better catalytic behavior. So far, perhaps the most well developed and supported mechanism for this class of reactions is that of Baiker and co-workers [25, 26] which is shown in Figure 1.6. They propose that on cinchonidine-modified palladium, alkenoic acids form dimers that hydrogen bond with the modifier quinuclidine group. The alcoholic OH group as well as the quinuclidine nitrogen of cinchonidine are hydrogen bonded to the reactant alkenoic acid in the enantiodifferentiation step. The Baiker group has provided support for this model through

both experimental and calculation methods [26]. Independently, Nitta [44] and Bartok [24] examined the enantioselective hydrogenation of α-phenylciannamic acid and 2-methyl-2-pentenoic acid. They agreed that both the OH group in C-9 position (Figure 1.2) and the quinuclidine nitrogen play key role in the interaction of modifier and alkenoic acid in the enantiodifferentiating step over Pd surfaces.

Experimental reactivity studies of enantioselective hydrogenation of alkenoic acids were performed with cinchonidine derivatives that had different elements or functional groups for R1 and R2, and connected to quinuclidine nitrogen. Results are shown in Table 1.1 [26]. Relatively low or even racemic products were achieved unless the R groups are H, and H is connected to quinuclidine nitrogen. For the modifier when there R=H and allyl or benzyl group was connected to quinuclidine nitrogen, the ee% was still similar with the one H for R and H connected to quinuclidine nitrogen. It seems to suggest that the H element in the quinulcidine nitrogen is not essential in the interaction. Baiker's group used NMR spectroscopy to exame the structure of the modifier with an allyl group connected to the quinuclidine nitrogen. It turned out that over 50% of the modifier underwent hydrogenolytic debenzylation over Pd surface. So the real part involved in the enantioselective hydrogenation is still the H connected to quinuclidine nitrogen.

Calculation with geometry optimizations were performed by ab initio calculations at the Hartree Fock level of theory using a 4-31G standard basis set. The calculation was performed on the simplest alkenoic acid - actylic acid. Dimer acid interacting with cinchonidine (CD) with two hydrogen bonds in a trans-arrangement is more stable than monomer acid interacting with CD. If the S product is the main product, assuming the

hydrogen was added from below the dimer acid, one of the C=C must point toward the quinolone ring of CD. To further confirm this CD-$(acid)_2$ dimer model, 1, 8-diazabicycloundec-7-ene (DBU) was added quantitatively. DBU is much stronger than the quinuclidine nitrogen in CD [26]. When the DBU:acid ratio is less than 1:2, the DBU addition did not change reaction rate or enantioselectivity. In contrast, the ee dropped linearly after the DBU:acid ratio exceeded 1:2, which suggests that the CD$(acids)_2$ connection is very strong with both base-acid interaction and H-bonding.

While this model seemed to be reasonably consistent with both the experimental kinetic and modeling studies, an IR study provided further, direct confirmation [25] Shown in Figure 1.7 are the IR spectra of 0.01M CD, 0.02M tiglic acid (TA) while DBU was titrated into the solution. The intensity of CD ν(OH) (3598cm^{-1}) increased with the increase of DBU concentration up to one equivalent DBU to TA, but then decreased when DBU concentration was increased further (not shown). The peaks around 3505 and 3365cm^{-1}were assigned to ν(OH) of free TA and ν(OH) from 1:2 CD-TA complexes, respectively. These two peak intensities gradually decrease with increasing DBU, suggesting that the TA was deprotonated by the stronger base DBU. Thus, the CD-TA_2 complexes were broken gradually until one equivalent DBU was reached. For the range of C=O stretching, the peaks at 1720 cm^{-1}(C=O monomer) and 1688cm^{-1} (C=O dimer) peaks decreased gradually with the increasing DBU and disappeared completely when one equivalent DBU was added. This showed that the TA was completely deprotonated by DBU. However, at the same time, the 1648cm^{-1} (protonated C=N) peak increased almost linearly and the 1613cm^{-1} peak (free C=N) was observable before equivalence was reached. This suggests that still some DBU was free from being protonation by TA. The

new signal at 1554cm^{-1} was assigned to carboxylate from 1:1 TA-DBU complex. These FTIR results suggest that the 1:2 CD-acids complex is the most important part in the process of enantioselective hydrogenation and that the complex was stable with DBU addition before 0.5 equivalent DBU added. The OH group and quinuclidine N in CD play the key role.

Mizukami group found that the excess enantiomer was opposite for aliphatic and aromatic substrates. Based on their kinetic results, the author hypothesized that the phenyl group in the β-position directs the adsorption mode due to a steric effect. So based on the Baiker's 1:2-CD aliphatic acid complex, they assume a CD-aromatic acid complex as shown in Figure 1.8. In this arrangement, the ring points away from the CD and is adsorbed on the catalyst surface opposite to the prochiral C=C for aliphatic acids. For hydrogenation of the dicarboxylic acids (e.g., mesaconic acid, citraconic acid), the opposite enantiomeric excess products were achieved though they are all aliphatic acid, which is proposed to be the reason of steric effect from second carboxylic acid group [22]. The hydrogenation performance is thus highly substrate dependent. It is believed that the bulky structure in the α position and electron donator in the β position is suitable for high selectivity [48]. Beside the effect of the substitutes on the interaction between acid and the modifier, the adsorption of the acid also affects the enantioselective hydrogenation [49-51].

In summary, three structural elements are crucial for cinchonidine to function as a chiral modifier: (i) an anchoring part represented by the flat aromatic ring system (quinolone moiety), which is responsible for adsorption onto the metal surface; (ii) the absolute configuration of C8 and C9, which controls the sense of chirality; (iii) a basic

nitrogen atom in the quinuclidine moiety and OH connecting to C9 that interacts with prochiral substrates.

1.2.5 SOLVENT AND ADDITIVE EFFECT

Nitta et al. mainly focussed on the study of (E)-α-phenylcinnamic acid as the substrate, and have investigated reaction variables that affect the activity and enantioselectivity, such as polarity of solvent [10, 13, 19, 20] support texture [6, 14, 16, 20] preparation method of catalyst [14, 20], transition metal loading [11, 14], hydrogen pressure [12, 18], modifier structure [17, 45], substrate structure [7, 9, 46, 47], additives [13, 15], reaction and pretreatment temperature [6, 8] and other factors. Varies effects are summarized in the following sections.

The nature of the solvents can greatly affect the performance in terms of both enantioselectivity and activity. For aromatic unsaturated compounds, the increase of the dielectric constant (εr), (which partly reflects polarity of solvent), leads to higher enantioselectivity for Pd/Al_2O_3 catalyst. In addition, some apolar solvents such as 1, 4 dioxane result in high e.e. of 49.5% for Pd/TiO_2 and Pd/C [13]. A contrary observation is that increasing the polarity of solvent leads to decrease of the e.e. for 2-methyl-2-pentenoic acid [37]. Generally speaking, aromatic and aliphatic substrates have opposite behavior with respect to polarity of the solvent. This is likely due to several reasons: 1) The ability of the solvent to facilitate desorption of the product, since this step has been proposed as rate determining for the modified sites [13]. 2) Solvents exhibiting less solubility towards cinchona alkaloids are desired, since this precipitates a high coverage of the modifier on the catalyst surface (resulting in fewer unmodified sites). 3) Solvent adsorption on Pd surface can result in less reactant adsorbed, thus lowering activity. 4)

Different adsorption mode for acids in different solvents. It is proposed that most carboxlic acids exist as dimers. However, in very dilute solution in non-polar solvents, or in the vapour phase, acid may exist as a monomer.

Several additives have been found to be effective for raising enantioselectivity and reaction rates. For example, the addition of as little as 1-2vol% water in dioxane can more than double the catalytic activity, while also affording a modest increase in enantioselectivity, which can be explained in term of dielectric constant. The addition of amines to the reaction mixture also produces notable increases in catalyst activity without sacrificing enantioselectivity, with the most dramatic effects observed for benzylamine (BA) [13, 21].The activity increase is explained by the acceleration of the product desorption from modified sites through acid-base interaction and adsorption-desorption equilibrium [13], since it is proposed that the product desorption step is the rate-determining step for the selective reaction on modified sites. It should be noted here that addition of BA is not valid for all substrates such as α-methylcinnamic acid (change from 23% to 20% e.e. with equivalent BA addition), mesaconic acid (10% to racemic) and citraconic acid (7% to racemic) [21].

1.2.6 HYDROGEN PRESSURE AND TEMPERATURE EFFECT

The effect of hydrogen pressure with respect to reaction rate and enantioselectivity was examined by Nitta [11] and Baiker's [36] group. The e.e. for hydrogenation of aromatic acid in polar solvent decreases with increasing hydrogen pressure [11], which is the opposite of what is observed for aliphatic hydrogenation in apolar solvent [11, 36]. The Nitta group studied hydrogenation of α-phenylcinnnamic acid and 2-methyl-2-butenoic acid as examples of aromatic acid and aliphatic acid using

a hydrogen pressure from 0.1 to 5 MPa. Aromatic acid in polar solvent shows an increase in the reaction rate and decrease of ee while aliphatic acid in apolar solvent shows increase reaction rate and e.e. This different behavior with hydrogen pressure was explained in terms of adsorption of various substrates on modified and unmodified sites. For aromatic substrates, it is proposed that the modifier and substate adsorbed on the catalyst strong enough that it was not affected by hydrogen pressure, while the reaction rate on unmodified metal surface accelerate with increasing hydrogen pressure. Thus, the reaction rate increased but not e.e.. In contrast, in the case of aliphatic acids, adsorption was weaker and surface hydrogen concentration increases with pressure on all sites.

So far, nearly all the asymmetric C=C hydrogenation reactions on these supported catalysts have been performed at room temperature. This is likely due to reports of Baiker [37] and Nitta [6] who found that for hydrogenation of 2-methyl-2-pentenoic acid and α-phenylcinnamic acid, the reaction rate increased and ee decreased with rising temperature for both aliphatic substrate in apolar solvent and aromatic substrate in polar solvent. It is proposed that the decrease of e.e. with increasing reaction temperature is caused by an increase of thermal fluctuation of the interactions between the substrate and the modifier on the catalyst surface and/or due to the suppressed solubility of hydrogen.

1.2.7 PD LOADING, MODIFICATION TEMPERATURE AND SUPPORT EFFECT

The relationship between e.e. and the dispersion of Pd particles on the Pd catalysts for the hydrogenation of α-phenylcinnamic acid (PCA) with and without BA addition was studied by Nitta's group (PCA 75 mmol L^{-1}, CD 15 mmol L^{-1}, BA 50 mmol L^{-1}, 318 K) [6]. The higher dispersion, the lower the selectivity will be, which suggests that larger Pd metal particles provide better performance. It is thus likely that

enantioselective hydrogenation is preferred at low index planes (i.e., Pd [111]). Pd/CeO_2 has lower enantioselectivity than Pd/TiO_2, which us explained by the latter having weaker metal-support interactions. It should be mentioned that works done by the same group around 1999-2004 indicate that the 20% dispersion 5wt% Pd/Al_2O_3 has the best selectivity for both aromatic and aliphatic acids [10, 11, 14].

Different than the effect of reaction temperature, the higher the modification temperature (temperature for hydrogen reduction) results in better selectivity [6] for hydrogenation of α-phenylcinnamic acid and (E)-2, 3-di (4-methoxyphenyl) propenoic acid over 5wt% Pd/C up to 360K, while keeping the reaction temperature as 296K. The most common explanation would be change of metal catalyst surface or the metal particle size. To further probe this effect, they tested the catalyst with flowing nitrogen at the same temperature, and no e.e. increase was detected. This suggested that some contamination on Pd metal surface was cleaned with hydrogen presence. They also find out that prereduce the Pd metal with hydrogen before CD introduced achieve better performance than pretreatment with both acids and CD. For support texture , nonporous or large pore size supports are favorable16, due to the space needed to allow both modifier and substrate interaction on the metal surface, and to allow the formation of an intermediate complex that is the required for enantioselectivity. In addition, alumina for Baiker's [25-38] group and titania for Nitta's [6-20] group supported Pd catalysts are most favorable support published so far.

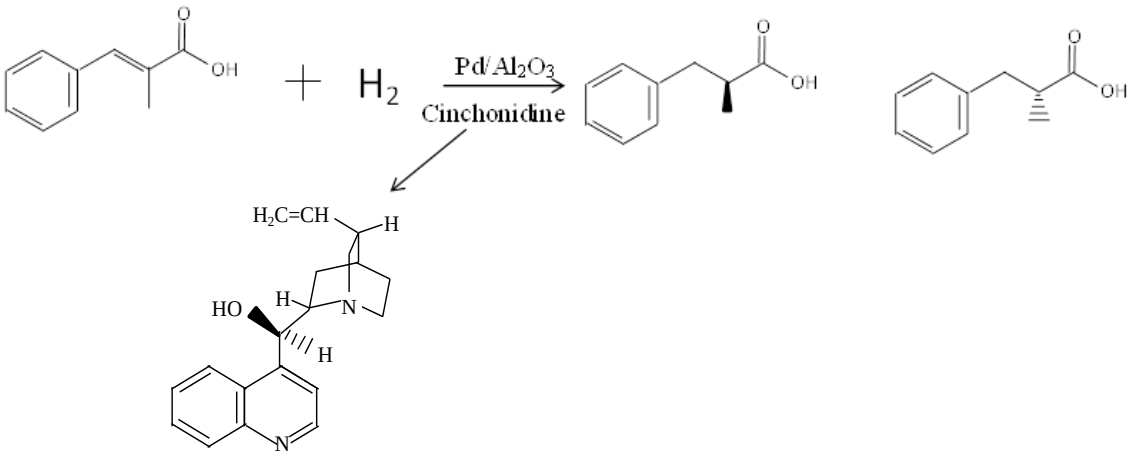

Figure 1.1 Hydrogenation of α-methylcinnamic acid (MCA).

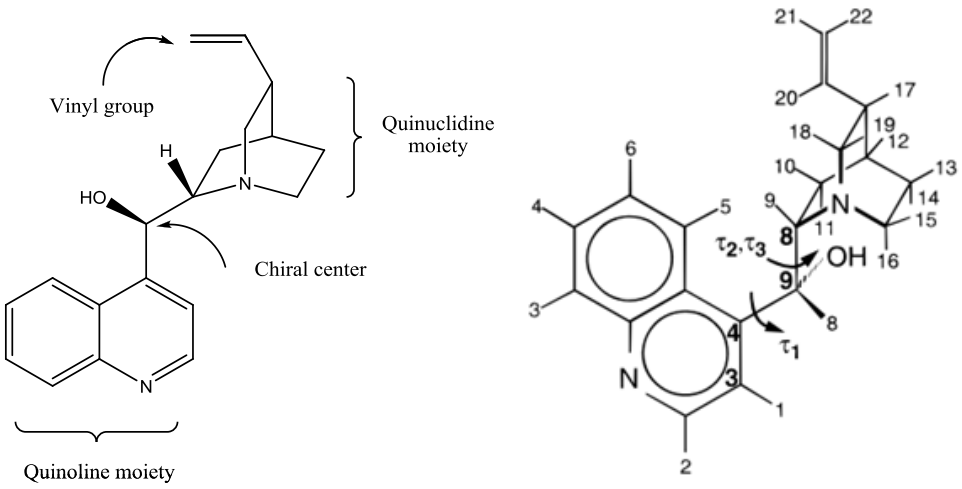

Figure 1.2 Cinchonidine structure and atom numbering. [61]

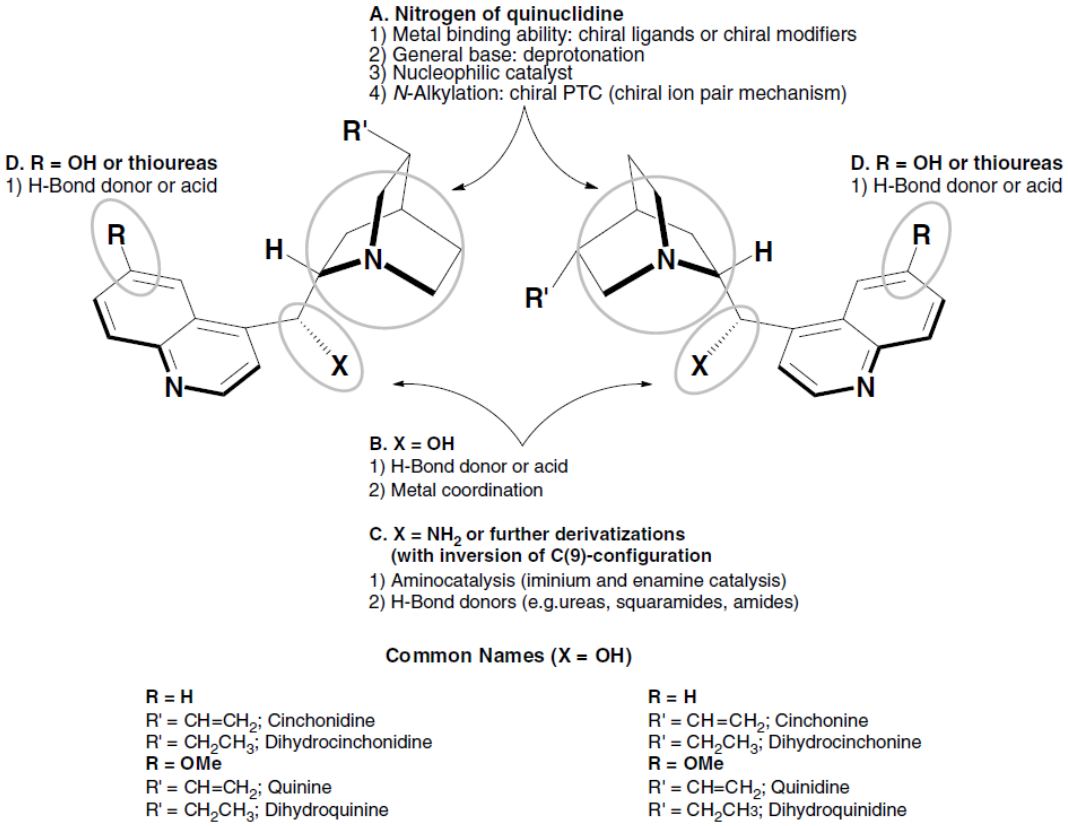

Figure 1.3 Active sites in cinchona alkaloid and their derivatives. [96]

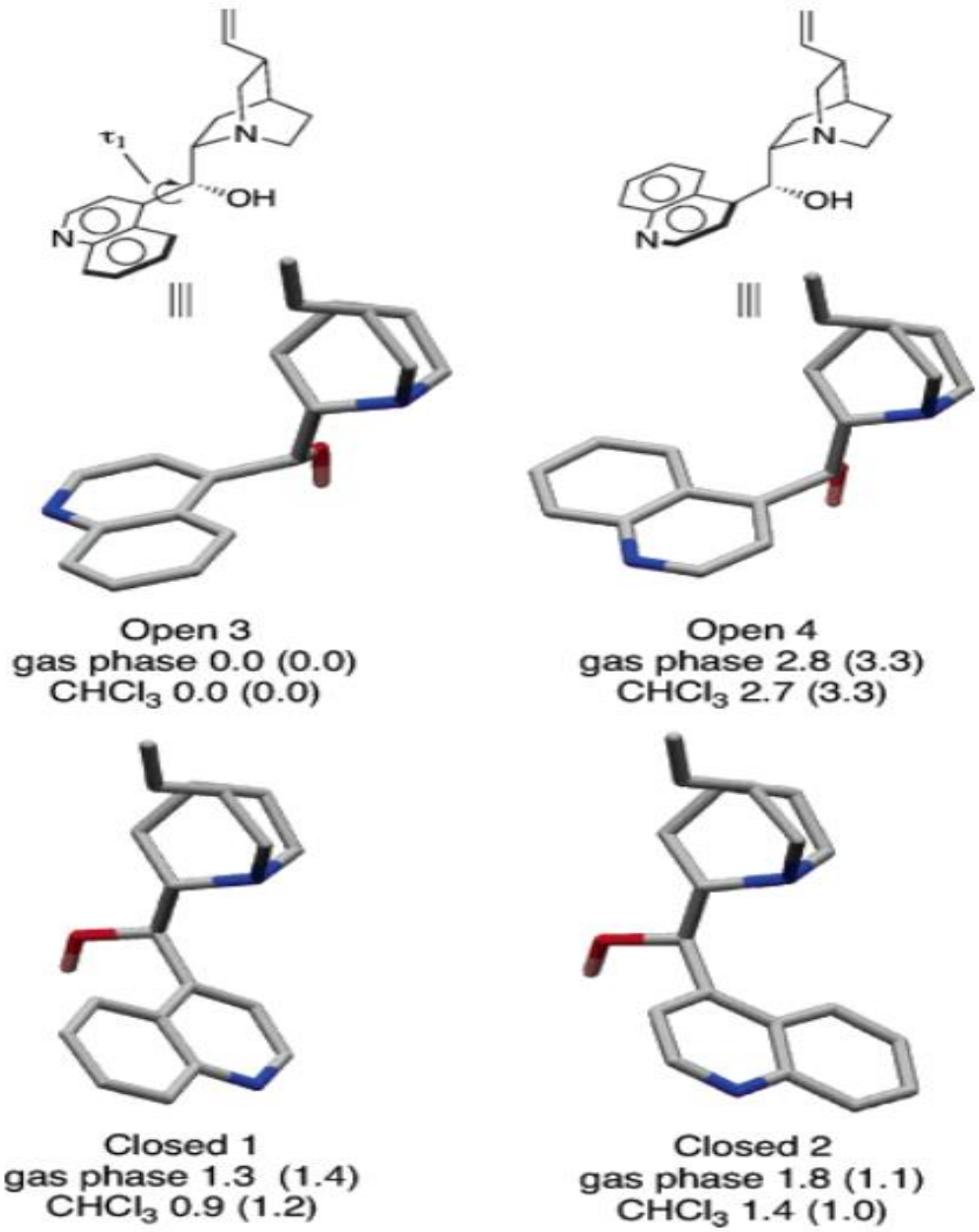

Figure 1.4 Structures and relative energies (kcal/mol) of low energy cinchonidine conformations B3LYP/6-31+G*/PCM(AMBER*/GB/SA/ [$CHCl_3$]). [63]

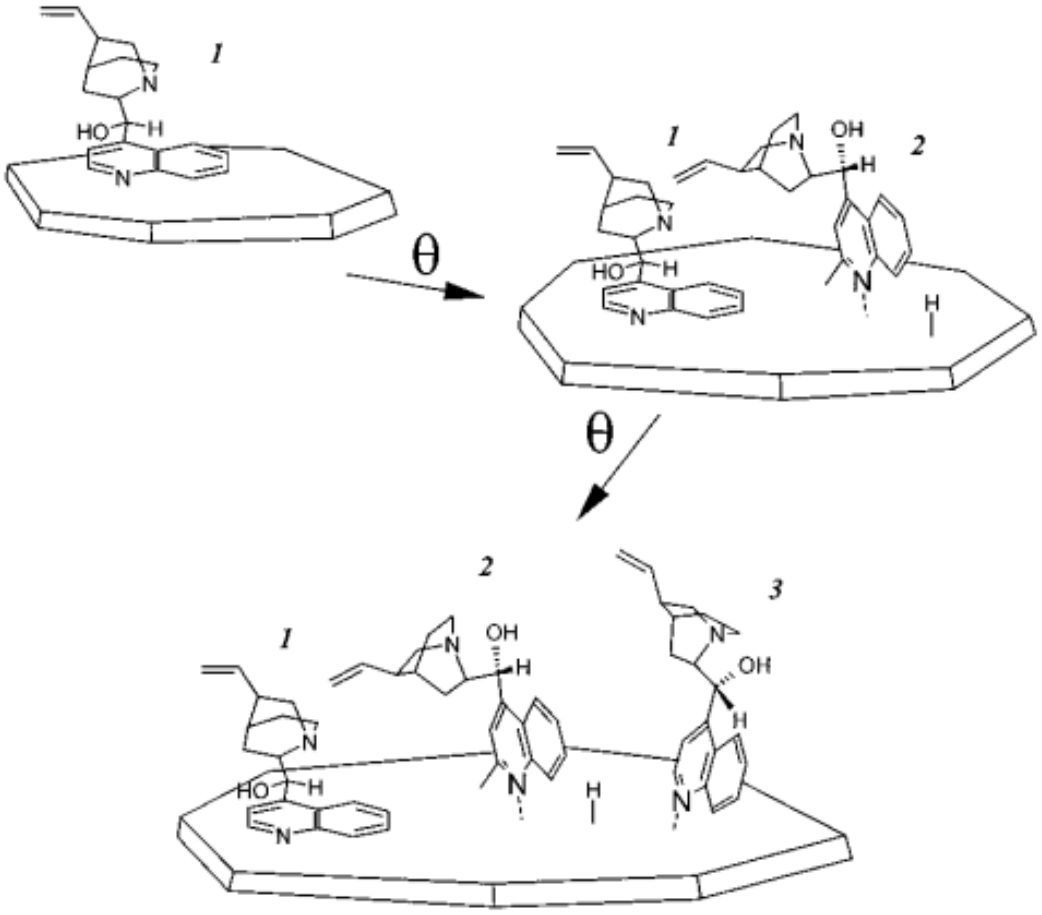

Figure 1.5 Suggested Adsorption Mechanism of Cinchonidine on Pt/Al_2O_3 at 283K from ATR-IR (θ is surface coverage, species 1: π-bonded, 2: α-H abstracted, 3: N lone pair bonded). [74]

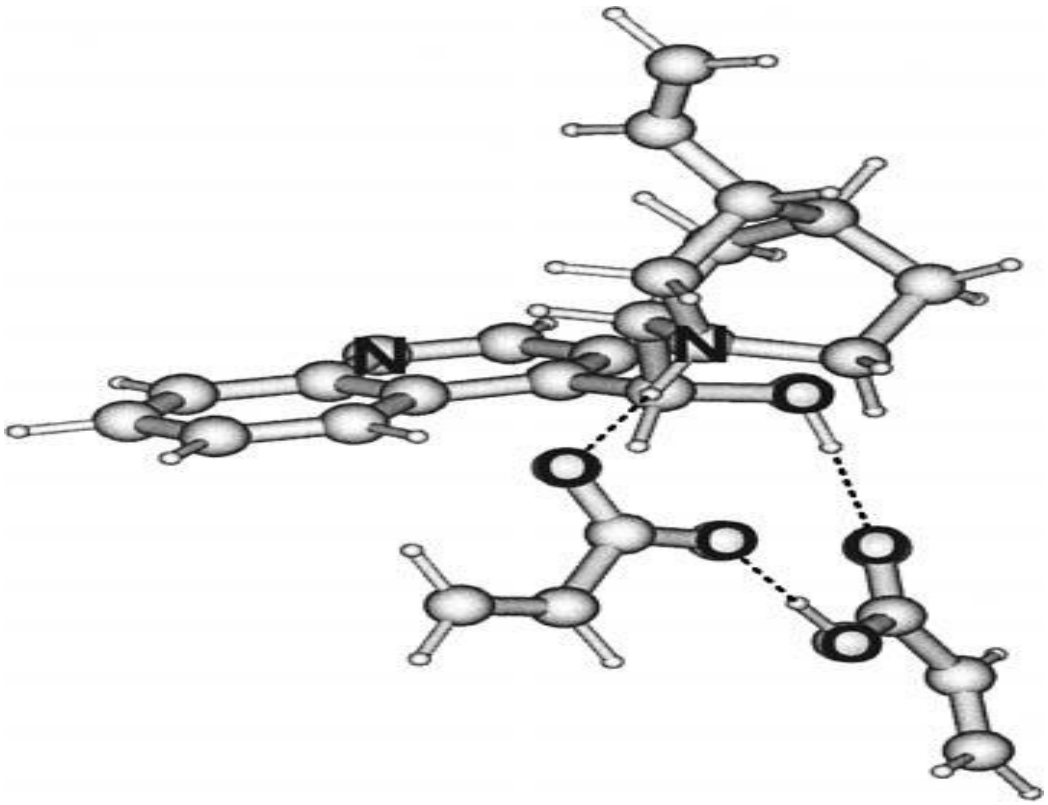

Figure 1.6 Hydrogen bonding in the energetically most stable acrylic acid dimer–CD species. [26]

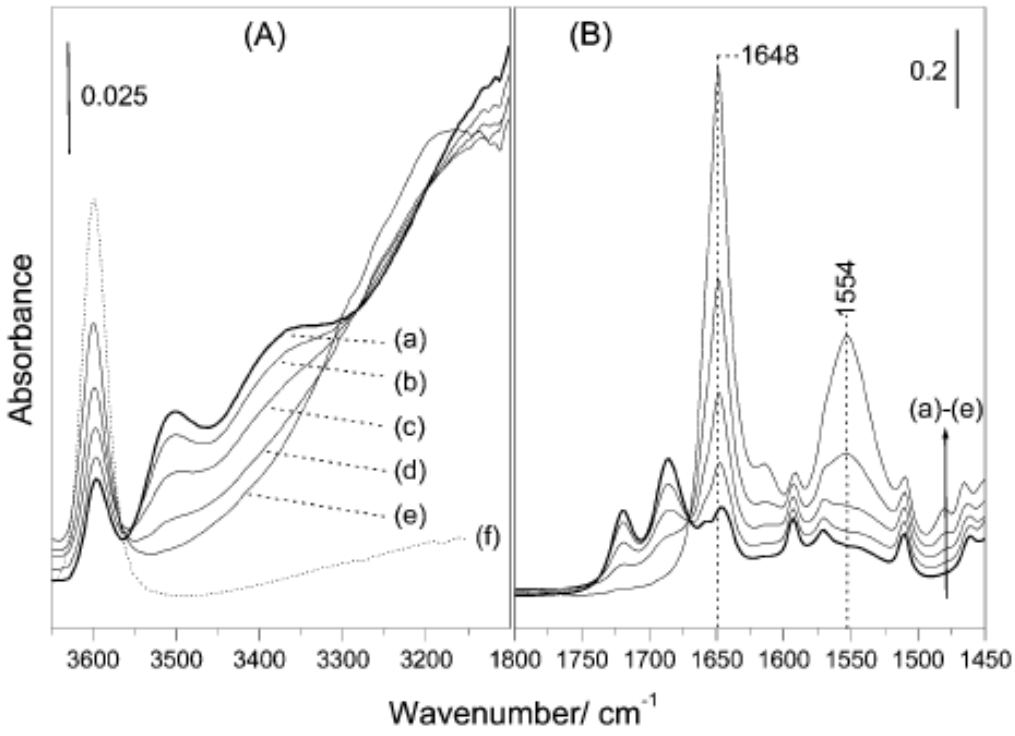

Figure 1.7 FTIR spectra of CD–TA–DBU solutions at increasing DBU concentration in CH_2Cl_2. CCD = 0.01 M, CTA = 0.02 M. Panel (A) shows the 3650–3100 cm^{-1} whereas panel (B) the 1800–1450 cm^{-1} spectral range. Traces (a)–(e) correspond to 0.0, 0.1, 0.25, 0.5 and 1.0 equivalent DBU with respect to TA. Trace (f) represents CD 0.01 M. [25]

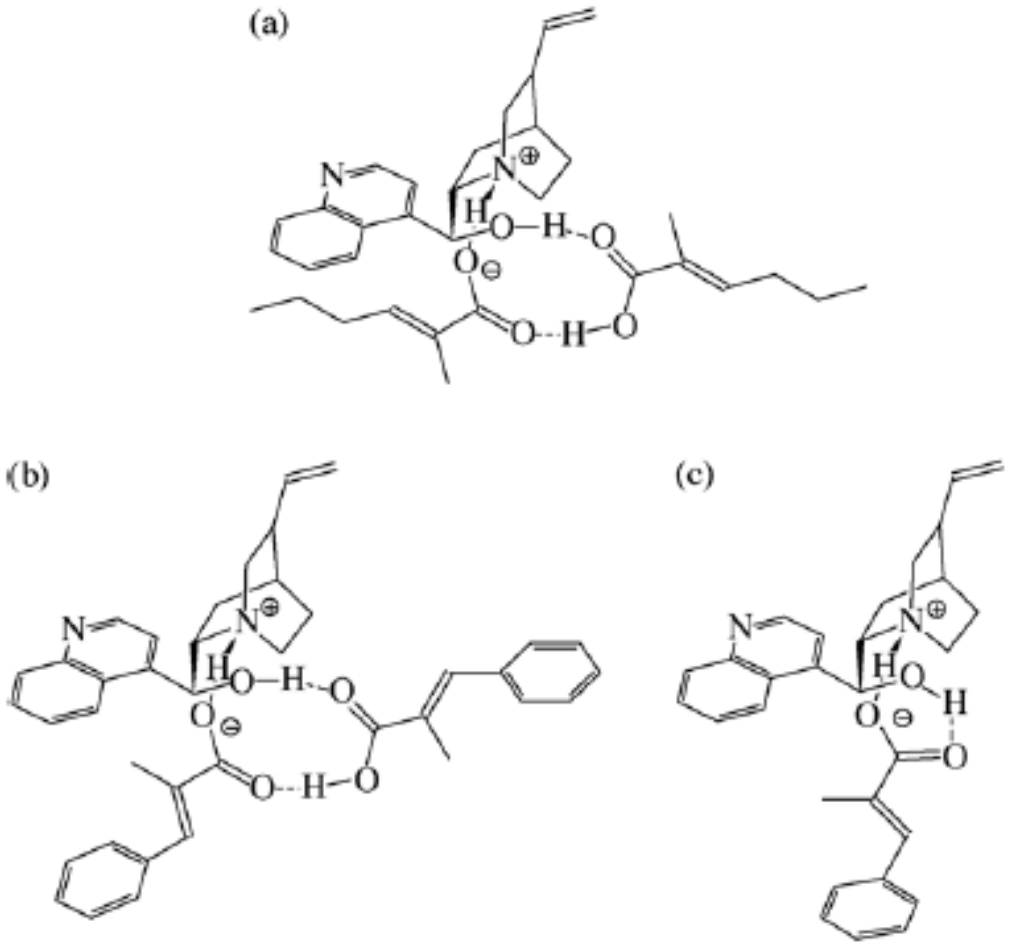

Figure 1.8 Proposed hypothetical structures for the (a) CD–(E)-2-methyl-2-hexenoic acid 1:2 complex; (b) CD–(E)-2-methyl-3-phenyl propenoic acid 1:2 complex and (c) CD–(E)-2-methyl-3-phenyl propenoic acid 1:1 complex. [22]

Table 1.1 Conversion and Enantioselectivity in the Hydrogenation of Tiglic Acid over 5 wt.% Pd/Alumina Modified with CD Derivatives. [26]

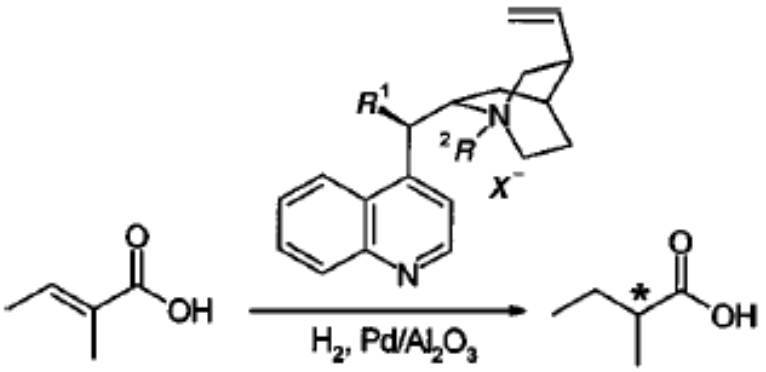

Modifier	R^1	R^2	X^-	Conversion (%)	ee (%) (*S*)
CD	OH	—	—	100	38
1	OH	H	Cl	47	26
2	OH	H	Br	21	29
3	OH	Allyl	Cl	29	17
4	OH	Benzyl	Cl	40	18
5	OH	Benzyl	Br	23	24
6	OH	CH_3	Cl	35	1
7	*O*-benzyl	Benzyl	Br	27	1.5
8	*O*-allyl	Allyl	Br	25	2
9	*O*-allyl	Benzyl	Br	7	2
10	—	—	—	100	1
11	OCH_3	—	—	100	2

CHAPTER 2 MCA ADSORPTION AND HYDROGENATION IN DICHLOROMETHANE

2.1 INTRODUCTION

The importance of synthesis of chemicals containing one or more chiral centers has been appreciated and addressed in the manufacture of pharmaceuticals, agrochemicals, and fragrances for decades. For example, the three top-selling drugs for 2008 – Lipitor (atorvastatin calcium), Plavix (clopidogrel bisulfate) and Nexium (esomeprazole magnesium), with total sales of $30 billion – were all single-enantiomer drugs [82]. The move towards enantiopure chemicals has been driven both by performance requirements and government regulations, as well as environmental concerns. While homogeneous catalytic asymmetric catalysis continues to progress rapidly, intrinsic drawbacks exist such as difficult (and expensive) catalyst separation and catalyst instability. Such issues may help to explain the relatively wide gap between R&D output from academics and industry versus commercial application [83]. In this respect, the eventual use of heterogeneous catalysts can offer several major advantages, including ease of catalyst separation, reduction of solvent usage, simplification of the synthetic route, and increased selectivity towards desired products. If optimized, these properties could result in significant economic and environmental benefits.

Cinchonidine-modified supported Pt-group metals are well-known and effective heterogeneous enantioselective catalysts, especially for the hydrogenation of prochiral

C=O bonds. In contrast, chiral C=C bond hydrogenation with these catalysts has been less successful. The first study was apparently published in 1985, and involved prochiral cinnamic acid hydrogenation over Pd/C catalysts [5]. Largely over the past decade, there have been a number of studies [6-51] that have followed up on this initial work. The groups of Nitta [6-20, 44, 45], Bartok [21-24, 48-51], and Baiker [25-38] have been the most active with the majority having explored hydrogenation of α, β- unsaturated C=C bonds adjacent to carboxylic acid groups with cinchonidine as modifier. It is suggested that cinchonidine (CD) and acids form a $CD(acid)_2$ complex during the enantioselective hydrogenation [32]. In addition, aromatic acids are more easily hydrogenated in polar solvents, as opposed to aliphatic acids that prefer non-polar environments. These (and other) studies of the cinchonidine-modified metal catalytic system have largely involved kinetics studies, as opposed to probing the surface molecular environment. In addition, the in-situ vibrational spectroscopic studies available have focused almost entirely on the cinchona alkaloid modifier interaction with the catalyst surface under different conditions [21, 25, 26].

This chapter reports an in-situ attenuated total reflection infrared spectroscopic study of the interaction of α-methylcinnamic acid with a Pd/Al_2O_3 catalyst. This molecule consists of a prochiral C=C bond located between COOH and phenyl groups (Figure 1.1), and is a good model compound for the study of C=C hydrogenation in aryl substituted substrates. Overall, the conversion and enantioselectivity of this molecule is reported to be very low over cinchonidine-modified catalysts [21, 22]. It was the aim of this work to begin to elucidate the surface molecular properties that may influence this behavior.

2.2 EXPERIMENT

2.2.1 MATERIALS

Dichloromethane (CHROMASOLV®), α-methylcinnamic acid (MCA, 99%) and α-methylhydrocinnamic acid (MHA, 98%) were obtained from Aldrich and used without further purification. The gas used for the experiments was ultrahigh purity hydrogen from National Welders Supply. $PdCl_2$ (Premion®, 99.999% (metals basis), Pd 59.5% min) and gamma aluminum oxide powder (99.5%, metal basis) were obtained from Alfa Aesar.

2.2.2 CATALYST PREPARATION

1 wt% Pd/γ- Al_2O_3 catalyst was synthesized via wet- impregnation. Palladium chloride was used as the precursor and the support γ- Al_2O_3 powder had a mean particle size of 37 nm and a surface area of $45 m^2/g$. The catalyst prepared had around 50% dispersion based on H_2 chemisorption, with a mean palladium particle size of 2.6 nm, confirmed by high-resolution transmission electron microscopy.

2.2.3 CATALYST CHARACTERIZATION

Atomic absorption spectroscopy is used to determine the concentration of a specific metal element in a solution. This technique relies strongly on the Beer-Lambert law. In short, the electrons of the atoms in the atomizer can be promoted to a higher energy level for a short amount of time by absorbing a set quantity of energy (i.e. light of a given wavelength). This amount of energy (or wavelength) is specific to a particular electron transition in a particular element, and in general, each wavelength corresponds to only one element. The quantity of energy (the power) generated by the flame is known, and thus when exposed to sample, the quantity remaining at the other side (at the

detector) can be measured. From the Beer-Lambert law, the concentration of the desired element can be determined. The Beer-Lambert Law is Where T =transmission; I0=intensity of the incident light; I =intensity of transmitted light; ε =molar absorptivity of the abs orber; l =path length; c = concentration

An atomic absorption spectrometer (Perkin Elmer model 3300) was used to analyze the exact palladium weight percent in the catalyst. Standard palladium solutions of 2ppm, 4ppm, 6ppm, 8ppm, and 10ppm were prepared first. The sample was dissolved with the help of acquaregia (HCl: HNO_3=6:1) and was heated to and held at 105°C for 4 hours. The sample solution was then diluted several times to the concentration of 2ppm to 10ppm, to stay within the detection limits of the instrument. 10% $LaCl_3$ was added to every palladium solutions to improve the AA signal. Though alumina should not yield a signal in the spectral region of interest, one pure alumina sample was still prepared in the same way to confirm this. A 1.89wt% Pd solid standard was used for comparison. The analytical spectra line is 244.79 nm, and is provided by a 20mA lamp from Scientific Products was used for elemental Pd analysis.

Chemisorption

To compare the effects of different Pd loadings, precursors and calcination, protocols, a 2.5wt% Pd $(NO_3)_2/Al_2O_3$ catalyst was prepared using Pd $(NO_3)_2$ as precursor. The rest of the steps are the same as described for $PdCl_2$. In addition, a 2.5wt% $PdCl_2/Al_2O_3$ was also prepared in addition to the 1wt% $PdCl_2/Al_2O_3$.

An Autochem II 2920[84] instrument manufactured by Micrometirics was used for chemisorption. Around 0.1g catalyst was installed in a pyrex U-tube and loaded into the equipment. The sample was first reduced at 200°C for 1 hour by flowing pure

hydrogen at 50cm^3/min, followed by a 50cm^3/min Argon purge for 1 hour to remove chemisorbed H_2, after cooling down to 40°C, the surface was saturated with hydrogen, followed by exposure to 10% O_2 and 100% Ar for half an hour each to saturate the Pd surface with adsorbed atomic oxygen, then 100% Ar for 30 min to remove residual O_2. The sample was then ready for pulse flow H_2 titration. At room temperature the adsorbed atomic oxygen reacts rapidly with the 10% H_2/balance Ar pulse (pulses repeated at 4 min intervals) to form H_2O and replace the adsorbed oxygen atom with atomic hydrogen. A TCD detector in the instrument measures the amount of unadsorbed gas flowing out of the sample cell. Peaks are continuously recorded until their sizes are equal (i.e., until the metal surface is saturated).

High-resolution Scanning Transmission Electron Microscopy (HR-STEM)

A JEOL 2100F with CEOS GmbH hexapole STEM probe corrector in the USC Electron Microscopy Center was used to image the 1wt% Pd/Al_2O_3 sample. This instrument is an advanced field emission electron microscope with an accelerating voltage of 80 to 200kV and a TEM point resolution 0.19nm. The imaging mode allows for determination of crystallographic structure at an atomic scale. It has very high resolution (the highest resolution so far is 0.08 nm), so it is an invaluable tool to study nanoscale properties of crystalline material such as semiconductors and metals.

Carbon monoxide Adsorption

Infrared spectroscopic characterization of supported and unsupported transition metal catalysts using CO as a probe molecule has been performed extensively in gas phase [85] and liquid phase [86]. In general, two bands associated with adsorbed CO have been observed on palladium. Linearly (i.e., terminal, atop) adsorbed CO typically

exhibits υCO frequencies between 2000 and 2100 cm^{-1}, while two-fold and three fold bridging CO typically lies between 1780 and 2000 cm^{-1}. The frequency of these bands is significantly affected by surface coverage, co-adsorbates, and electric field dipole coupling effects. As a result, CO is a good choice for initial probing of catalyst films in liquid solvents using ATR-IR spectroscopy.

The adsorption of CO from water was examined using ATR-IR spectroscopy. An FTIR spectrometer (Nicolet 670) equipped with an ATR-IR accessory (SpectraTech) was used for these studies. The accessories are compatible with several custom designed liquid flow cells. The detail of this technique will be presented in the Section 3.3.0. A background spectrum was taken after flowing DI water through the ATR cell for at least 4 hours, and it was used for all other spectra acquired during the experiment. The spectra were taken automatically every 158 seconds using 128 scans with a resolution of 4 cm^{-1}. Pure water is flowed through cell for 2 hours followed by CO saturated water for 2 hours. Finally the flow was switched back to pure water for 2 hours. The spectrum in Figure 11 is the last spectrum taken after flowing CO saturated DI water for 2 hours.

In addition to water, identical experiments were performed using dichloromethane, which is one of the solvents chosen for study of the C=C hydrogenation reaction.

2.2.4 ATR-IR SPECTROSCOPY

An FTIR spectrometer (Nicolet 670) equipped with an ATR-IR accessory (SpectraTech) was used for these studies, as reported previously [87, 88]. In the accessory there are two mirrors that allow the horizontal infrared light to be reflected verticallyinto the ATR-IR cell. Two holes in the bottom of the cell are designed to let the

infrared light enter the ZnSe element sealed within the cell. A 60° zinc selenide (ZnSe) crystal (Spectra Tech) was selected for use as the ATR element upon which the catalyst film is deposited. The film was coated onto the ATR element using a suspension of 25mg catalyst in 20ml DI water. This mixture had been first placed in an ultrasonic bath overnight in order to obtain a uniform suspension. A thin layer of this suspension was spread into the ATR element and dried under a lamp. This procedure was repeated four times, giving an average film thickness of 10±2 μm, as found using optical microscopy (Olympus BX50 microscope and Simple PCI image analysis software by Compix).

The liquid solutions are kept in glass flasks (i.e., reservoirs) with magnetic stirring. Two separate reservoirs were used during the experiment without mixing between acid solutions and pure solvent (CH_2Cl_2). Gas can be bubbled into the solution for hydrogenation experiments using an H_2 line attached to porous glass frit capped tube submerged in the reservoir. Pumps recycle the solution from the reservoirs, through the flow cell and back during the experiment. The flow path was altered by three-way valves that were automated and controlled using Labview (National Instruments). All experiments were carried out at room temperature and atmospheric pressure.

For acid adsorption experiments, pure solvent was flowed through the flow cell overnight prior to taking the background. At time zero, a spectral background was acquired and utilized for all the spectra taken during the experiment. Spectra were acquired continuously every ca 2 min during the experiment with 128 scans per spectrum using a resolution of 4 cm^{-1}. Pure solvent was continued for 1 hour, followed by 2mM MCA in CH_2Cl_2 for 1 hour. Then the cycle is repeated, with solvent followed by acid solution, but for 16 mM acid and 8 mM acid, ending with a final solvent flush. For

hydrogenation, after spectrawere acquired in H_2-saturated pure solvent for 2 h, the flow was switched to H_2-saturated 0.016M acid solution for 2 h. Finally the solution was purged with H_2-saturated solvent for 2 h. The adsorption and hydrogenation of α-methylhydrocinnamic acid (which is the product of the hydrogenation reaction) on 1 wt% Pd/Al_2O_3 was studied with ATR-IR to help interpret the hydrogenation spectra. In these experiments, a background was taken after bubbling hydrogen in solvent for 1 h, after which spectra in pure solvent were collected for 1 h. This was followed by 0.016 M product acid for 1 h, and finally pure solvent.

Vibrational assignments were assisted using spectral curve fitting to deconvolute overlapping peaks. Specific band assignments were aided by density functional theory (DFT) calculations on a single molecule in the gas phase using Gaussian 03 W, Revision B.02 [89] with the Becke three-parameter-Lee-Yang-Parr (B3LYP) method and the 6-31 G(d) basis set. The results were corrected by scaling factor 0.97.

2.3 RESULTS AND DISCUSSION

2.3.1 CATALYST CHARACTERIZATION

The absorptions of the standard Pd solutions with concentration of 0ppm, 2ppm, 4ppm, 6ppm, 8ppm, and 10ppm were measured by the AA equipment. The corresponding concentration versus absorbance plot shows a linear relationship. The first two samples in the table are alumina samples, the following two are the catalyst sample while the last one is the 1.89wt% palladium solid standard. The average weight percent of two sample solutions prepared is 0.99wt.%, suggesting minor loss of metal during the preparation steps.

Chemisorption

As shown in Figure 2.1, with everything else the same, $PdCl_2$ as a precursor works better than Pd $(NO_3)_2$, with the dispersion increase from $PdCl_2$ to Pd $(NO_3)_2$. Higher loading will result in clearly lower dispersion; 2.5wt% $PdCl_2/Al_2O_3$ has 10% dispersion at the beginning while 1wt% has 26% dispersion. Thus, the largest dispersion difference comes from changing the loading. Washed catalyst and calcined catalyst have higher dispersion but the difference is not as significant. The Figure 2.1a) is the chemisorption result for Pd/Al_2O_3 catalysts using the method of hydrogen chemisorption while Figure 2.1b) is b) Pd/Al_2O_3 catalysts using the method of hydrogen titration of oxygen-precovered sites. Though there was higher dispersion at 400 $^{\circ}$C compared to 300°C, but the dispersion difference is small. We choose 300°C as our H_2 reduction temperature for the catalyst considering the problem of increasing the particle size with higher reduction temperature. There are several processes occurring during calcination [90]: loss of the chemically bonded water or CO_2, active phase generation and stabilization of mechanical properties, modification of the texture through sintering (i.e., small crystals or particles that turn into bigger ones), and modification of the structure. When the loading is 1 wt%, the dispersion at 300°C is 45% for hydrogen chemisorption and 25% for O_2-H_2 titration, and the corresponding diameter is 2.5 nm for hydrogen chemisorption and 4.4 nm for O_2-H_2 titration which is calculated using equation [84]:

$$APS = \frac{6}{(D_{calc}) \times (\frac{W_S}{GMW_{calc}}) \times (6.023 \times 10^{23}) \times (SA_{calc})}$$

where APS is the active particle size, Dcalc is the calculated metal density (g/cm^3), Ws is the sample weight, (g), GMWcalc is the gram molecular weight (g/g-mole), and SAcalc is the calculated specific surface area (per gram of metal).

High-resolution Scanning Transmission Electron Microscopy (HR-STEM)

As seen in Figure 2.2, the imaging reveals that Pd particles are present in the form of small bright spherical particles, supported on the larger (30-40 nm) Al_2O_3 particles. Over 400 particles in 17 HR-STEM images were measured, yielding a volume-surface mean diameter of 2.7 nm, which is consistent with the results from hydrogen chemisorption.

CO Adsorption

As shown in Figure 2.3, two clear peaks are observed in CO stretching region. For CO adsorption in water, they are 1932 and 2064 cm^{-1}. While for CH_2Cl_2, A blue-shift about 10 cm^{-1} wavenumbers with the positions at 1940 and 2078 cm^{-1} are observed, respectively. At full CO adsorption an intense absorption band at 1990-2100cm^{-1} corresponds to atop CO adsorbed on palladium, peaks at 1830-1950cm^{-1} indicating the presence of CO adsorbed on 2-fold bridging sites. These results show expected CO adsorption behavior and indicate that the palladium catalyst is typical of those used for catalytic studies. In addition, the dichloromethane solvent has little effect on frequency shift for CO adsorption.

2.3.2 REACTANT ACID ADSORPTION

The first step to study the hydrogenation of α-methylcinnamic acid is to understand the adsorption behavior of this reactant on the γ-Al_2O_3 support and Pd/Al_2O_3 catalyst. Prior to this, the ATR-IR spectra of the acid solution in contact with the bare

ZnSe element were examined. The first plot in Figure 2.4 shows typical spectra taken from acid solution in contact with the bare element as a function of the concentration profile described before. The seven spectra shown from the bottom to the top were the spectra taken at the end of each indicated experimental step. Two clear peaks are observed at 1715 cm^{-1} and 1685 cm^{-1}. From the literature [25], the 1715 cm^{-1} peak is associated with C=O stretching from acid monomers,while the 1685 cm^{-1} peak is associated with acid dimer species. The small peak at 1492 cm^{-1} is assigned to the ring vibration,while peaks at 1448 cm^{-1} and 1407 cm^{-1} correspond to methyl group vibrations. Usually, the monomer acid is favored in very dilute solution in non-polar solvents, or in the vapor phase. Indeed, the relative sizes of the peaks change with concentration, showing that the dimer species is favored at higher concentrations. However, most importantly, these liquid phase peaks disappear completely upon switching to pure solvent; this confirms that there is no strong adsorption on the ZnSe surface.

Figure 2.5 shows ATR-IR spectra obtained in the same fashion, but for an Al_2O_3 film. As can be seen, the peak intensities are increased and there are peaks remaining after removal of liquid-phase acid, suggesting that acid is adsorbed on the alumina. The peak associated with monomer C=O decreased, while the dimer-related peak increased, relative to the liquid phase. In addition, there is prominent peak at around 1640 cm^{-1}, which is assigned to C=C stretching [25]. Peaks around 1350 cm^{-1} to 1500 cm^{-1} were mainly associated with C–H bending vibrations in the methyl group, while the features from 1500 to 1600 cm^{-1} arise from ring stretching vibrations. All of these assignments are shown in Table 2.1, and were made based on comparisons with characteristic frequency tables and the DFT calculation results. Figure 2.6 shows that similar spectra were

observed for the same experiment performed on the 1wt% Pd/Al_2O_3 sample, although some peak intensities are a little higher. Indeed, the peaks from 1500 to 1600 cm^{-1} are clearly increased compared to Al_2O_3 alone, while the ratio of peaks found between 1600-1700 cm^{-1} and 1350-1500 cm^{-1} changed.

The spectra during adsorption experiments are complex and contain many overlapping peaks from a variety of sources, especially at the highest acid concentration of 0.016 M. To distinguish more clearly the peaks arising from bulk liquid and adsorbed species, the spectra were deconvoluted using least squared regression analysis. Before fitting could proceed, the peaks used to model liquid phase were determined. This was accomplished by fitting the IR spectra obtained from the bare element in 0.016 M acid, as shown in Figure 2.5. The peaks at 1450, 1407, 1492, 1680, and 1715 cm^{-1} can be readily assigned to liquid-phase acid. The resulting parameters for these liquid peaks were then used when fitting the IR spectra obtained in the presence of a film (i.e. Al_2O_3 or Pd/Al_2O_3). Initial inputs for surface adsorbed acid-related peaks were chosen based on the shape of the overall spectra and examination of residuals after subtraction of such liquid signals. The peaks from liquid-phase acid were modeled by pure Gaussian lineshapes, while the peaks from adsorbed species were modeled by a hybrid Lorentzian/Gaussian function. Several constraints were placed on the liquid peak parameters during the fitting routine within a given data set. The ratios, positions, and full widths at half maximum (FWHM) of the liquid peaks were kept constant, with only the intensity of the peaks allowed to vary. The same constraints were placed on the peak parameters for adsorbed acid on alumina when fitting the 1 wt.% Pd/Al_2O_3 spectrum. Finally, the intensities of any adsorbed acid peaks on Pd were allowed to vary while

keeping other parameters constant. All the fitted spectra shown in the right plots in Figs. 2.4-2.7 were those taken for the highest concentration acid (0.0016 M) flowing through the cell. In these spectra, the red peaks are those arising peaks from liquid-phase acid, blue are those coming from adsorbed acid on alumina, and green are those observed on the Pd metal.

Based on this curve fitting, and vibrational frequencies calculated by DFT, peak assignments have been made and are summarized. Of particular interest are the peaks ~1529 cm^{-1} and ~1384 cm^{-1}, which are confidently assigned as asymmetric and symmetric COO^- vibrations base on the available literature [91, 92]. The presence of these peaks shows that the reactant acid is dissociatively adsorbed on both the alumina and Pd surfaces. It is well known that different binding structures of carboxylates can be assigned based on the difference between asymmetric and symmetric COO^- vibration peaks. For example, a difference between 350 cm^{-1} to 500 cm^{-1} indicates a unidentate mode, 150-180 cm^{-1} indicates a bridging bidentate mode, and 60-100 cm^{-1} indicates a chelating bidentate. Thus, the bidentate bridging configuration, with the two oxygen atoms of the carboxylate bridging between two sites on the surface, is apparently favored under the conditions examined here. Overall, considering the C=O stretching bands in these curve fitted plots, both monomer and dimer acid species exist in the bulk liquid phase. In contrast, only dimer is present on the alumina surface, and no significant dimer or monomer peaks are observed Pd. Thus, these spectra reveal that the acid adsorbs both molecularly and dissociatively on alumina but only dissociatively on Pd, at these conditions. It has been suggested previously [32] that on the cinchonidine (CD)-modified Pd surface, a $CD(acid)_2$ complex is present during the enantioselective hydrogenation.

The present spectra obtained during adsorption suggest that such complexesmay indeed be necessary to facilitate molecular adsorption on the surface.

2.3.3 HYDROGENATION

After examining the adsorption of acid onto Al_2O_3 and Pd/Al_2O_3 catalyst, preliminary studies of α-methylcinnamic acid hydrogenation were performed. Based on the literature, this hydrogenation can be carried out effectively at roomtemperature and atmospheric hydrogen pressure, albeit with low activity. Fig. 2.7 A and B show typical spectra for hydrogenation of 0.016 M acid on alumina and 1 wt.% Pd/Al_2O_3, respectively. The relevant spectra for reactant adsorption in the absence of H_2 at the same concentration are taken from Fig. 2.5. Finally, a spectrumis included for the adsorption of the product α-methylhydrocinnamic acid in dichloromethane directly after exposure of the catalyst to a 0.016 M concentration step for 1 h. It was expected that the Al_2O_3 would not show any surface reactivity towards hydrogenation. Indeed, Fig. 2.7A supports this supposition, since the spectrum taken in the presence of H_2-saturated acid is essentially identical to that obtained in H_2-free solution. In contrast, Fig. 2.7B shows that in the case of catalyst, a very significant shoulder appears above 1700 cm^{-1} in the presence of H_2. Based on comparison with the spectrum obtained during product adsorption, this new peak can readily be assigned to the C=O stretch of dimerized adsorbed product acid. Both the monomer and dimer C=O stretching frequencies for the product are blue shifted by about 50 cm^{-1}, due to the absence of an adjacent C=C bond. In addition, there is a broad feature around 1600 cm^{-1}, which can be assigned to ring stretching combined with the higher frequency C=C stretching peak from the reactant, which is still also adsorbed on both Pd and Al_2O_3. The C=C bond, the benzene ring is another possible unsaturated bond

that can be hydrogenated. However, preliminary batch kineticstudies (not shown) of the same catalyst for this hydrogenation system at the same temperature and pressure indicate that only the C=C bond is hydrogenated under these conditions.

2.4 CONCLUSIONS

The adsorption of α-methylcinnamic acid in dichloromethane at room temperature on Al_2O_3 and 1 wt.% Pd/Al_2O_3 powder thin films was characterized by ATR-IR. While both monomer and dimer acid species are present in the liquid phase, the only molecular adsorption on Al_2O_3 was in dimer form. In contrast, there was essentially no observed molecular adsorption on the Pd surface. The presence of asymmetric and symmetric COO- vibration peaks and their band separation indicated adsorbed bidentate bridging carboxylate species on both Al_2O_3 and Pd. Thus, this substituted acid adsorbs both molecularly and dissociatively on Al_2O_3, but only dissociatively on Pd. Introduction of solution phase hydrogen had no effect on the surface speciation on Al_2O_3 alone. In contrast, strongly adsorbed product was formed in the presence of Pd/Al_2O_3, where it may reside on the metal and/or the support.

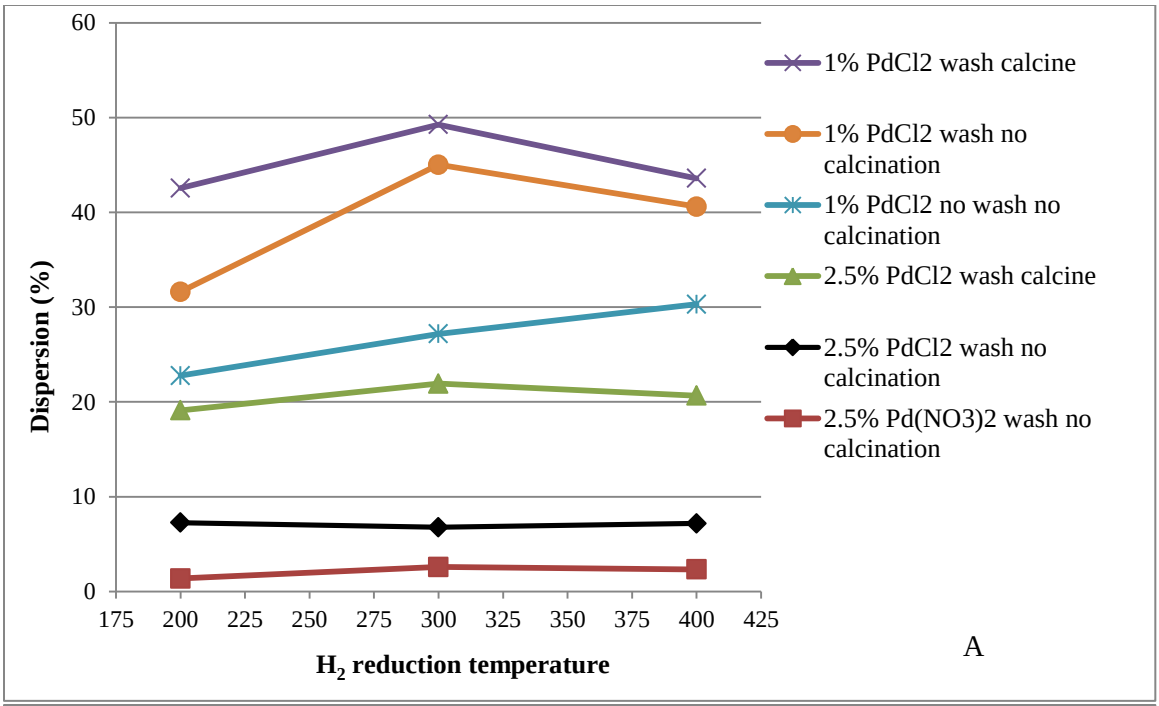

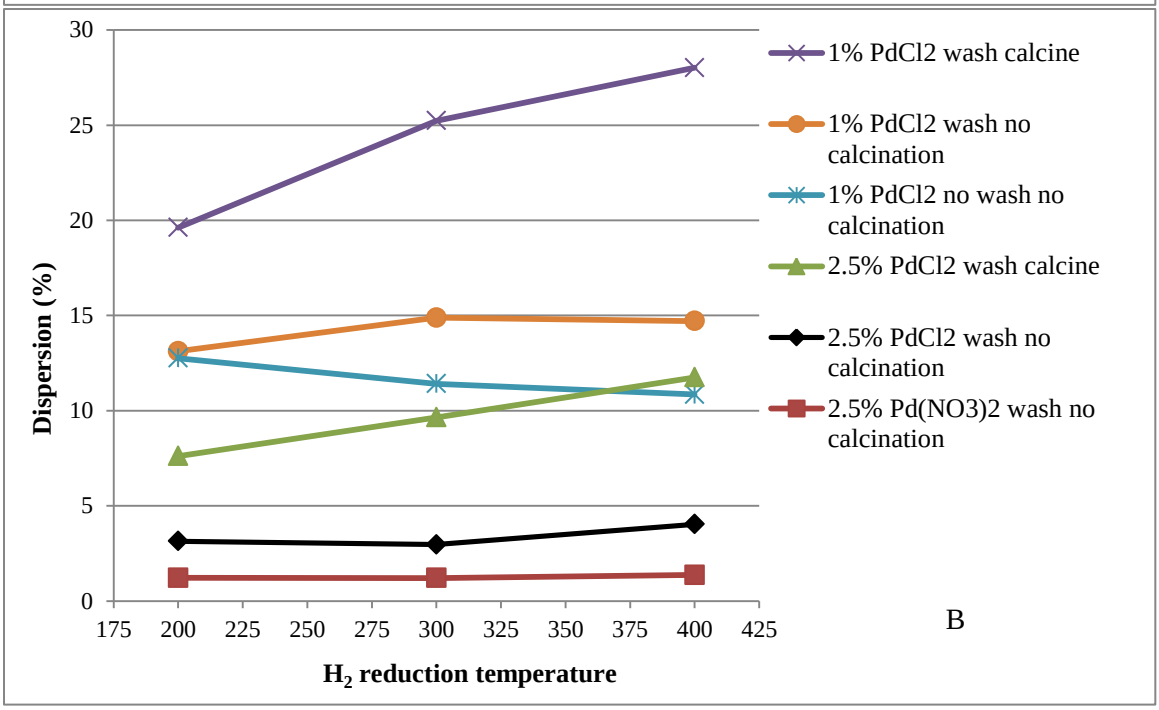

Figure 2.1 Chemisorption results for A) Pd/Al_2O_3 catalysts using the method of hydrogen chemisorption B) Pd/Al_2O_3 catalysts using the method of hydrogen titration of oxygen-precovered sites.

A

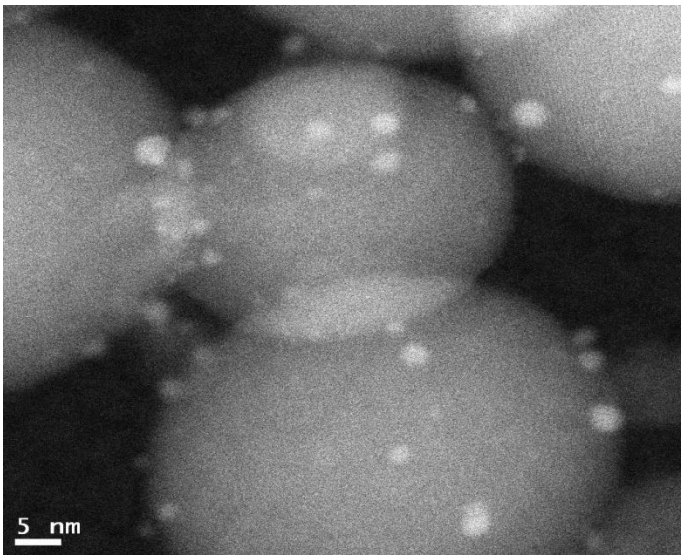

B

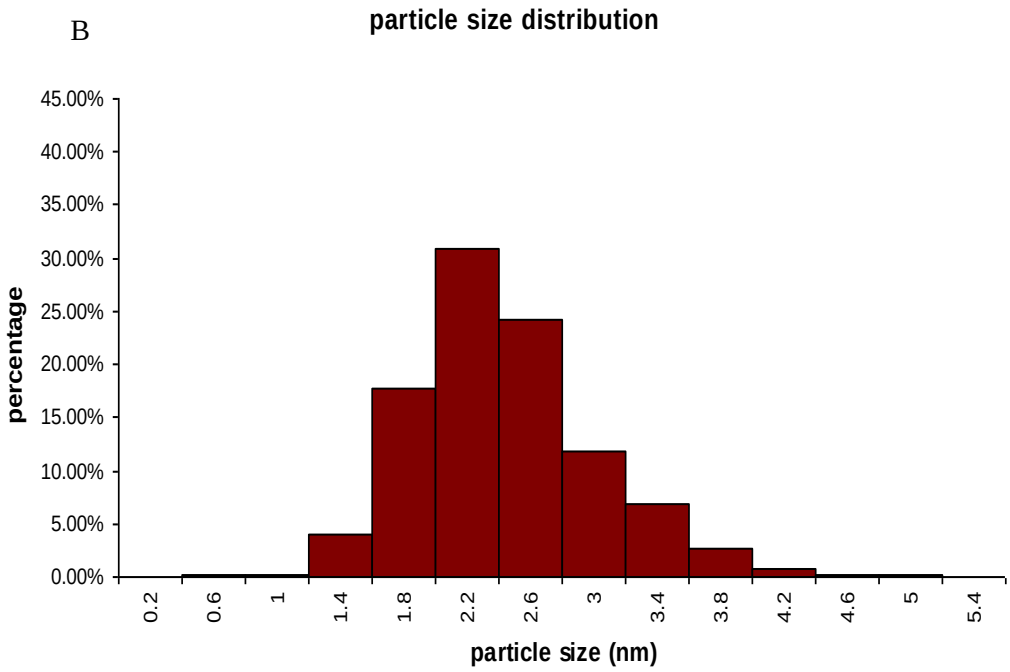

Figure 2.2 A) HR-STEM image of 1wt%Pd/Al_2O_3, B) Over 400 particle's diameter results from HR-TEM.

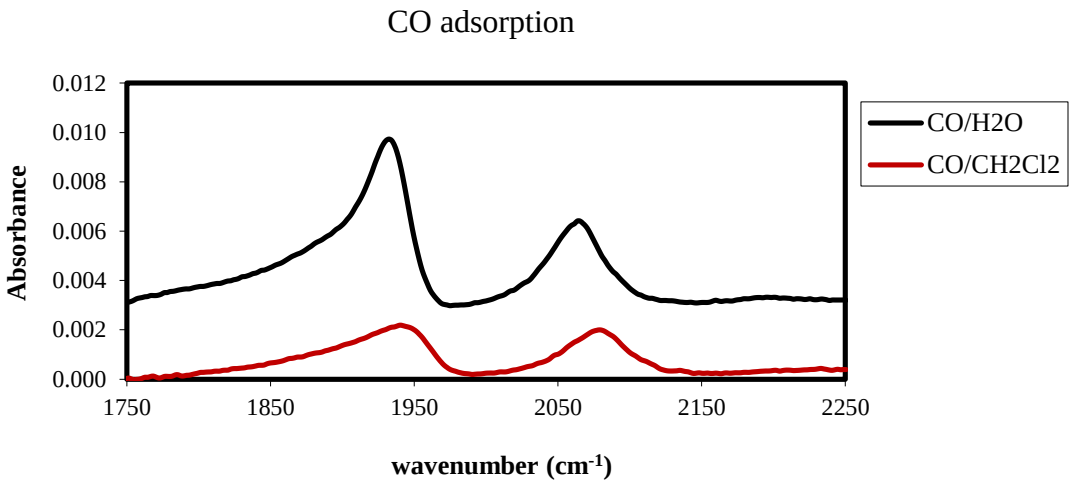

Figure 2.3 CO adsorption on 1wt% Pd/Al_2O_3 with DI water and dichloromethane as solvent.

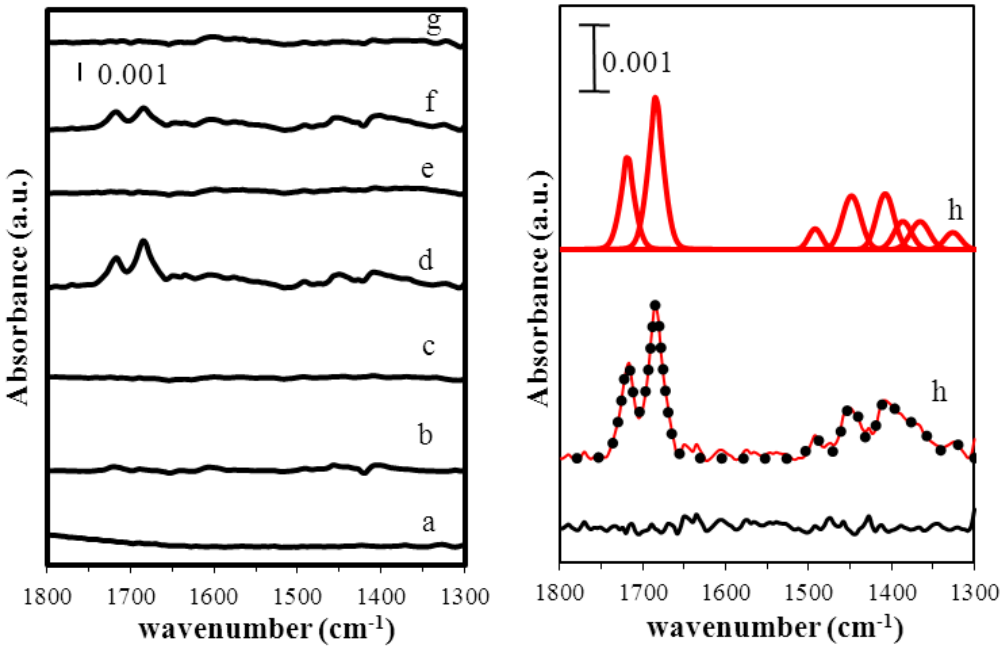

Figure 2.4 ATR-IR spectra for α-methylcinnamic acid (MCA) in contact with a bare ZnSe element. The spectra were acquired in order after exposure to a) pure solvent, b) 2 mM MCA, c) pure solvent, d) 16mM MCA, e) pure solvent, f) 8mMMCA and g) pure solvent. The plots on the right (h) are curve fitting for d). See text for details.

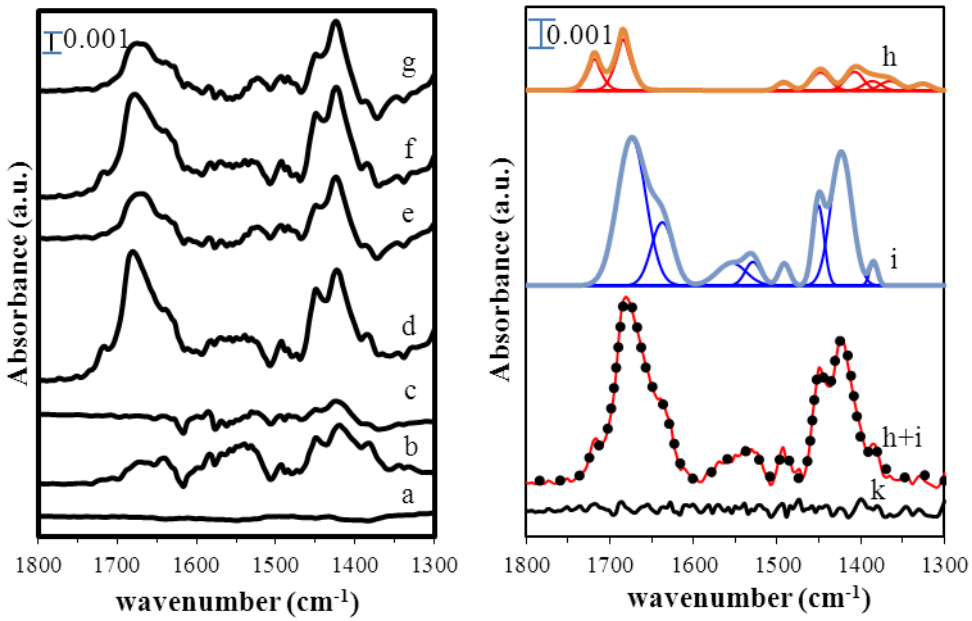

Figure 2.5 ATR-IR spectra for α-methylcinnamic acid (MCA) adsorption on Al_2O_3. The spectrawere acquired in order after exposure to a) pure solvent, b) 2 mM MCA, c) pure solvent, d) 16 mM MCA, e) pure solvent, f) 8 mM MCA and g) pure solvent. The plots on the right are curve fitting for d), with the curves indicated for spectral contributions from the h) liquid and i) adsorption on alumina. See text for details.

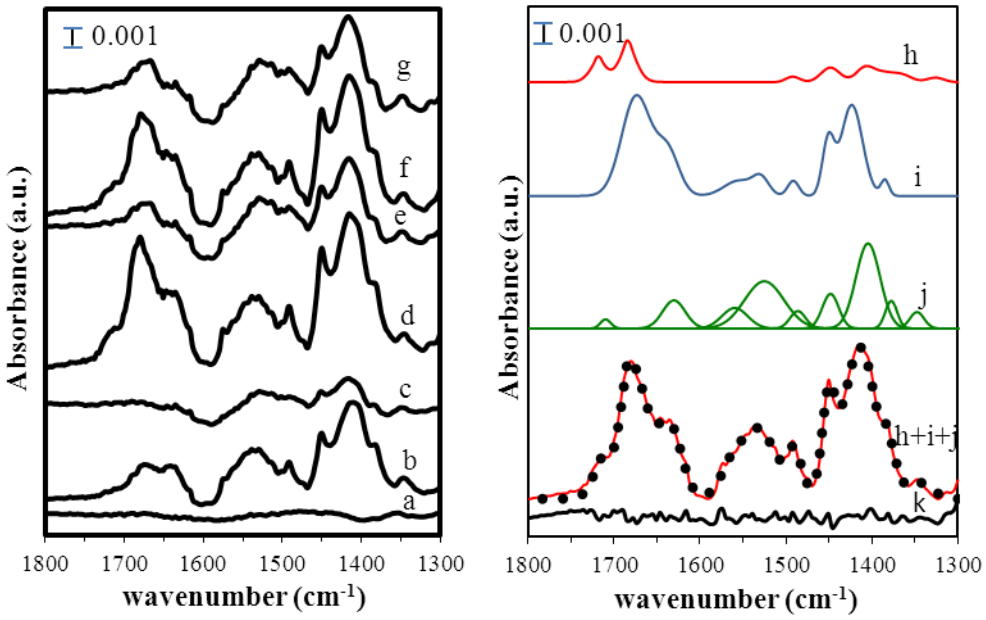

Figure 2.6 ATR-IR spectra for α-methylcinnamic acid (MCA) adsorption on 1 wt.% Pd/Al_2O_3. The spectra were acquired in order after exposure to a) pure solvent, b) 2 mM MCA, c) pure solvent, d) 16 mM MCA, e) pure solvent, f) 8 mM MCA and g) pure solvent. The plots on the right are curve fitting for spectrum d), with the curves indicated for spectral contributions from h) liquid, i) adsorption on alumina, and j) adsorption on Pd. See text for details.

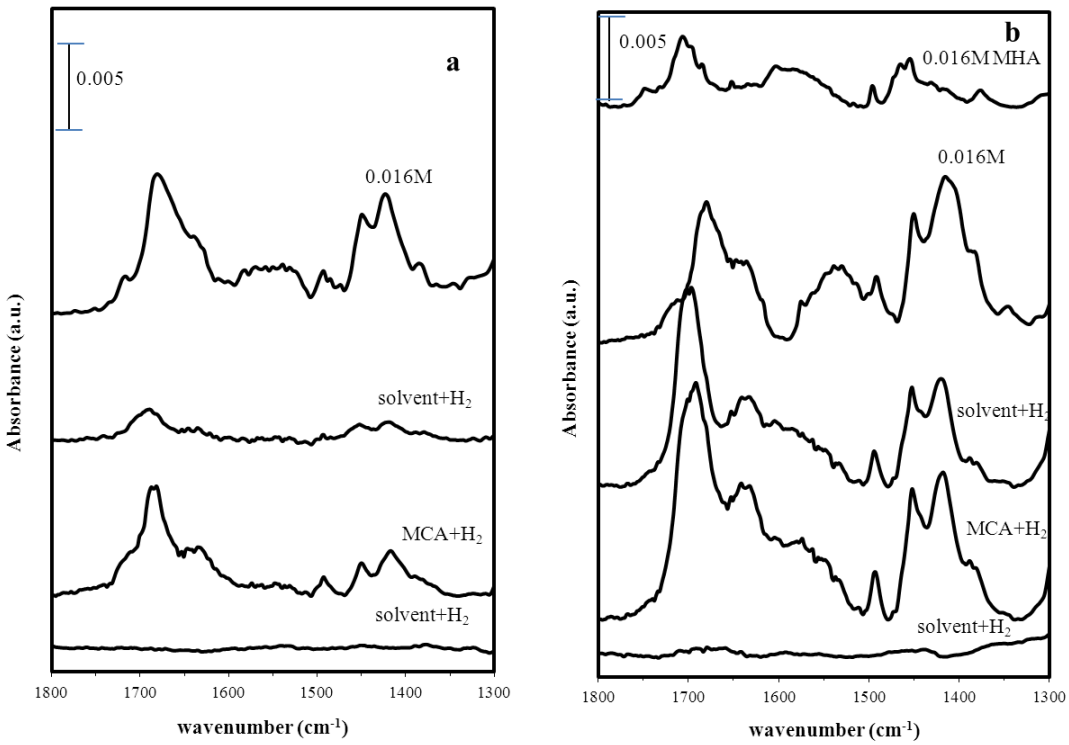

Figure 2.7 ATR-IR spectra obtained during hydrogenation of MCA on alumina and 1 wt.% Pd/Al_2O_3.MCA and product (MHA) adsorption spectra acquired in separate adsorption experiments in the absence of H_2 are shown for comparison.

Table 2.1 Vibrational peak assignments

Vibrational Mode	Peak Assignment			
	Experimental			Calculation
	bare element	Al_2O_3	1wt% Pd/Al_2O_3	B3LYP/6-31G(d)
C=O str. (monomer)	1716		1710	1738
C=O str. (dimer)	1684	1672		1738
C=C str.		1637	1632	1621
ring str.		1554	1547	1566
asymmetric COO- vib		1529	1522	
ring symmetric vib.	1492	1491	1491	1483
methyl group asymmetric C-H vib	1448	1450	1447	1457
methyl group symmetric C-H vib	1407	1423	1403	1392
symmetric COO- vib	1386	1384	1378	
C-H vibration(H-C=C)			1346	1359

CHAPTER 3 KINETIC STUDY OF SOLVENT, TEMPERATURE AND PRESSURE EFFECT

3.1 INTRODUCTION

Enantiopure chemicals are important in living systems, such as in amino acids, proteins and sugars, etc., and they are important for the manufacture of pharmaceuticals, agrochemicals, and fragrances. While homogeneous catalysts are widely used in industry, intrinsic drawbacks exist, such as difficult (and expensive) catalyst separation and catalyst instability. Such issues may help to explain the relatively wide gap between R&D output from academics and industry versus commercial application [83]. In this respect, the eventual use of heterogeneous catalysts can offer several major advantages, including ease of catalyst separation, reduction of solvent usage, simplification of the synthetic route, and increased selectivity towards desired products. If optimized, these properties could result in significant economic and environmental benefits.

Largely over the past decade, there have been a number of studies [6-51] exploring the hydrogenation of α, β- unsaturated C=C bonds adjacent to carboxylic acid groups over Pd catalysts with cinchonidine as a chiral modifier, especially from the groups of Nitta [6-20, 44, 45], Bartok [21-24, 48-51], and Baiker [25-38]. Via spectroscopic detection, the modifier cinchonidine (CD) has been shown to form a $CD(acid)_2$ complex during the enantioselective hydrogenation [32]. Based on kinetic studies, it is suggested that aromatic acid hydrogenation is favored in polar solvents, as

opposed to aliphatic acid hydrogenation that is prefer in non-polar environments. However, the kinetic studies available have focused almost entirely on the final conversion and selectivity [7-24], rather than exploring kinetic parameters such as rates, reaction orders, or activation energies.

This chapter reports a detailed kinetic study of the hydrogenation of α-methylcinnamic acid with 5wt% Pd/Al_2O_3 catalyst as shown in Figure 1.1. This molecule consists of a prochiral C=C bond located between COOH and phenyl groups, and is a good model compound for the study of C=C hydrogenation in aryl substituted substrates. Overall, the substrate has not been very well studied, with conversion and desired enantioselectivity reported to be very low over cinchonidine-modified catalysts [21, 22]. The aim of this work is to begin to study in detail, the kinetic parameters such as reaction order, activation energy and any possible product inhibition effects.

3.2 EXPERIMENTAL SECTION

The materials were as follows and used as received: α-methylcinnamic acid (MCA, 99%, Sigma-Aldrich), α-methylhydrocinnamic acid (MHA, 98%, Sigma-Aldrich), cinchonidine (CD, TCI), dichloromethane (99.9 %, Sigma-Aldrich), isopropanol (99+%, Alfa-Aesar), 1,4-dioxane (99.9%, Sigma-Aldrich), N,N-dimethylformamide (Sigma-Aldrich) and 5 wt% Pd/Al_2O_3 powder (Alfa-Aesar, 14% metal dispersion); H_2 (UHP), N_2 (UHP), and 20 % H_2/N_2 (2,000 psi) were supplied by Airgas.

Hydrogenation of MCA was carried out in a stainless steel EZE-Seal® batch reactor (Autoclave Engineers) with 100 ml capacity equipped with thermocouple, a pressure gauge and a stirring motor. In a typical reaction, the reactor was loaded with 48

ml solvent, and 0.1g catalyst. For enantioselective hydrogenation, 0.088 g modifier (CD) was added into the reactor. After sealing, a leak check using 200 psi N_2 was performed three times, followed by three pressure/vent cycles in order to remove any residual oxygen from the system. The water-cooled stirring motor was set at a rate of 1,000 rpm based on rate measurements made at varying speeds, and was chosen to ensure that reactions were carried out free of external mass transfer limitations. H_2 was flowed for one hour to pre-reduce the catalyst. The reaction was then initiated by an introduction of 0.97g substrate (MCA) in 12ml solvent solution into the reactor. In this way, the modifier/reactant ratio is fixed at ca. 1/20, which is a typical ratio for this kind of asymmetric hydrogenation [21]. The temperature of the liquid in the reactor was monitored with the thermocouple in real time during the reaction, and had a maximum deviation of 1–2 ºC.

The samples collected from the reactor at different reaction times were injected automatically with a Hi-Tech 300A liquid auto sampler from Overbrook Scientific. The quantitative analysis of the product mixture was performed using a Hewlett Packard 5890 Series II gas chromatograph with a flame ionization detector (FID), equipped with an a DB-1 column (15m*0.53mm, J&W Scientific Inc). The ee value was determined using a CyclosilB column (30m*0.25mm, J&W Scientific Inc.) after transforming the products to methyl esters. According to the literature, the (R)-product is in excess [21] [22], and the enantiomeric excess (e.e.) value was calculated with the equation: e.e.(%) = 100*([R] - [S])/([S] + [R]).

3. 3 RESULTS AND DISCUSSION

3.3.1 REACTION ORDERS IN ISOPROPANOL

Prior to examination of the solvent and temperature effects, the reaction orders for MCA and H_2 were determined in isopropanol. Several parameters were fixed for the hydrogenation reaction, including initial substrate concentration, solvent, and temperature. Both the racemic and enantioselective reactions were tested at different H_2 pressures from 1 to 30 atm. The experimental concentration versus time plots were well fitted by applying least square regression to an empirical exponential function $c = a \times \exp(bt^2 + dt)$, where a, b, and d are parameters that allowed to vary and t is time. The hydrogenation reaction rate can be expressed in a typical power law form as: $r = -\frac{dC}{dt} = kP_{H_2}^{\beta} C^{\alpha} = k_{app} C^{\alpha}$. Therefore, using the differential method by plotting ln(-dC_{MCA} /dt) versus ln(C_{MCA}) yields the reaction order (α) and the apparent reaction constant (k_{app}) with respect to the acid substrate. As shown in Figure 3.1, the MCA reaction order is ca. 1 with or without modifier in isopropanol. Similar plots were obtained for other hydrogen pressures, showing that the acid reaction order is independent of H_2 pressure.

Figure 3.2 shows further analysis by plotting lnk_{app} versus lnP_{H_2}, which allows for the evaluation of the reaction order with respect to H_2 pressure. The reaction exhibits a zero order dependence on H_2 pressure for both the racemic and modified cases. These and the previous results show that the presence of cinchonidine does not affect the reaction order with respect to either acid or H_2 pressure in isopropanol The zero order in hydrogen suggests that hydrogen adsorption and activation is fast and equilibrated, while

the first order in acid suggests that the rate determining step might be the adsorption and activation of MCA.

3.3.2 SOLVENT EFFECTS

A summary of kinetic data obtained in various solvents is shown in Table 3.1. As the data indicates, this type of hydrogenation reaction is strongly solvent-dependent in terms of the activity. Among the five chosen solvents, four solvents exhibit first order in MCA, which can be explained by a Langmuir-Hinshelwood mechanism. Interestingly, the reaction is zero order in MCA in CH_2Cl_2 with or without modifier. The reason for this difference is at present unclear. For activity, isopropanol is superior, followed by 1, 4-dioxane + 1.5vol% DI water, 1, 4 dioxane and N, N-dimethylformamide (DMF), and finally, CH_2Cl_2, which exhibits very low activity. In all cases, cinchonidine has a significant inhibiting effect on the reaction rate.

Selectivity in all these five solvents was similar and low. Previous studies have focused on the effect of solvent polarity on enantioselectivity. Generally, the increased polarity of solvent leads to a poorer catalytic performance for aliphatic acids, while in contrast it enhances performance for aromatic acids [26]. However, the effect of solvent polarity on activity has not been extensively examined. There are several possible reasons for different activity including H_2 solubility, MCA solubility and the dielectric constant, to name a few. The solubility of H_2 in these five solvents at 298.15 K and 0.1 MPa is in the order of isopropanol>CH_2Cl_2>dioxane>dioxane+DI water>DMF. For isopropanol, it has the highest H_2 solubility and highest activity, but for CH_2Cl_2, it has higher H_2 solubility than the other solvents but affords the lowest activity. Thus, H_2 solubility definitely will affect the activity, but it is not the main reason for these trends.

MCA solubility in different solvents was compared and found to decrease in the order of CH_2Cl_2>DMF>dioxane>dioxane+DI water>isopropanol. This is exactly the reverse order of activity. It is reasonable because the more MCA is preferred to be in the liquid phase, the less thermodynamic driving force for MCA adsorption. This result also indicates the MCA adsorption and activation might be the rate determining step. The dielectric constant decreases in the order of DMF>isopropanol>CH_2Cl_2>dioxane+DI water>dioxane, which does not correlate with the activity trend.

In the case of selectivity, the cinchonidine solubility in different solvents is a possible factor, and these values have been tabulated in literature [97] for DMF, isopropanol, dioxane, and dioxane+DI water as follows: DMF>isopropanol>dioxane>dioxane+DI water. However, this order does not correlate with the present findings. Another possible reason for different selectivity is the ratio between unmodified initial reaction rate and modified initial reaction rate. This difference in isopropanol is 7 times difference, 3.7 for Dioxane, 4.2 for Dioxane+DI water, and 3.5 for DMF. The unmodified reaction rate is much faster than the modified one in isopropanol, so the enantioselectivity is lowest, while DMF has smallest difference with highest enantioselectivity. Addition of DI water leads to an increase in both unmodified and modified reaction rates, and the ratio between these two rates, along with a concurrent increase in the enantioselectivity. All these results suggest that not only the polarity, but also the protic character of the solvent, seem to play an important role in determining activity and for enantioselectivity, polar aprotic solvent> polar protic>nonpolar solvent.

3.3.3 TOF CALCULATION

To estimate the turnover frequency on modified sites from the apparent rate of reaction data obtained during the modified reaction, an analysis was performed by making several assumptions. First, the total number of sites (S) remains constant during the racemic and enantioselective hydrogenation. Second, unmodified sites (U) exhibit the same activity, whether in the absence or presence of modified sites. Third, modified sites (M) exhibit a perfect selectivity, directing the hydrogenation 100 % towards the R-enantiomer. These assumptions have been used effectively in our recent previous study of enantioselective hydrogenation of alkenoic acid over Pd catalyst [93]. A series of mathematical manipulations yields the following equations:

Racemic reaction: $r_{rac}= (S)* (TOF)_U$

Selective reaction: $r_R=1/2(U)*(TOF)_U$

$$r_S=1/2(U)* (TOF)_U+(S-U)*(TOF)_M$$

$$r_{sel}= (U)*(TOF)_U+ (S-U)*(TOF)_M$$

where r_{rac} is the initial rate of racemic reaction, r_R and r_S are the initial rate of R and S product of enantioselective reaction, respectively. Using these equations, the modified sites (S) can be calculated, revealing ~91% modified sites coverage in isopropanol, 76% for dioxane, 81% for dioxane+DI water and 77% for DMF.

Figure 3.3 shows the corresponding estimated turnover frequencies (TOF) of modified and unmodified sites. The ratio of unmodified/modified site TOF is isopropanol>dioxane>dioxane+DI water>DMF in the region of 16–130. . This followed similar trend with enantioselectivity (DMF> Dioxane+DI water> Isopropanol> Dioxane),

DI water addition increase both TOF_u and TOF_m but preferentially accelerate TOF_m. It suggests that the TOF difference between modified and unmodified sites might be the key reason for different selectivity, since the modified coverage is high and similar in all the solvents. The implication from this analysis is that from the standpoint of balancing the activity and the selectivity, the catalyst should be carefully modified, since the high percentage and rather low TOF of modified sites will result in a dramatic decrease in the overall reaction rate. It is interesting to note that this is different than the enantioselective C=O hydrogenation of a-ketoesters (and related compounds) over cinchonidine-modified Pt catalysts [55]. In that system, a ligand acceleration effect causes the enantioselective rates to be enhanced by at least an order of magnitude over racemic rates. Regardless of the validity of the assumptions made in the present analysis, it is apparent that such a ligand acceleration effect is not occurring in the present case of enantioselective C=C bond hydrogenation.

3.3.4 ACTIVATION ENERGY

The activation energy was calculated by using the Arrhenius equation $lnk_{app} = lnA - \frac{E_a}{RT}$, where k_{app} is the apparent rate constant for the reaction, A is pre-exponential factor, Ea is the activation energy for the reaction, R is the ideal gas constant in joules per mole kelvin, T is the temperature in kelvins. Plotting ln(k) versus 1/T yields –Ea/R as slope. Experiments were carried out in isopropanol at 298, 306, and 313K, with results shown in Figure 3.4 For the racemic reaction (solid circles), E_a = 44 ± 20 kJ/mol = 10.5 ± 4.7 kcal/mol while for the modified reaction, E_a = 45 ± 10 kJ/mol = 10.8 ± 2.4 kcal/mol. The activation energy for the racemic and modified reactions are similar to each other, likely because of the relatively fast reaction rate on unmodified compared to

modified sites, as described above (cf. Table 3.1). In isopropanol, the TOF for unmodified sites is 130 times faster than modified sites, so k_{app} for modified reaction is almost the same as for the unmodified reaction.

3.3.5 PRODUCT EFFECT ON REACTION RATE

Product desorption has been determined to be the rate determining step in several enantioselective hydrogenations [13, 21, 93, 94]. To test this possibility in the present case, two sets of experiments were carried out for the racemic reactions. First, the initial rate was probed with varying amounts of product injected into liquid mixture prior to the start of the hydrogenation, with other reaction conditions kept constant. For reactions with 0.1M MCA, 0.1M MCA + 0.1M MHA, and 0.1MMCA + 0.2 MMHA, the initial rates of reaction are similar (185 ± 25, 186, ± 25 and 194 ± 25 mmol/h/gcat, respectively). This result suggests that the presence of product has no significant effect on reaction rate. In the second set of experiments, the effect off adding reactant over a long reaction time was examined. The reaction was run with 0.1M MCA at the beginning, and then a certain amount of MCA was added every 40 mins. The overall reaction rate constants in these three periods decreased only slightly as shown in Figure 3.5 Overall, these results show the product has essentially no effect on activity for this reaction, suggesting that its possible adsorption on the catalyst surface does not compete effectively for active sites.

3.4 CONCLUSIONS

The kinetics of C=C bond hydrogenation in α-methylcinnamic acid over Pd/Al_2O_3 catalyst with and without cinchonidine modifier was carried out in a semi-batch reactor. The hydrogenation reaction exhibits a strong solvent-dependent behavior, with

isopropanol showing the best activity performance likely due to its strong polarity and protic nature. Regardless of the absence or presence of modifier, the reaction rate is independent on H_2 pressure and first order in the acid substrate. The TOF on unmodified sites are much faster than modified ones, which results in the low enantioselectivity. Apparent activation energies for reaction with and without modified are similar. Finally, the product has no effect on the reaction rates or enantioselectivity, suggesting that substrate adsorption and activation may be the rate determining step.

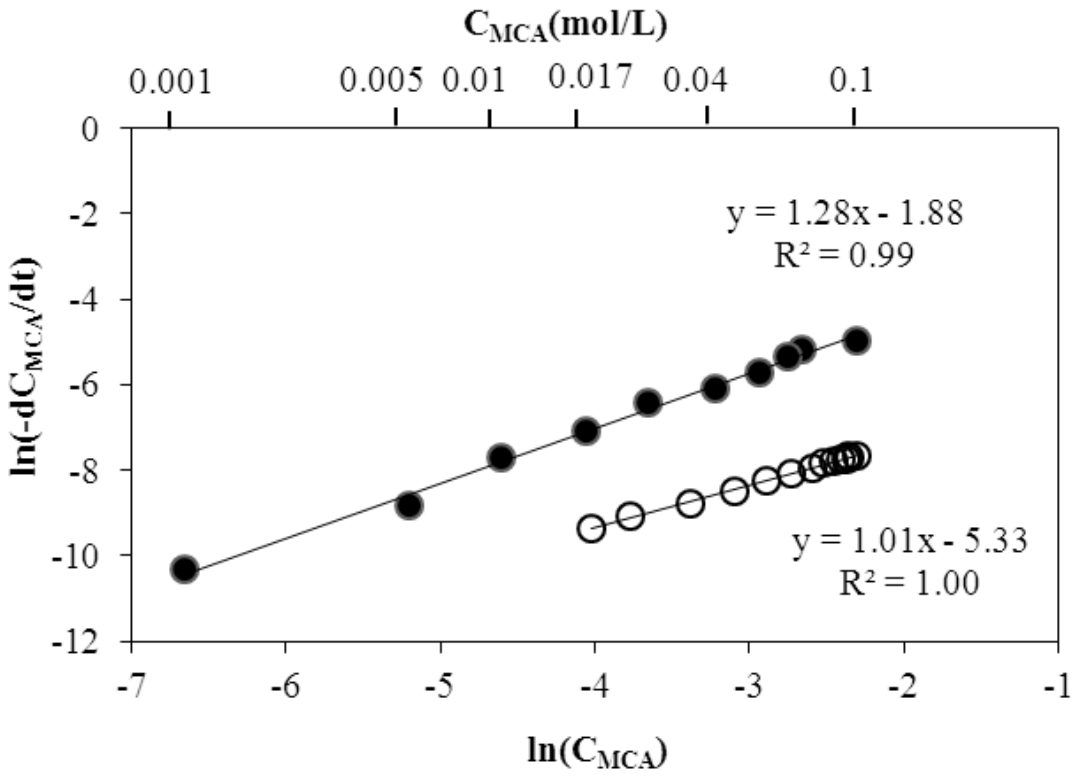

Figure 3.1 Reaction orders with respect to substrate in absence (solid circles) and presence (open circles) of modifier.

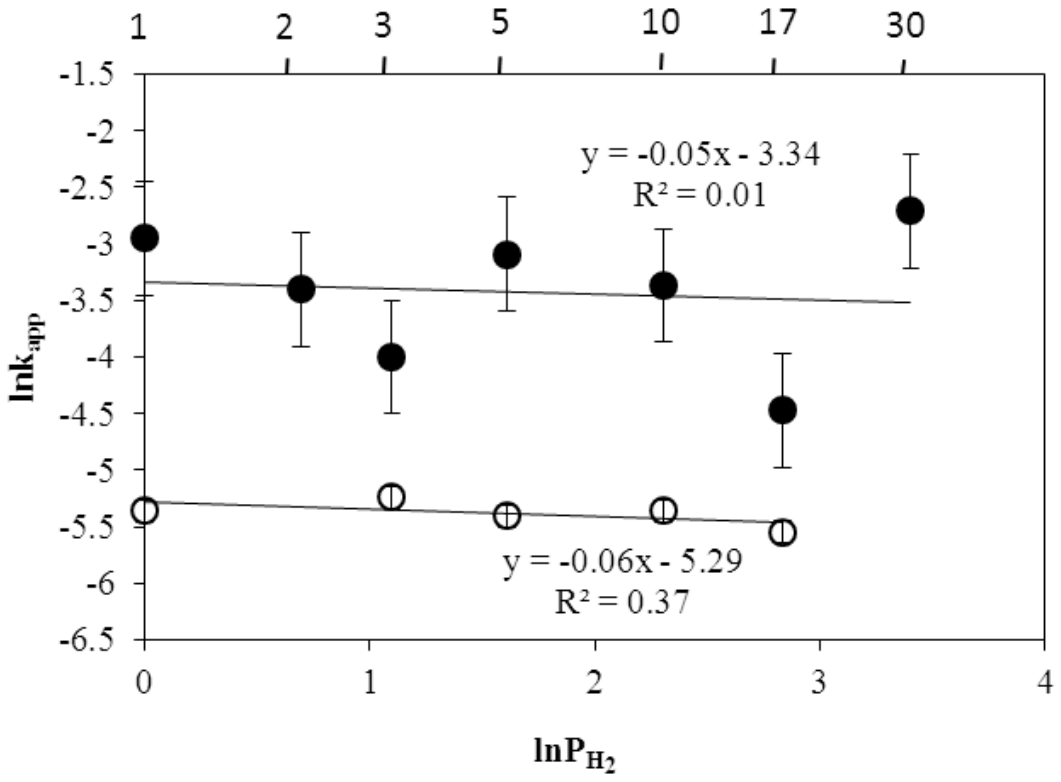

Figure 3.2 Reaction orders with respect to hydrogen in absence (solid circles) and presence (open circles) of modifier.

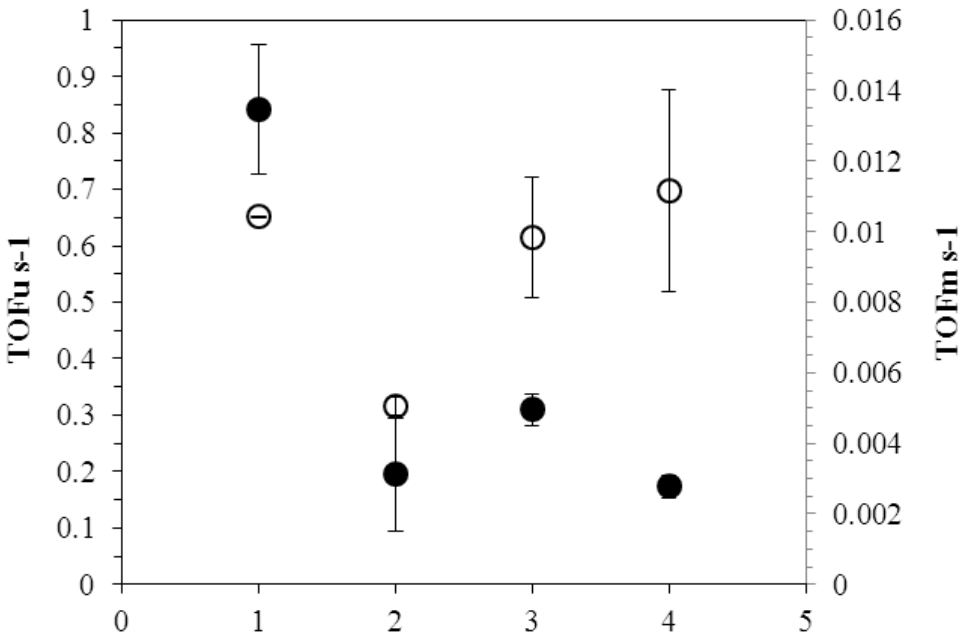

Figure 3.3 TOF for unmodified sites (solid circles) and modified sites (open circles). 1). Isopropanol 2). Dioxane 3). Dioxane+DI water 4). N, N-dimethylformamide (DMF).

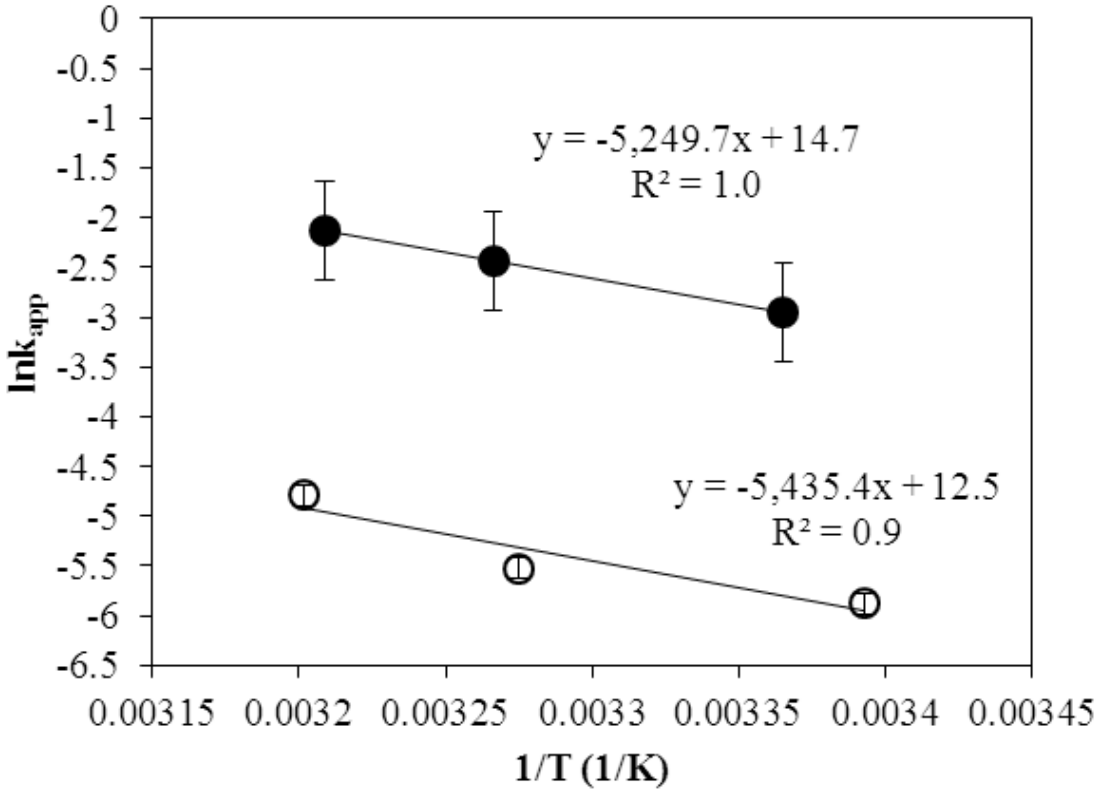

Figure 3.4 Activation energy in absence (solid circles) and presence (open circles) of modifier.

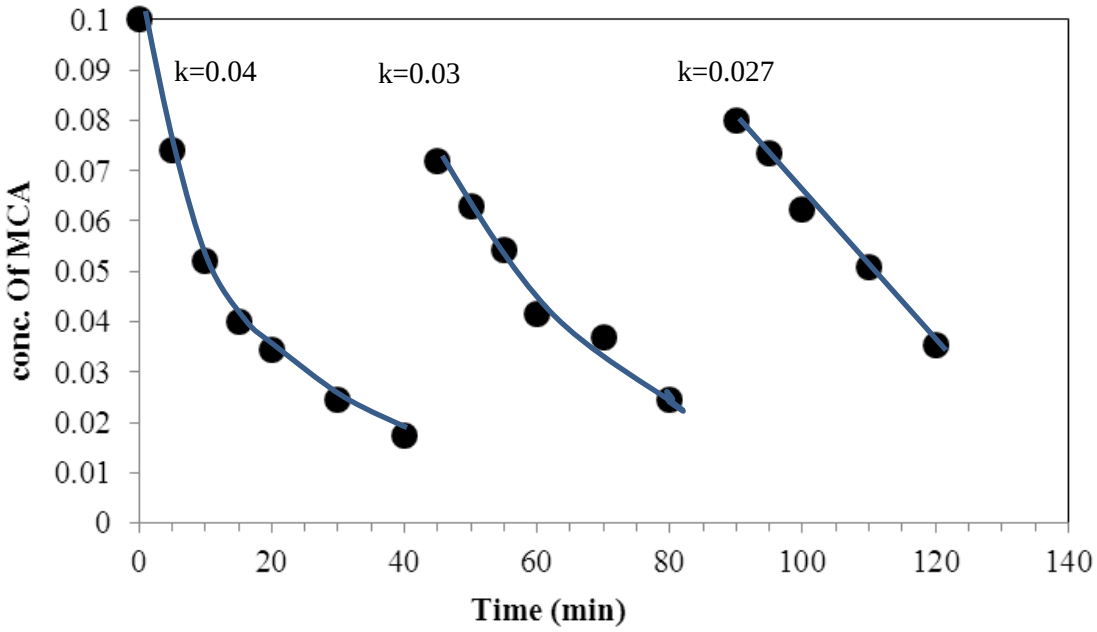

Figure 3.5 Effect of adding reactant during a long run. The lines are drawn to guide the eye.

Table 3.1 Summary of kinetic results of solvent effect

	Cinchonidine (mM)	order	Conversion (%)	r_{ini} (mmol/h/gcat)	ee (%)
Isoproponal	0	1	100*	185±25	0
Isoproponal	5	1	97	26.5±0.4	7.5±0.5
Dioxane	0	1	74	52±12	0
Dioxane	5	1	43	14±0.6	5.5±0.5
Dioxane+DI	0	1	99	68.6±5	0
Dioxane+DI	5	1	70	16.2±1.2	10.5±0.5
N,N-dimethylformamide	0	1	83	38.2±4	0
N,N-dimethylformamide	5	1	39	11±1.2	17±0.5
CH_2Cl_2	0	0	100	18.2	0
CH_2Cl_2	5	0	20	3	--

CHAPTER 4 IN-SITU ATR-IR INVESTIGATION OF HYDROGENATION OF MCA IN ISOPROPANOL

4.1 INTRODUCTION

Chirality is a property of three-dimensional asymmetry; enantiomers have the same molecular formula but different geometry arrangement, just like the mirror image of left and right hands. Though the structural difference is minor, it can give enantiomers very different function in human pharmacology and toxicology. The drug thalidomide is a very famous example: the (S)-enantiomer is a sedative effective against morning sickness, while the (R)-enantiomer causes birth defects. So the synthesis of enantiopure chemicals has been of great importance in the manufacture of pharmaceuticals, agrochemicals, and fragrances for decades, and draws more and more attention recently because patents are beginning to expire. For example, three of the four top-selling drugs from 2007 until 2010 – Lipitor (atorvastatin calcium), Plavix (clopidogrel bisulfate) and Nexium (esomeprazole magnesium) – were all single-enantiomer drugs [82], while Lipitor and Plavix lose patent protection in 2011 and 2012 [95]. Performance requirements and government regulations, as well as environmental concerns, all drive the move towards enantiopure chemicals. While homogeneous catalytic asymmetric catalysis continues to progress rapidly, intrinsic drawbacks exist such as difficult (and expensive) catalyst separation and catalyst instability. Such issues may help to explain

the relatively wide gap between R&D output from academics and industry versus commercial application [83]. In this respect, the eventual use of heterogeneous catalyst can offer several major advantages, including ease of catalyst separation, reduction of solvent usage, simplification of the synthetic route, and increased selectivity towards desired products. If optimized, these properties could result in significant economic and environmental benefits.

The first study of C=C hydrogenation was apparently published in 1985 for prochiral cinnamic acid hydrogenation over Pd/C catalysts [5]. Largely over the past decade, there have been a number of studies [6-51] that have followed up on this initial work. The groups of Nitta [6-20, 44, 45], Bartok [21-24, 48-51], and Baiker [25-38] have been the most active, and the majority of studies have explored hydrogenation of α, β-unsaturated C=C bonds adjacent to carboxylic acid groups with cinchonidine as the chiral modifier. It has been suggested that cinchonidine (CD) and reactant acids form a $CD(acid)_2$ complex during the enantioselective hydrogenation [32]. In addition, aromatic acids favor polar solvents, as opposed to aliphatic acids that prefer non-polar environments. These (and other) studies of the cinchonidine-modified metal catalytic system have largely involved kinetics studies, as opposed to probing the surface molecular environment. In addition, the in-situ vibrational spectroscopic studies available have focused almost entirely on the cinchona alkaloid modifier interaction with the catalyst surface under different conditions [21, 25, 26, 64, 73, 74, 76, 77].

This chapter reports an in-situ attenuated total reflection infrared spectroscopic study of the hydrogenation of α-methylcinnamic acid over a 5wt% Pd/Al_2O_3 catalyst in isopropanol. This molecule consists of a prochiral C=C bond located between COOH and

phenyl groups [81], and is a good model compound for the study of C=C hydrogenation in aryl substituted substrates. The solvent was chosen for comparison with our previous spectroscopic study in dichloromethane [81], and based on recent batch kinetic investigations of solvent effects on the hydrogenation of this molecule (Chapter 2). Overall, the conversion and enantioselectivity of this molecule is relatively low over cinchonidine-modified catalysts [16, 17]. It is the aim of this chapter to begin to elucidate the surface molecular properties that may influence this behavior.

4.2 EXPERIMENTAL SECTION

4.2.1 MATERIALS

The substrate α-methylcinnamic acid (MCA, 99%) and product α-methylhydrocinnamic acid (MHA, 98%) were obtained from Aldrich and used without further purification. Isopropanol (99+%) was obtained from Alfa Aesar and cinchonidine was obtained from TCI America. The gas used for the experiments was ultrahigh purity hydrogen from National Welders Supply. 5wt% Pd/Al_2O_3 was obtained from Alfa Aesar with 14% dispersion as measured by O_2-H_2 chemisorption methodology [99].

4.2.2. ATR-IR SPECTROSCOPY

An FTIR spectrometer (Nicolet 670) equipped with an ATR-IR accessory (SpectraTech) was used for these studies, as reported previously [81, 87, 88]. In the accessory there are two mirrors that allow the horizontal infrared light to be reflected vertically into the ATR-IR cell. Two holes in the bottom of the cell are designed to let the infrared light enter the ZnSe element sealed within the cell. A 60° zinc selenide (ZnSe) crystal (Spectra Tech) was selected for use as the ATR element upon which the catalyst film is deposited. The film was coated onto the ATR element using a suspension of 20

mg catalyst in 20 ml DI water. This mixture had been first placed in an ultrasonic bath overnight in order to obtain a uniform suspension. A thin layer of this suspension was spread into the ATR element and dried under a lamp. This procedure was repeated four times, giving an average film thickness of 10±2μm, as found using optical microscopy (Olympus BX50 microscope and Simple PCI image analysis software by Compix).

The liquid solutions are kept in glass flasks (i.e., reservoirs) with magnetic stirring. Two separate reservoirs were used during the experiment without mixing between acid solutions and pure solvent (isopropanol). Gas can be bubbled into the solution for hydrogenation experiments using an H_2 line attached to porous glass frit capped tube submerged in the reservoir. Pumps recycle the solution from the reservoirs, through the flow cell and back during the experiment. The flow path was altered by three-way valves that were automated and controlled using Labview (National Instruments). All experiments were carried out at room temperature and atmospheric pressure.

For the ATR experiments, pure solvent was flowed overnight (at least 12 hours) to ensure system stability. For each experiment, at time zero, a spectral background was acquired and utilized for all subsequent spectra acquired. Spectra were acquired continuously every ca 2 mins during the experiment with 128 scans per spectrum using a resolution of 4 cm^{-1}. The exact protocols involving the alternating flow of liquids with or without saturation of hydrogen are described in each relevant section below.

Vibrational assignments were assisted using spectral curve fitting to deconvolute overlapping peaks. Specific band assignments were aided by density functional theory (DFT) calculations on a single molecule in vacuum using Gaussian 03W, Revision

B.02[89] with the Becke three-parameter-Lee-Yang-Parr (B3LYP) method and the 6-31G(d) basis set. The results were corrected by scaling factor 0.97 [81].

4.3 RESULTS AND DISCUSSION

4.3.1 REACTANT ACID ADSORPTION

Before the study of hydrogenation, it is important to understand the adsorption behavior of this reactant (α-methylcinnamic acid) on the γ-Al_2O_3 support and Pd/Al_2O_3 catalyst. Pure solvent was flowed through the flow cell overnight prior to taking the background. Pure solvent was continued for 1 hour, followed by 2mM MCA in isopropanol for one hour. Then the cycle is repeated, with solvent followed by acid solution, but for 16mM acid and 8mM acid, ending with a final solvent flush. Prior to this, the ATR-IR spectra of the acid solution in contact with the bare ZnSe element were examined. The first plot in Figure 4.1A shows typical spectra taken from acid solution in contact with the bare element as a function of the concentration profile described before. The seven spectra shown from the bottom to the top were the spectra taken at the end of each indicated experimental step. A prominent peak was observed at 1693 cm^{-1}, which based on the literature [25] is associated with an acid dimer species. The small peak at 1566 cm^{-1} is assigned to the ring vibration, while peaks at 1458 cm^{-1} and 1395 cm^{-1} correspond to methyl group vibrations. Usually, the monomer acid is favored in very dilute solution in non-polar solvents, or in the vapor phase. There is almost no monomer peak observed in this polar solvent (isopropanol) in this concentration. Most important from the standpoint of the adsorption and hydrogenation studies, these liquid phase peaks disappear completely upon switching to pure solvent; this confirms that there is no strong adsorption on the ZnSe surface.

Figure 4.1B shows ATR-IR spectra obtained in the same fashion, but for an Al_2O_3 film. As can be seen, the peak intensities are increased and there are peaks remaining after removal of liquid-phase acid, suggesting that acid is adsorbed on the alumina. The peak associated with dimer C=O remains the same as for the liquid phase and decreases significantly when switching to pure solvent. In addition, there is a prominent peak at around 1640 cm^{-1}, which is assigned to C=C stretching [25]. Peaks around 1350 cm^{-1} to 1500 cm^{-1} were mainly associated with C-H bending vibrations of the methyl group, while the features from 1500 to 1600 cm^{-1} arise from ring stretching vibrations. All of these assignments are shown in Table 4.1, and were made based on comparisons with characteristic frequency tables and the DFT calculation results. Figure 4.2A shows that similar spectra were observed for the same experiment performed on the 5wt% Pd/Al_2O_3 sample. It is notable that the peaks are clearly increased compared to Al_2O_3 alone.

The spectra during adsorption experiments are complex and contain many overlapping peaks from a variety of sources, especially at the highest acid concentration of 0.016M. To distinguish more clearly the peaks arising from bulk liquid and adsorbed species, the spectra were deconvoluted using least squared regression analysis described before [81]. All the fitted spectra shown in the right plots in Figures 4.1 and 4.2 were those taken for the highest concentration acid (16mM) flowing through the cell. In these spectra, the red peaks are those arising from liquid-phase acid, blue are those coming from adsorbed acid on alumina and green are those observed on the Pd metal. The same fitting was applied to 22 spectra selected, with 3 to 4 spectra per step. Figure 4.2B shows a typical time-dependent infrared signal for adsorbed MCA on Pd from peak solving for the peak at 1377 cm^{-1}. It shows a response correlates strongly with the presence of acid in

solution. However, in contrast to the square-like profile for the liquid MCA signal, the progression of the surface signal suggests an adsorption and desorption process over the course of the experiment. The peaks at 1547cm^{-1} , 1334 cm^{-1}, 1450 cm^{-1}, 1492 cm^{-1}, 1599 cm^{-1}, 1642 cm^{-1} and 1405 cm^{-1} follow almost the same trend with 1377cm^{-1}, This suggests that these peaks likely come from the same species, which in this case is the surfaced adsorbed MCA.

Based on this curve fitting, and vibrational frequencies calculated by DFT, peak assignments have been made and are summarized in Table 4.1. Of particular interest are the peaks at ~1547cm^{-1} and ~1377cm^{-1}, which are confidently assigned as asymmetric and symmetric COO^- vibrations based on the available literature [81, 91, 92] and comparison between adsorbed spectra and solid phase MCA (shown in Figure 4.2C). The presence of these peaks shows that the reactant acid is dissociatively adsorbed on both the alumina and Pd surfaces. It is well known that different binding structures of carboxylates can be assigned based on the difference between asymmetric and symmetric COO^- vibration peaks. For example, a difference between 350 cm^{-1} to 500 cm^{-1} indicates a unidentate mode, 150-180 cm^{-1} indicates a bridging bidentate mode, and 60-100 cm^{-1} indicates a chelating bidentate. Thus, the bidentate bridging configuration is apparently favored under the conditions examined here. Overall, considering the C=O stretching bands in these curve fitted plots, only dimer acid species exist in the bulk liquid phase and the intensity of this feature is very similar on alumina and Pd surface. In addition, there is only a very weak C=O peak left after solvent flush. Thus, these spectra reveal that the acid is predominantly dissociatively adsorbed on alumina and Pd under these conditions, with only a very small coverage of molecularly adsorbed species.

A similar set of MCA adsorption experiments was previously carried out in dichloromethane (Fig. 4.3A) and in 1, 4-dioxane (Fig. 4.3B). Table 4.2 shows the comparison of carboxylate peaks and C=O stretching peak intensity in these three solvents based on curve fitting. The intensity of carboxylate peaks decrease in the order of Isopropanol>Dioxane>Dichloromethane, and it is the same with the order of hydrogenation activity (Chapter 3). It suggests that the MCA dissociative adsorption may be the rate-determining step or that the adsorbed carboxylate is an important intermediate.

4.3.2 PRODUCT ADSORPTION AND PRODUCT-REACTANT COADSORPTION

Before studying hydrogenation of MCA, the product α-methylhydrocinnamic acid (MHA) adsorption on Pd/Al_2O_3 was explored. In this experiment, solvent was flowed first for one hour, followed by 16mM MHA for one hour, and then switching to solvent flushing for one hour. As shown in Figure 4.4, several clear peaks show up at around 1700, 1600, 1550, 1500, 1450 and 1250cm^{-1}. Negative peaks around 1380 and 1130cm^{-1} are solvent peaks. By DFT calculation and comparison between adsorbed MHA and solid phase MHA spectra (Fig 4.4 iv), peaks around 1550cm^{-1} and 1250cm^{-1} can be assigned to carboxylate peaks. From the difference between asymmetric and symmetric COO^- vibration peaks, it is almost in the range of unidentate mode. In addition, the C=O stretching band at around 1700 cm^{-1} maintains a constant intensity after solvent flushing which is not available for both bridging bidentate and chelating bidentate mode. Molecularly adsorbed species may have C=O stretching but molecularly adsorbed species are usually weakly adsorbed, so solvent flushing will decrease the intensity of C=O

stretching. These features all suggest the unidentate configuration is apparently favored for MHA under the conditions examined.

The intensity after the final flush of solvent decreases little compared to in the presence of MHA solution, suggesting that the product adsorbs strongly on surface. It is therefore interesting to study the MCA and MHA coadsorption in sequence to compare the adsorption strengths of the reactant and product. Figure 4.5A shows the result when MCA is introduced first to the surface, followed by exposure to MHA. Figure 4.5B shows the results from the reverse order experiment. The main difference in the vibrational spectra between MHA and MCA is C=C stretching around 1640cm^{-1} present only in the latter. Comparing the last spectra in both cases, the C=C stretching band is almost decreased half that compared to MCA adsorption. This suggests the adsorption strength for MCA and MHA are similar, which is consistent with kinetic results published before.

4.3.3 RACEMIC HYDROGENATION

After examining the adsorption of MCA and MHA on Pd/Al_2O_3, studies of α-methylcinnamic acid hydrogenation were performed. Based on the literature [10, 12, and 15] and our previous kinetic study (Chapter 3), this hydrogenation can be carried out effectively at room temperature and atmospheric hydrogen pressure. For hydrogenation of liquid phase MCA, after spectra were acquired in pure solvent for two hours, the flow was switched to 0.016M acid solution. Then, after taking the first spectrum of MCA, hydrogen was bubbled into acid solution for two hours. Figure 4.6A shows typical spectra for hydrogenation of 0.016 M MCA on 5wt% Pd/Al_2O_3. Two spectra of MHA adsorption are included in Figure 4.6B for comparison. The decrease of the 1640 cm^{-1}

peak is a direct indication of C=C hydrogenation. The 1370 cm^{-1} band is the symmetric carboxylate peak of MCA, but in MHA this carboxylic peak shifts to 1250 cm^{-1}. The MHA asymmetric carboxylic peak is at 1550 cm^{-1}, which is a 5 cm^{-1} blue shift compared to MCA (1545 cm^{-1}). The C=O stretching band for MHA is at 1700 cm^{-1}, which is blue shifted 7 cm^{-1} compared to MCA (1693 cm^{-1}). Comparing the last spectrum for hydrogenation and MHA adsorption, it is clear that MCA was hydrogenated and that this hydrogenation can be detected by ATR-IR. When hydrogen began to bubble into the acid solution, a very significant decrease of peaks at 1370 cm^{-1} and 1640 cm^{-1} was observed and the peak at 1250 cm^{-1} increased. Based on comparison with the spectrum obtained during product adsorption, these phenomena all arise from the difference between adsorbed reactant and product.

To better understand the hydrogenation of adsorbed reactant on surface, another hydrogenation experiment was carried out. For hydrogenation of surface adsorbed MCA on both catalyst and alumina, pure solvent was first flowed through cell for one hour after background was taken, and then switched to 16mM MCA solution for one hour, followed by pure solvent for one hour. This step eliminated liquid phase MCA from the flow cell, leaving only strongly adsorbed species mostly in the form of bridging adsorbed carboxylate. After this, the pure solvent was saturated with hydrogen and the spectra were followed in real time. Figure 4.7 clearly shows that the 1640 cm^{-1} C=C band is disappearing and peak at around 1370 cm^{-1} decreases, while the 1250 cm^{-1} band increases. These observations all suggest that the surface adsorbed reactant is hydrogenated. In this case, it suggests that the bridging adsorbed MCA is reactive.

It was expected that there would be no activity for hydrogenation of adsorbed MCA on the alumina support. Indeed, Figure 4.8A supports this supposition, since the spectrum taken in the presence of H_2-saturated solvent is essentially identical to that obtained in H_2-free solution. There are also often problems regarding whether the benzene ring in MHA can be hydrogenated or not, and whether features seen in adsorbed MCA hydrogenation are coming from hydrogen replacing MCA or not. To answer these two problems, the hydrogenation of surface adsorbed MHA was performed. Figure 4.8B compares the spectrum taken after H_2-rich solvent flow and H_2-free solvent, revealing that the spectra are identical. This suggests benzene ring is not hydrogenated and that the hydrogen replacement (at least of the product) is not a problem to consider under this condition. This is also consistent with the reaction kinetic studies presented in Chapter 3.

4.3.4. CINCHONIDINE ADSORPTION AND CINCHONIDINE-REACTANT INTERACTION

Two sets of experiments were carried out to explore cinchonidine adsorption on Pd in dichloromethane and isopropanol, with results shown in Figure 4.9. Since cinchonidine adsorption was studied before in dichloromethane [98], the experiment here with dichloromethane was for comparison. Compared to ATR-IR studies of cinchonidine adsorption on Pd published by Baiker [98], the spectra are essentially identical. The peaks at around 1450 cm^{-1}, 1500 cm^{-1} and 1600 cm^{-1} suggests that cinchonidine adsorbed in two ways on the catalyst 1) parallel through π-bonding between the quinolone moiety and the metal and 2) with the quinolone ring tilted with respect to the surface. Comparing cinchonidine adsorption in isopropanol with dichloromethane, no clear peaks show up at low concentration (i.e., 5mM). However, by 50mM the spectra are identical to cinchonidine adsorption in dichloromethane. Therefore the only significant difference

between cinchonidine adsorption in dichloromethane and isopropanol is the appearance of adsorbed species at lower concentrations in the former. This phenomenon may be due to the very different solubility of cinchonidine in these two solvents [97] which is reported to be 12 g/L for dichloromethane and 25g/L for isopropanol. The solubility for cinchonidine in isopropanol is 2 times larger than it is in dichloromethane, so there is more driving force for cinchonidine to be adsorbed in dichloromethane as opposed to isopropanol.

The cinchonidine-reactant interaction was tested on bare element, Al_2O_3 and Pd/Al_2O_3 with three ratios (CD: MCA: 1:20; 1:2; 1:1). After solvent (isopropanol) flow, 0.1M MCA solution was flowed through the cell, followed by flushing with pure solvent. Cinchonidine (5mM, 50mM, 0.1M) was then added to the MCA solution gradually in three steps to reach each desired ratio, followed by a final, solvent flush. Each step takes one hour. The results of these experiments are shown in Figures 4.10A, 4.10B, and 4.10C. The 1:20 ratio is the one that has been used in previous kinetic studies in the literature [22][25][26], As discussed in Chapter 1, it has been proposed that on cinchonidine-modified Pd, alkenoic acids form dimers or monomers that hydrogen bond with the modifier quinuclidine group. The quinuclidine nitrogen is then protonated and hydrogen bonds to OH group of acid and the OH group of cinchonidine is hydrogen bonded to C=O group of acid. Similar to MCA adsorption, there are only C=C and C=O stretching bands observed over the bare element, while the peak intensities increase dramatically on the Al_2O_3 and Pd/Al_2O_3 surfaces. Figure 4.10D calculated spectra obtained by subtracting the bare element spectra of liquid phase MCA from the bare element spectra of the liquid phase CD+MCA. These calculated spectra are compared to

spectra obtained for CD in solution over the bare element. Peaks at around 1450 cm^{-1}, 1500 cm^{-1} and 1600 cm^{-1} are from CD adsorption. However, the new broad peak at around 1550 cm^{-1} suggests the formation of $CD(acid)_x$ complexes. For example, $CD(acid)_1$ interaction has been observed at 1559 cm^{-1} while a $CD(acid)_2$ interaction has been observed at 1540 cm^{-1} [25]. Thus, the peak at 1550 cm^{-1} is the combination of these two peaks. In the 1:1 liquid phase ratio, this combined peak blue shifts, suggesting there is a more $CD(acid)_1$ interaction occurring at this ratio compared to 1:2 solution ratio. Figure 4.10E is the spectra of CD+MCA on Pd/Al_2O_3 (Figure 4.10C) with 0.7 times the spectra of CD+MCA on bare element (Figure 4.10A) at the same CD: MCA ratio. The ratio 0.7 comes from the difference of C=O stretching for spectra of MCA on the Pd/Al_2O_3 and on bare element. As described before in the section of MCA adsorption, the C=O stretching peak mostly arises from liquid phase MCA. So the residual spectra are the peaks from species adsorbed on the surface. The 1:20, 1:2, and 1:1 ratio spectra after this mathematical manipulation are identical, with the 1600 cm^{-1} peak arising from MCA ring stretching, the 1573 cm^{-1} band coming from flat adsorbed CD, and again the 1550 cm^{-1} peak being the combined $CD(acid)_1$ and $CD(acid)_2$ interaction peaks. Compared to MCA spectra, addition of CD decreases the C=O stretching feature around 1690 cm^{-1} slightly and the peak at around 1573cm^{-1} increases. However, but all of these differences are small compared to the effect of adding CD in the liquid phase. This suggests $CD(acid)_x$ interaction is essentially the same on the surface as in the liquid phase. That may be the reason why the 1:20 ratio affords similar enantioselectivity as higher ratios [24].

4.3.5 CINCHONIDINE HYDROGENATION AND HYDROGENATION OF MCA ON CINCHONIDINE MODIFIED Pd/Al_2O_3

Cinchonidine (0.1M) hydrogenation was examined on Al_2O_3 and Pd/Al_2O_3 with ATR-IR, with results shown in Figure 4.11. The C=C band decreased on Pd/Al_2O_3 (Fig. 4.11A) while there was no change on Al_2O_3 (Fig. 4.11B). This suggests that the CD is hydrogenated on Pd/Al_2O_3 in the presence of H_2, suggesting that during the enantioselective reaction the real modifier is the hydrogenated cinchonidine (i.e., 10, 11-dihydrocinchonidine), which is consistent with previous studies [26]. Peaks related to CD adsorption at around 1450cm^{-1}, 1500cm^{-1} and 1600cm^{-1} did not change when C=C was hydrogenated, suggesting that the hydrogenated cinchonidine adsorbs the same way as cinchonidine.

Since kinetic studies in Chapter 3 were based on a CD: MCA ratio of 1:20, the same ratio was used for this ATR-IR study. Hydrogenation of surface adsorbed CD-MCA (16 mM MCA, 0.8 mM CD)/(0.1M MCA, 5mM CD) was performed on Pd/Al_2O_3 in the same fasion. Pure solvent was flowed through the cell followed by MCA+CD solution for 1 hour. This was then followed by solvent flush for 1h, and then hydrogen bubbling into the pure solvent for 1 hour. Results are shown in Figure 4.12. The C=C band decreases in 1 hour and the C=O band increases, similar with the observation during racemic reaction. The decrease of the 1640 cm^{-1} peak is a direct indication of C=C hydrogenation. The 1547 cm^{-1} feature of the asymmetric carboxylate peak in MCA is blue shifted and the 1370 cm^{-1} symmetric carboxylate peak decreases. Comparing the last spectrum for hydrogenation and MHA adsorption, it is clear that MCA was hydrogenated. This modified reaction of surface adsorbed MCA+CD finishes in 10 min

compared to 5 min for the racemic reaction of MCA, suggesting that the modified reaction is slower than racemic one, consistent with kinetics. The C=C peak intensity for adsorbed MCA under both conditions suggests saturation of the surface. The stronger carboxylate peak and small intensity of the C=C peak remaining after hydrogenation under the higher concentration likely results from the larger amount of MCA adsorbed on Al_2O_3 under this condition.

4.4 CONCLUSIONS

The kinetics of C=C bond hydrogenation in α-methylcinnamic acid over Pd/Al_2O_3 catalyst with and without cinchonidine modifier was carried out in a semi-batch reactor. The hydrogenation reaction exhibits a strong solvent-dependent behavior, with isopropanol showing the best activity performance likely due to its strong polarity and protic nature. Regardless of the absence or presence of modifier, the reaction rate is independent on H_2 pressure and first order in the acid substrate. The TOF on unmodified sites are much faster than modified ones, which results in the low enantioselectivity. Apparent activation energies for reaction with and without modified are similar. Finally, the product has no effect on the reaction rates or enantioselectivity, suggesting that substrate adsorption and activation may be the rate determining step.

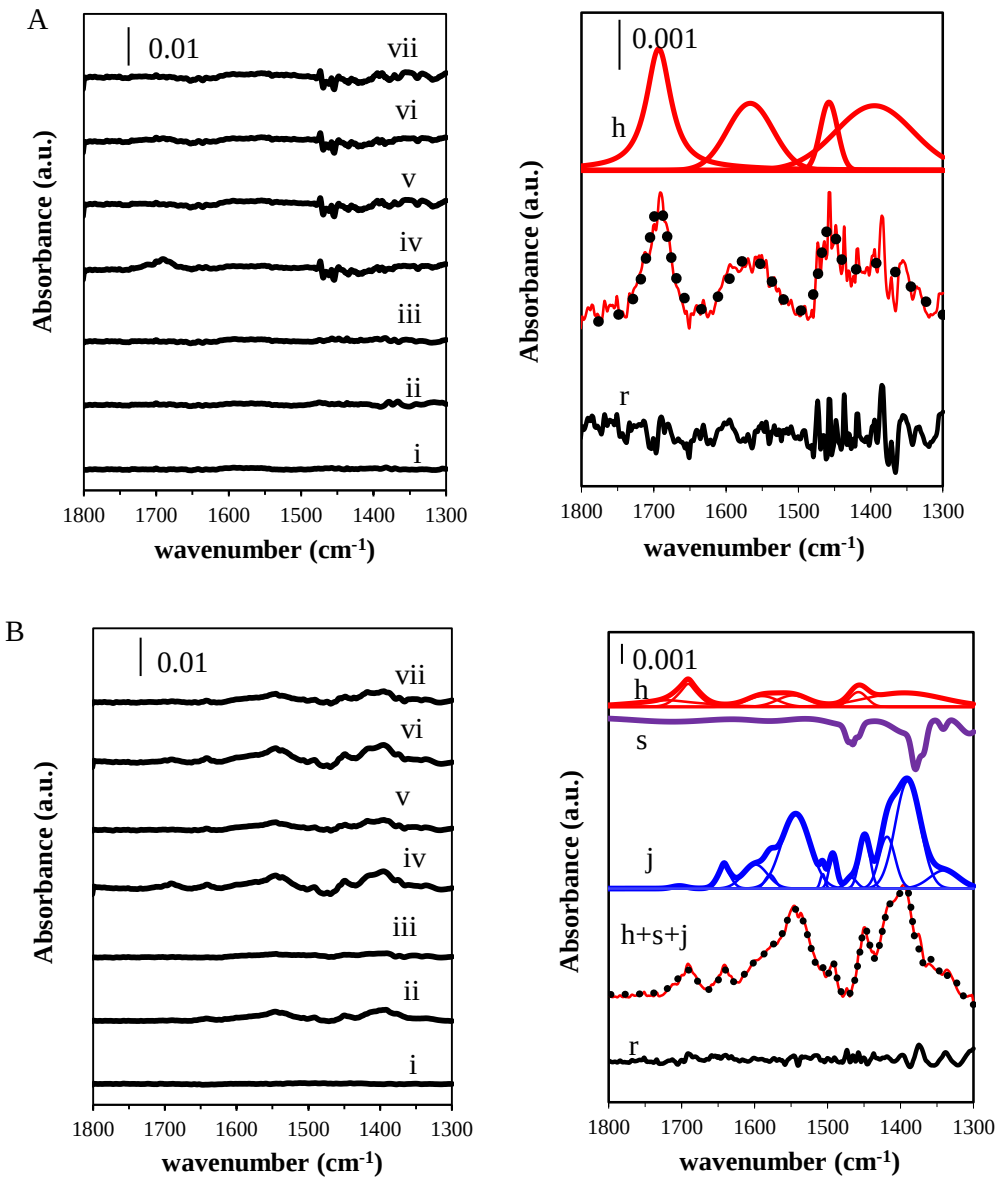

Figure 4.1 MCA adsorption and peak solving on A) bare element and B) alumina in isopropanol. The spectra were acquired in order after exposure to i) pure solvent, ii) 2 mM MCA, iii) pure solvent, iv) 16 mM MCA, v) pure solvent, vi) 8 mM MCA and vii) pure solvent. The plot on the right contains the following traces: (h) curve fitting for iv) in a), (s) solvent, (j) adsorption on alumina, and (r) residual from subtracting all curve fits (h+s+j) from the raw data. See text for details.

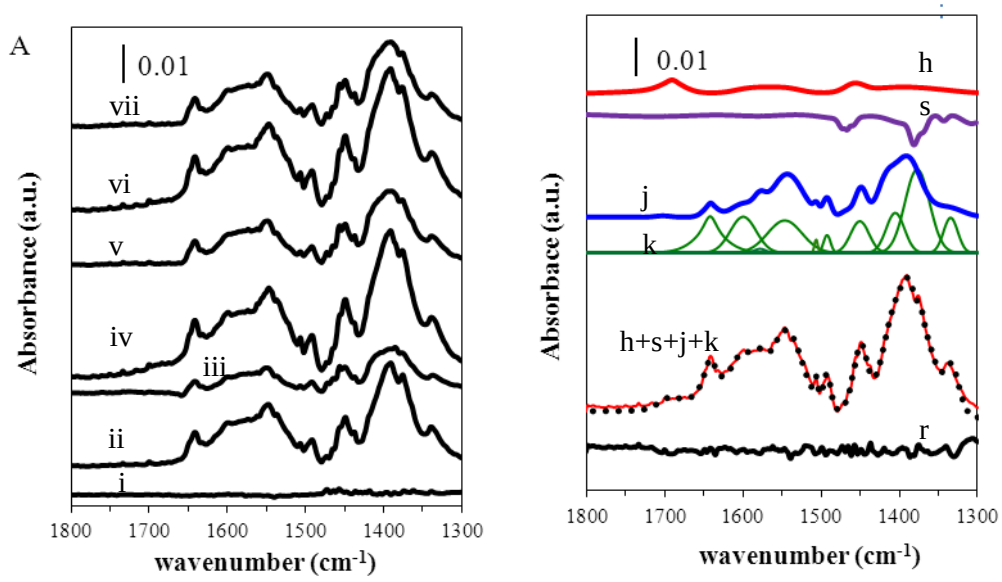
A
0.01
vii
vi
v
iv
iii
ii
i
Absorbance (a.u.)
1800 1700 1600 1500 1400 1300
wavenumber (cm-1)
0.01
h
s
j
k
h+s+j+k
r
Absorbace (a.u.)
1800 1700 1600 1500 1400 1300
wavenumber (cm-1)

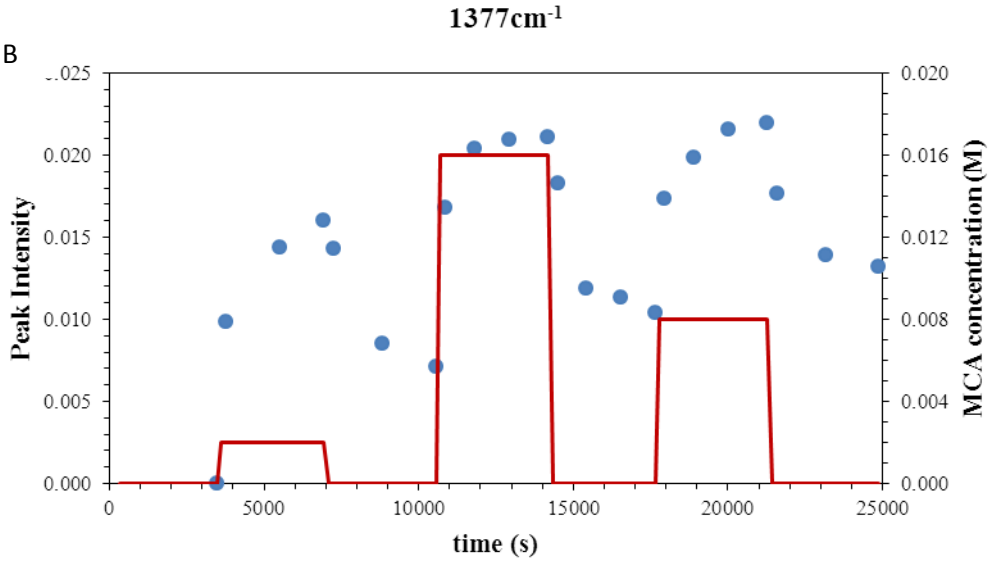
1377cm-1
B
.025
0.020
0.015
0.010
0.005
0.000
Peak Intensity
0.020
0.016
0.012
0.008
0.004
0.000
MCA concentration (M)
0 5000 10000 15000 20000 25000
time (s)

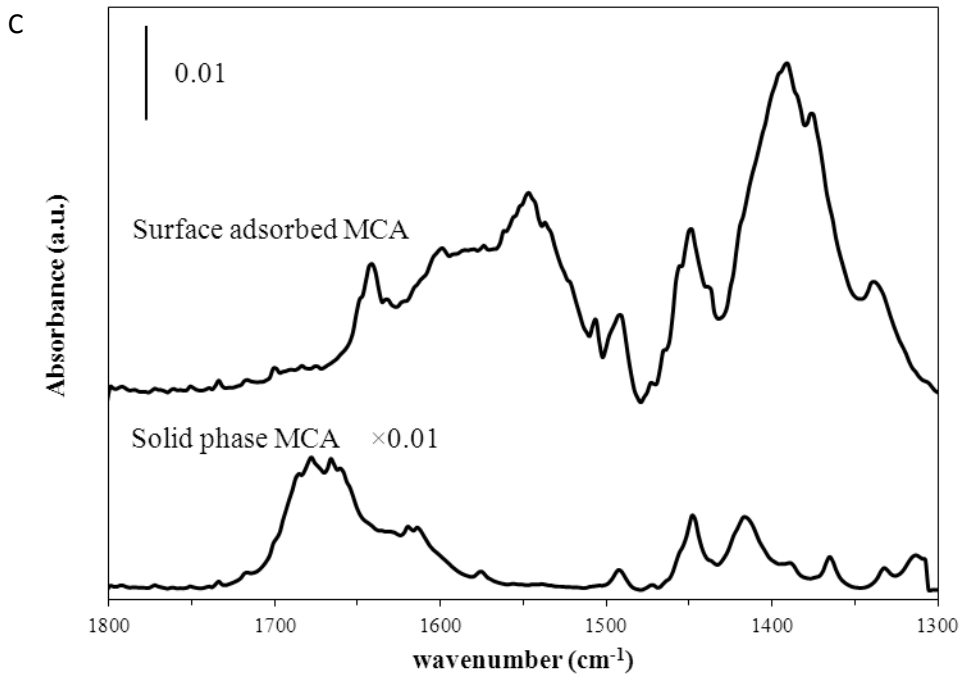

Figure 4.2 A) MCA adsorption on 5wt% Pd/Al_2O_3 and peak solving in isopropanol, The spectra were acquired in order after exposure to i) pure solvent, ii) 2 mM MCA, iii) pure solvent, iv) 16 mM MCA, v) pure solvent, vi) 8 mM MCA and vii) pure solvent. The plot on the right contains the following traces: (h) curve fitting for iv) in a), (s) solvent, (j) adsorption on alumina, (k) adsorption on Pd, and (r) residual from subtracting all curve fits (h+s+j+k) from the raw data. B) Time-dependent infrared signal of the 1377 cm^{-1} adsorbed MCA feature on Pd (dotted line) obtained from peak solving. The solid line is the liquid-phase MCA concentration profile over the same time period. C) Spectrum of surface adsorbed MCA compared with the spectrum of solid phase MCA. See text for details.

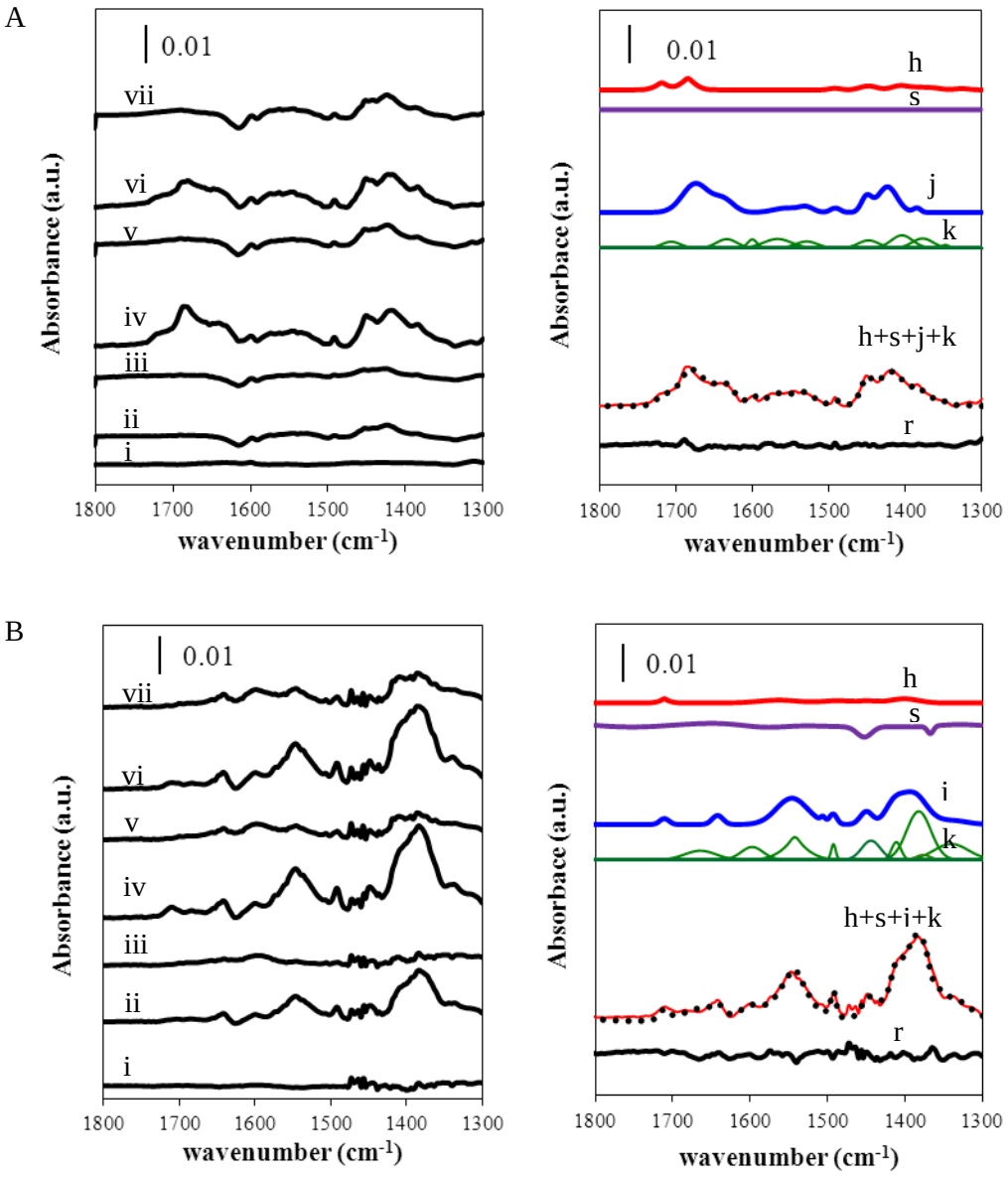

Figure 4.3 MCA adsorption on 5wt% Pd/Al_2O_3 and peak solving in A) dichloromethane and B) dioxane. The spectra were acquired in order after exposure to i) pure solvent, ii) 2 mM MCA, iii) pure solvent, iv) 16 mM MCA, v) pure solvent, vi) 8 mM MCA and vii) pure solvent. The plot on the right contains the following traces: (h) curve fitting for iv) in a), (s) solvent, (j) adsorption on alumina, (k) adsorption on Pd, and (r) residual from subtracting all curve fits (h+s+j+k) from the raw data.

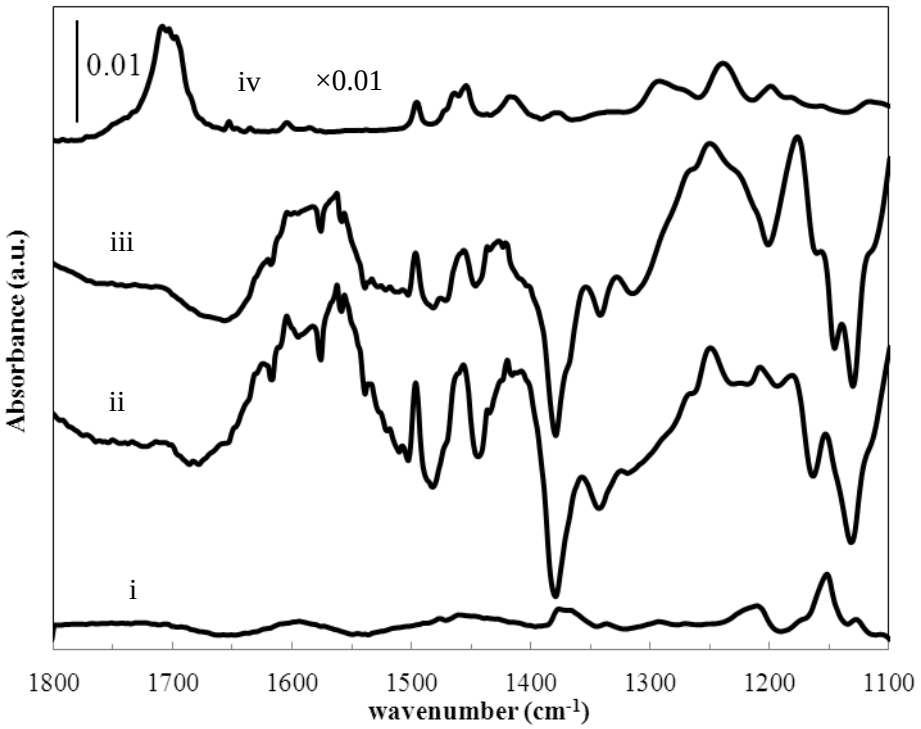

Figure 4.4 MHA adsorption on Pd/Al_2O_3 in isopropanol. The spectra were acquired in order after exposure to i) pure solvent, ii) 16 mM MHA, iii) pure solvent. See text for details. iv) Spectrum of solid phase MHA with absorbance multiplied by a factor of 0.01.

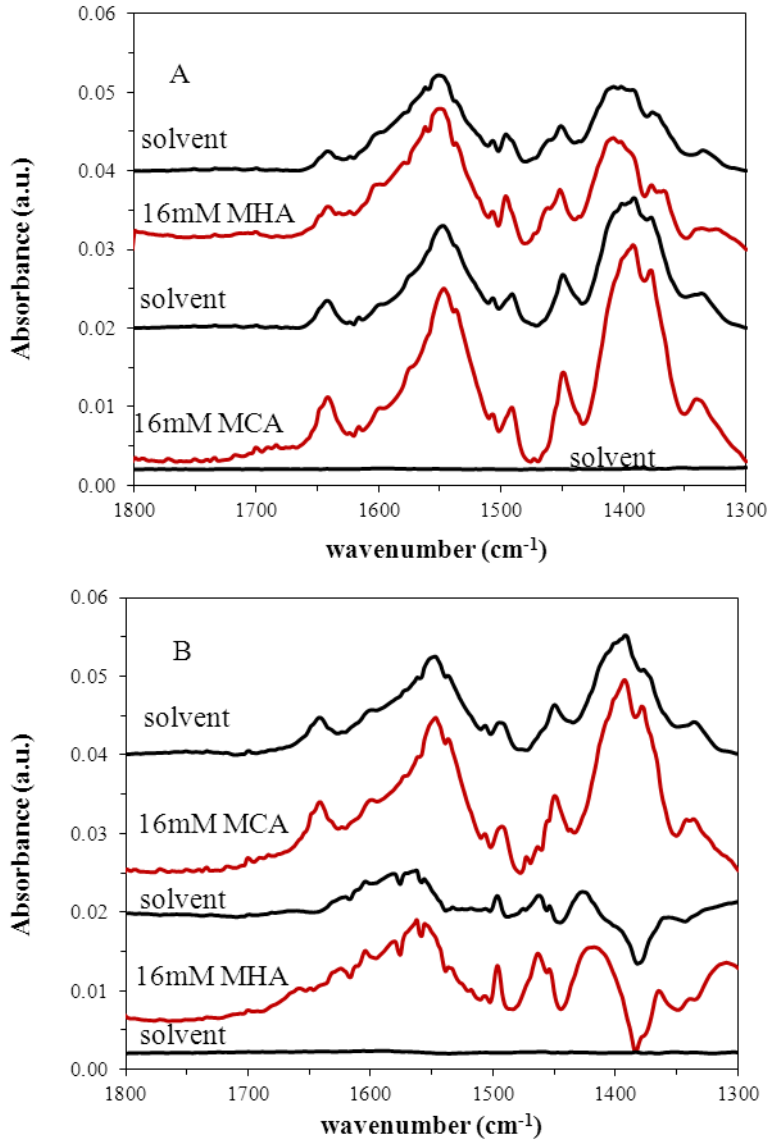

Figure 4.5 MCA and MHA coadsorption in isopropanol. A) MCA then MHA, B) MHA then MCA.

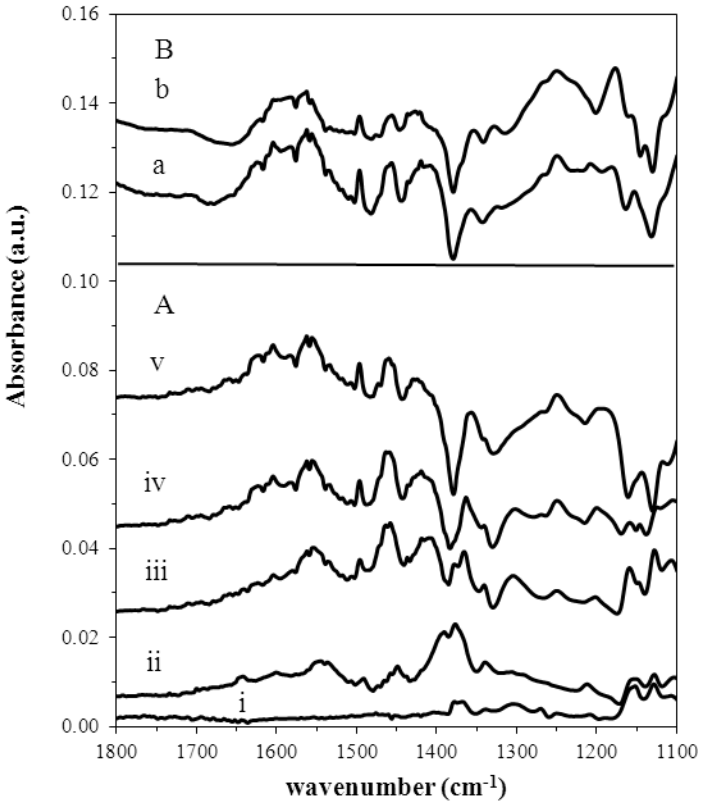

Figure 4.6 MCA hydrogenation on 5wt% Pd/Al_2O_3 in isopropanol. A) i) solvent (isopropanol). ii) 16mM MCA solution in isopropanol. iii) H_2 bubbled into 16mM MCA solution for 8 mins. iv) H_2 bubbled into 16mM MCA solution for 1 hour. v) H_2 bubbled into 16mM MCA solution for 2 hours. B) MHA adsorption on 5wt% Pd/Al_2O_3 in isopropanol. a) 16mM MHA in isopropanol for 1 hour. b) solvent (isopropanol) flush after acid solution.

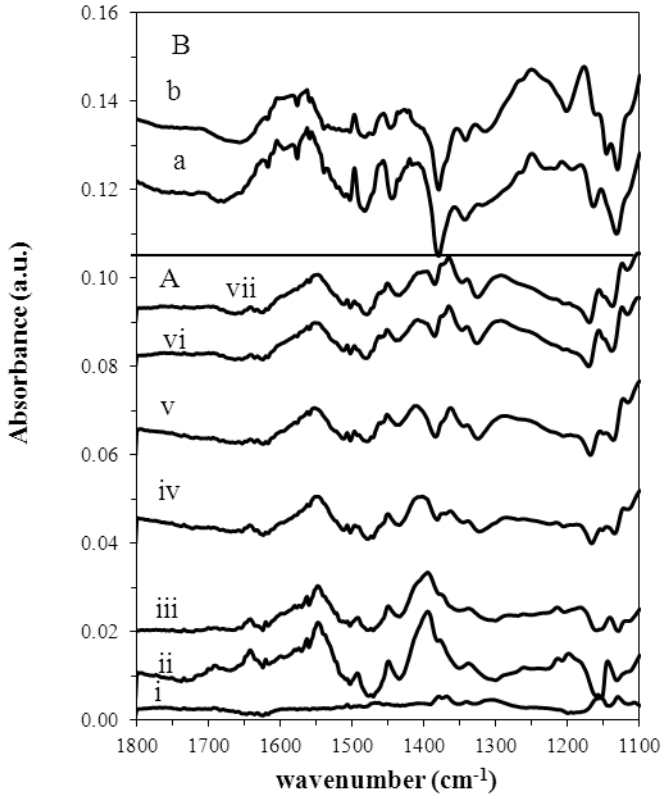

Figure 4.7 MCA hydrogenation on 5wt% Pd/Al_2O_3 in isopropanol. A) i) solvent (isopropanol). ii) 16mM MCA solution in isopropanol. iii) solvent flush for 1 hour. iv) first spectra after H_2 bubbled into solvent. v) H_2 bubbled into solvent for 5 mins. vi) H_2 bubbled into solvent for 1 hour. vii) H_2 bubbled into solvent for 2 hours. B) MHA adsorption on 5wt% Pd/Al_2O_3 in isopropanol. a) 16mM MHA in isopropanol for 1 hour. b) solvent (isopropanol) flush after acid solution.

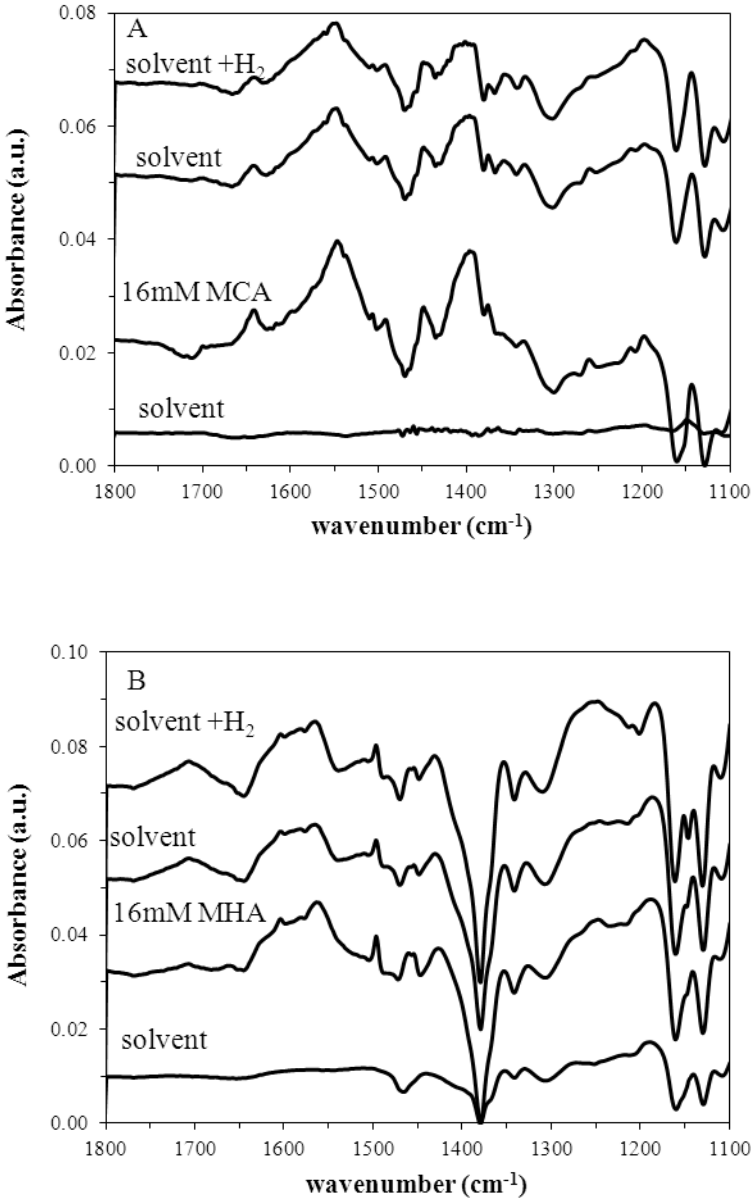

Figure 4.8 A) MCA hydrogenation on Al_2O_3 in isopropanol. B) MHA hydrogenation in isopropanol on Pd/Al_2O_3.

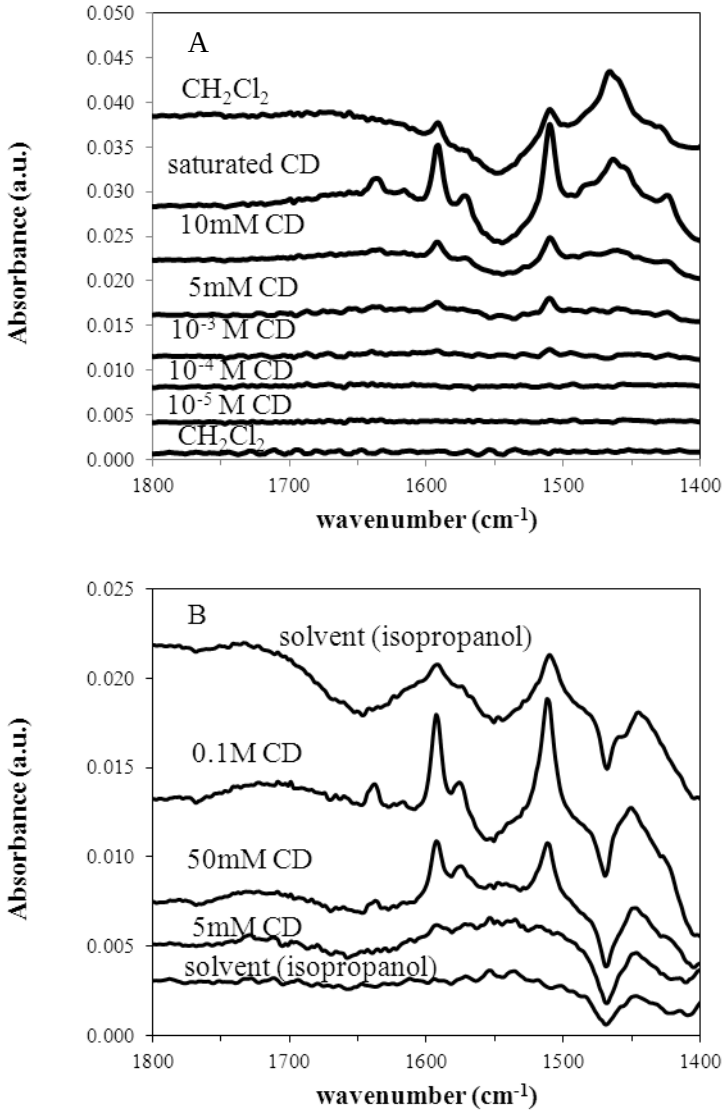

Figure 4.9 Cinchonidine (CD) adsorption on Pd/Al_2O_3 in A) dichoromethane and B) isopropanol.

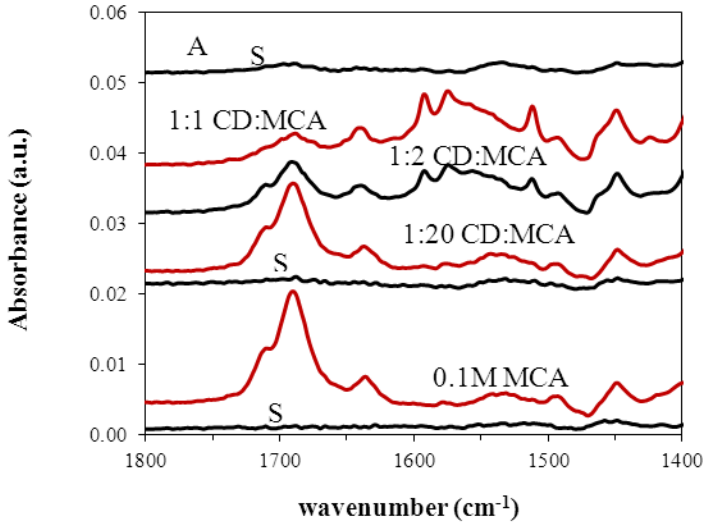
A
S
1:1 CD:MCA
1:2 CD:MCA
1:20 CD:MCA
S
0.1M MCA
S
Absorbance (a.u.)
wavenumber (cm-1)

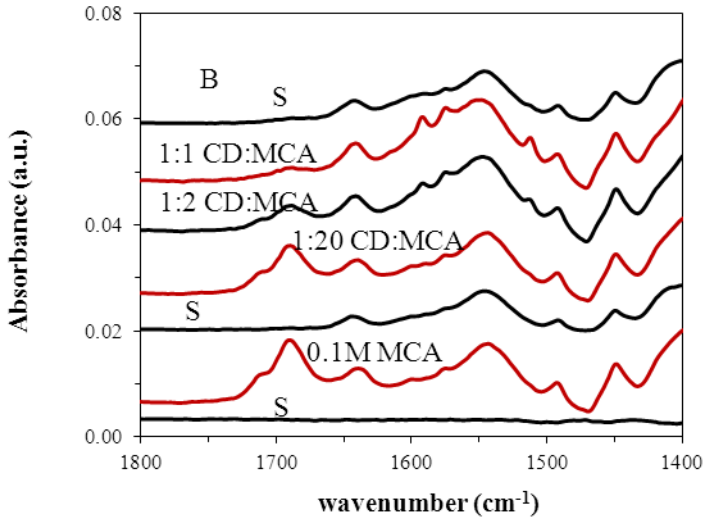
B
S
1:1 CD:MCA
1:2 CD:MCA
1:20 CD:MCA
S
0.1M MCA
S
Absorbance (a.u.)
wavenumber (cm-1)

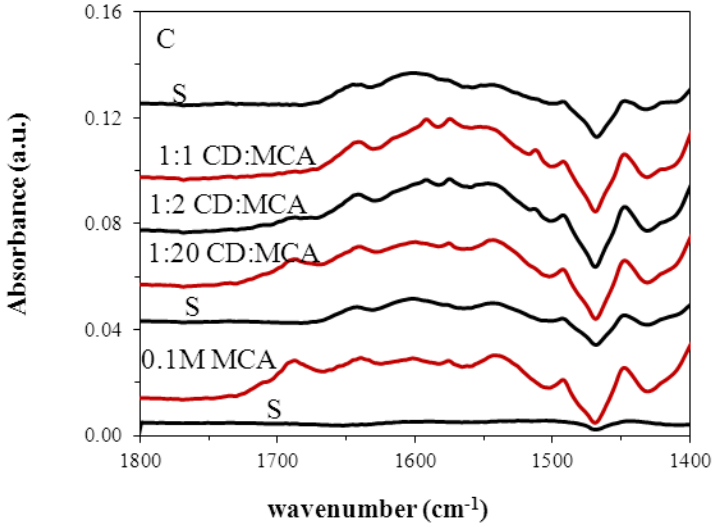
C
S
1:1 CD:MCA
1:2 CD:MCA
1:20 CD:MCA
S
0.1M MCA
S
Absorbance (a.u.)
wavenumber (cm-1)

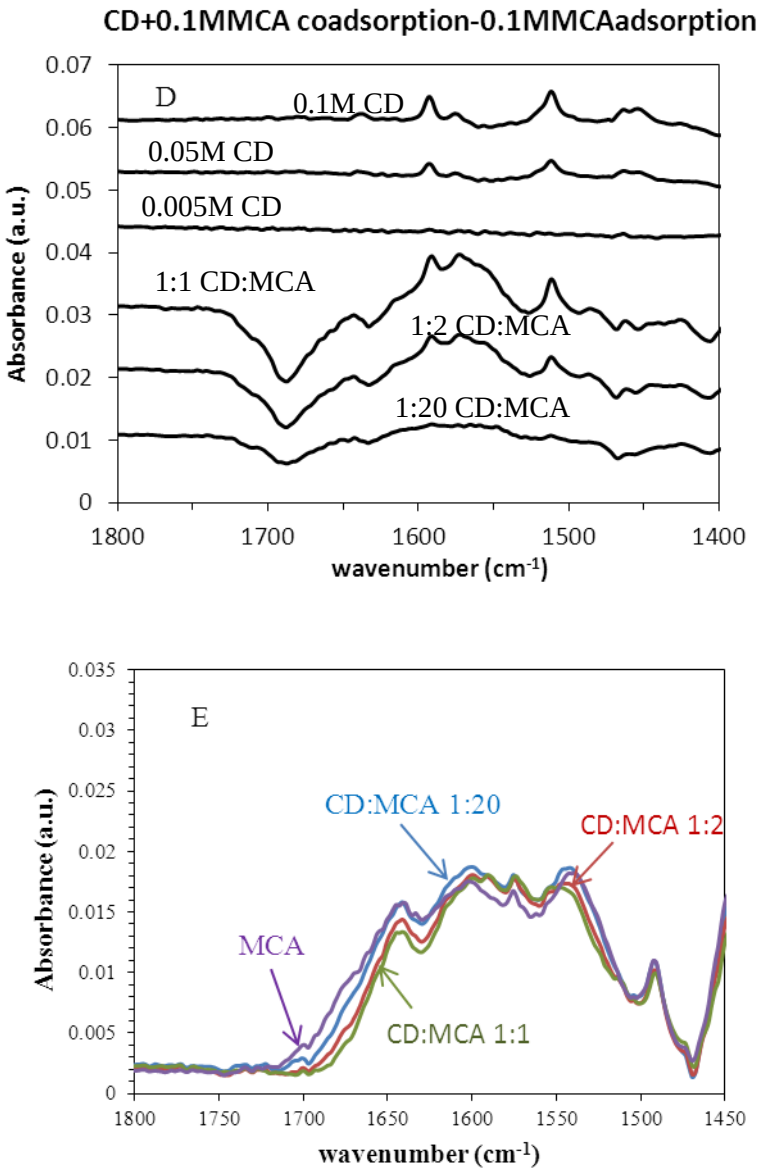

Figure 4.10 MCA gradually added cinchonidine in solution up to 0.1M with CD:MCA ratios of 1:20, 1:2, 1:1 on A) bare element, B) alumina, and C) Pd/Al_2O_3, D) Spectra of CD+MCA over bare element with the MCA on bare element subtracted, compared with the spectrum of cinchonidine over the bare element. E) Spectra of MCA+CD (1:20, 1:2, 1:1) from C) with 0.7 times the apectrum of the same step from A subtracted.

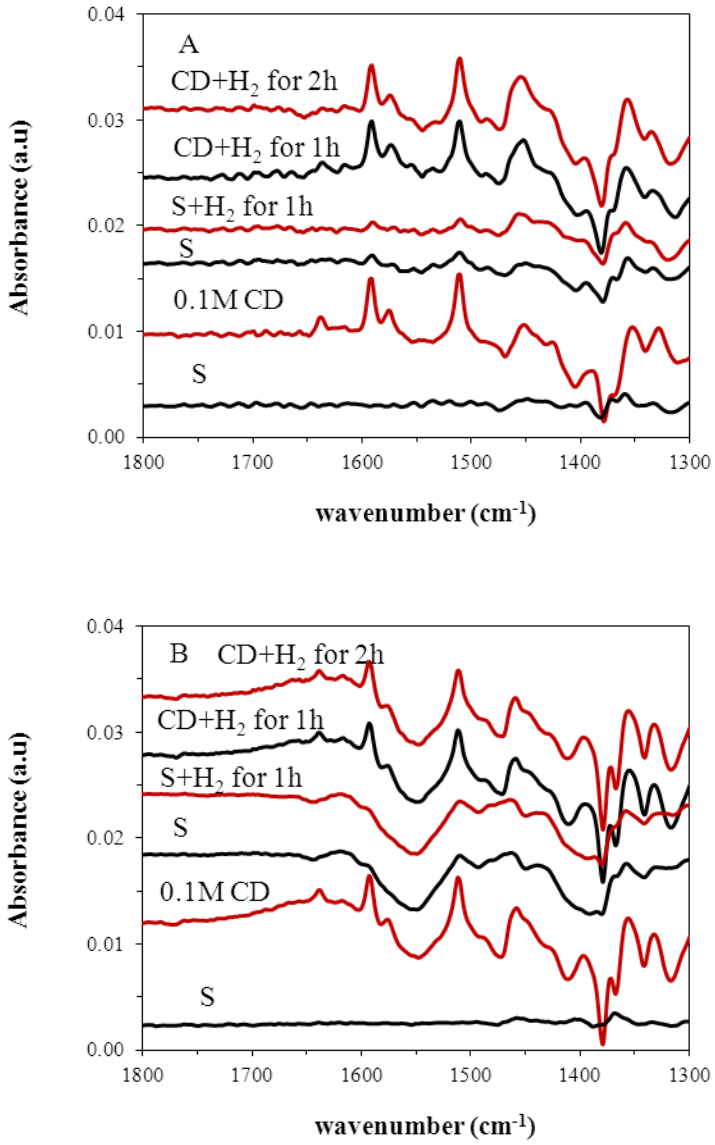

Figure 4.11 Cinchonidine hydrogenation. (0.1M CD) on A) Pd/Al_2O_3 and B) Al_2O_3.

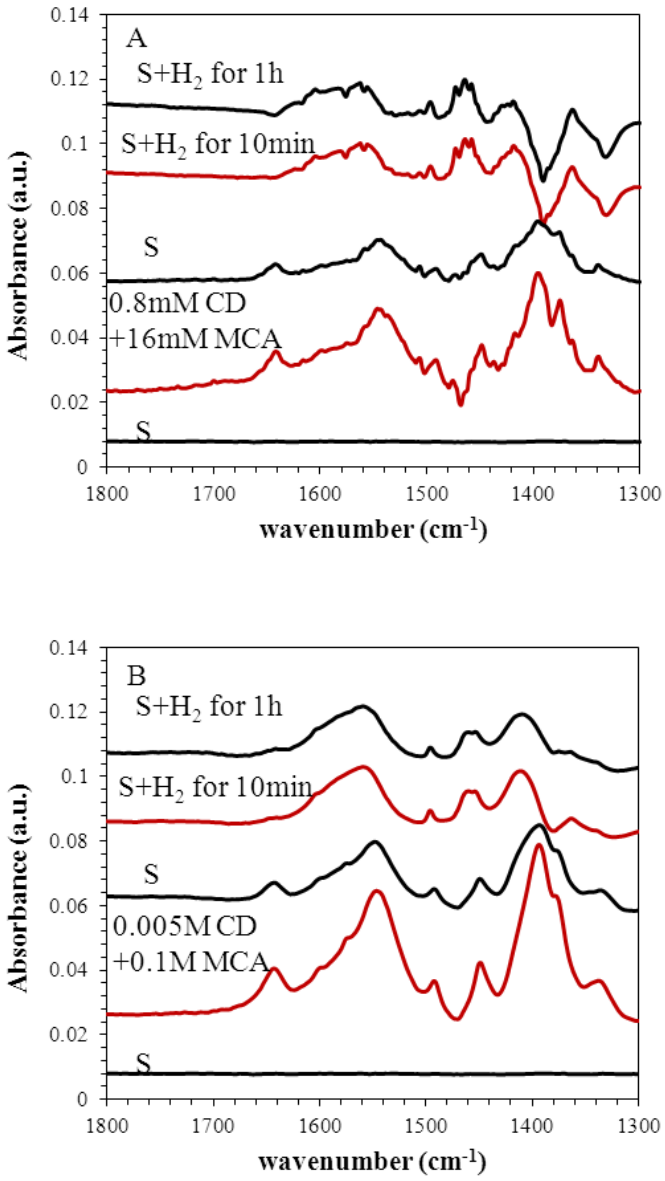

Figure 4.12 Hydrogenation of MCA with cinchonidine on Pd/Al_2O_3 at A) 16mM MCA + 0.8mM CD and B) 0.1M MCA + 0.005mM CD .

Table 4.1 Vibrational Peak Assignments

Vibrational Mode	Peak Assignment			
	Experimental			Calculation
	bare ZnSe element	Al_2O_3	5wt% Pd/Al_2O_3	B3LYP/ 6-31G(d)
C=O str. (dimer)	1693			
C=C str.		1642	1642	1621
ring in plane sym str.	1566	1594	1600	1593
ring in plane asym str.		1578	1578	1566
asymmetric COO^- vib		1545	1547	
ring symmetric vib.		1506	1506	1483
ring symmetric vib.		1493	1493	1483
C-H vibration (CH_3)		1468		1461
methyl group asymmetric C-H vib	1458	1449	1450	1457
methyl group symmetric C-H vib		1418	1405	1392
symmetric COO^- vib		1390	1377	
C-H vibration(H-C=C)		1340	1334	1359

Table 4.2 Carboxylate peak comparison

	Asym COO^-		**Sym COO^-**		**C=O**	
	cm^{-1}	**Intensity**	**cm^{-1}**	**Intensity**	**cm^{-1}**	**Intensity**
Isopropanol	1547	$8*10^{-3}$	1377	$2*10^{-2}$	1693	0
Dioxane	1542	$5*10^{-3}$	1382	$1*10^{-2}$	1710	0
Dicholoromethane	1529	$1.7*10^{-3}$	1377	$2*10^{-3}$	1706	$1.7*10^{-3}$

REFERENCES

1. Collins, A. N.; Sheldrake, G. N.; Crosby, J., eds., "Chirality in industry II: Developments in the commercial manufacture and applications of optically active compounds," Wiley, New York (1997).

2. T. Yoshida, and K. Harada, B Chem Soc Jpn 44 (1971) 1062-&.

3. Nasar, K.; Fache, F.; Lemaire, M.; Beziat, J. C.; Besson, M.; Gallezot, P. "Stereoselective reduction of disubstituted aromatics on colloidal rhodium" J. Mol. Catal. 87, 107 (1994).

4. Haruna, N.; Acosta, D. E.; Nakagawa, S.; yamaguchi, K.; Tai, A.; Okuyama, T.; Sugimura, T. "Asymmetric Hydrogenation of Furan-containing Ketones over Tartaric Acid-modified Raney Nickel Catalyst" Heterocycles 62, 375 (2004).

5. Perez, J. R. G.; Malthete, J.; Jacques, J. "Asymmetric hydrogenation of prochiral cinnamic acids in the presence of palladium on activated carbon and of chiral bases," C. R. Acad. Sci. Paris Serie II 300, 169 (1985).

6. Kubota, T.; H. Kubota, et al. "Enantioselective hydrogenation of (E)-α-phenylcinnamic acid over cinchonidine-modified Pd catalysts supported on TiO_2 and CeO_2," Catal Lett 129, 387 (2009).

7. Sugimura, T.; Watanabe, J.; Uchida, T.; Nitta, Y.; Okuyama, T. "Highly enantioselective hydrogenation of α-alkyl-β-arylpropenoic acids over cinchonidine-modified palladium catalyst," Catal. Lett. 112, 27 (2006).

8. Nitta, Y.; Watanabe, J.; Okuyama, T.; Sugimura, T. "Activation-temperature dependence in enantioselective hydrogenation of unsaturated carboxylic acids over cinchonidine-modified Pd/C catalysts," J. Catal. 236, 164 (2005).

9. Sugimura, T.; Watanabe, J.; Okuyama, T.; Nitta, Y. "The effect of the substrate structure on the stereoselectivity in the asymmetric hydrogenation of unsaturated carboxylic acids over cinchonidine-modified palladium catalyst," Tetrahedron: Asymmetry 16, 1573 (2005).

10. Nitta, Y.; Kubota, T.; Okamoto, Y. "Solvent effect on the structure sensitivity in enantioselective hydrogenation of α, β-unsaturated acids with modified palladium catalysts," J. Mol. Catal. A: Chem. 212, 155 (2004).

11. Nitta, Y.; Kubota, T.; Okamoto, Y. "Effect of palladium dispersion on the enantioselective hydrogenation of α, β-unsaturated acids with modified Pd/TiO_2 catalysts," Bull. Chem. Soc. Jap. 74, 2161 (2001).

12. Nitta, Y. "Hydrogen pressure dependence in enantioselective hydrogenation of α, β-unsaturated acids with cinchonidine-modified Pd/TiO_2 catalysts," Bull. Chem. Soc. Jap. 74, 1971 (2001).

13. Nitta, Y. "Enantioselective hydrogenation of (E)-α-phenylcinnamic acid with cinchonidinemodified Pd/TiO_2: influence of solvents and additives," Top. Catal. 13, 179 (2000).

14. Nitta, Y.; Kubota, T.; Okamoto, Y. "Preparation of cinchonidine-modified palladium catalysts for the enantioselective hydrogenation of (E)-α-phenylcinnamic acid," Bull. Chem. Soc. Jap. 73, 2635 (2000).

15. Nitta, Y. "Importance of product desorption in enantioselective hydrogenation of phenylcinnamic acid with a cinchonidine-modified Pd/TiO_2 catalyst: effect of additives," Chem. Lett. 28, 635 (1999).

16. Nitta, Y.; Okamoto, Y. "Effect of support texture on enantioselective hydrogenation of (E)-α- phenylcinnamic acid with cinchonidine-modified palladium catalysts," Chem. Lett. 27, 1115 (1998).

17. Nitta, Y.; Shibita, A. "Enantioselective hydrogenation of (E)-α-phenylcinnamic acid on Pd/TiO_2 catalyst modified by cinchona alkaloids: effect of modifier structure," Chem. Lett. 27, 161 (1998).

18. Nitta, Y.; Kobiro, K. "Conversion dependence of enantioselective hydrogenation of (E)-α- phenylcinnamic acid on cinchonidine-modified Pd/TiO_2 catalyst," Chem. Lett. 25, 897 (1996).

19. Nitta, Y.; Kobiro, K. "Solvent effect on enantioselective hydrogenation of (E)-α-phenylcinnamic acid with cinchonidine-modified palladium catalysts," Chem. Lett. 24, 165 (1995).

20. Nitta, Y.; Ueda, Y.; Imanaka, T. "Enantioselective hydrogenation of (E)-α-phenylcinnamic acid over cinchonidine-modified palladium catalysts," Chem. Lett. 23, 1095 (1994).

21. Szollosi, G.; Hanaoka, T.; Niwa, S.; Mizukami, F.; Bartok, M. "Increased enantioselectivity in the presence of benzylamine in the heterogeneous hydrogenation of α,β-unsaturated carboxylic acids," J. Catal. 231, 480 (2005).

22. Szollosi, G.; Niwa, S.; Hanaoka, T.; Mizukami, F. "Enantioselective hydrogenation of α,β-unsaturated carboxylic acids over cinchonidine-modified Pd catalysts: effect of substrate structure on the adsorption mode," J. Mol. Catal. A: Chem. 230, 91 (2005).

23. Szori, K.; Szollosi, G.; Felfoldi, K.; Bartok, M. “A novel asymmetric heterogeneous catalytic reaction: hydrogenation of ethyl 2-acetoxyacrylate on cinchonidine modified Pd and Pt catalyst,” React. Kinet. Catal. Lett. 84, 151 (2005).

24. Kun, I.; Torok, B.; Felfoldi, K.; Bartok, M. “Heterogeneous asymmetric reactions Part 17: asymmetric hydrogenation of 2-methyl-2-pentenoic acid over cinchona modified Pd/Al_2O_3 catalysts,” Appl. Catal. A: Gen. 203, 71 (2000).

25. Ferri, D.; Burgi, T.; Baiker, A. “FTIR study of chiral modifier-reactant interactions: the cinchonidine-akenoic acid system,” J. Chem. Soc., Perkin Trans. 2, 437 (2002).

26. Borszeky, K.; Burgi, T.; Zhaohui, Z.; Mallat, T.; Baiker, A “Enantioselective hydrogenation of α,β- unsaturated carboxylic acids over cinchonidine modified palladium: nature of modifier-reactant interaction,” J. Catal. 187, 160 (1999).

27. Borszeky, K.; Mallat, T.; Baiker, A “Palladium-catalyzed enantioselective hydrogenation of alkenoic acids. Role of isomerization,” Catal. Lett. 59, 95 (1999).

28. Borszeky, K.; Mallat, T.; Baiker, A “Enantioselective hydrogenation of α, β-unsaturated acids. Substrate-modifier interaction over cinchonidine modified Pd/Al_2O_3,” Tetrahedron: Asymmetry 8, 3745 (1997).

29. Maris, M; Burgi, T.; Mallat, T., Baiker, A. “Enantioselective hydrogenation of furancarboxylic acids: a spectroscopic and theoretical study,” J. Catal. 226, 393 (2004).

30. Maris, M; Huck, W.-R.; Mallat, T., Baiker, A. “Palladium-catalyzed asymmetric hydrogenation of furan carboxylic acids,” J. Catal. 219, 52 (2003).

31. Huck, W.-R.; Burgi, T.; Mallat, T.; Baiker, A. “Enantioselective hydrogenation on cinchona modified metal catalysts: mechanistic implications of acid additives,” J. Catal. 205, 213 (2002).

32. Huck, W.-R.; Burgi, T.; Mallat, T.; Baiker, A. “Asymmetric hydrogenation of 4-hydroxy-6-methyl-2-pyrone: role of acid-base interactions in the mechanism of enantiodifferentiation,” J. Catal. 200, 171 (2001).

33. Huck, W.-R.; Mallat, T.; Baiker, A. “Potential and limitations of palladium-cinchona catalyst for the enantioselective hydrogenation of a hydroxymethylpyrone,” J. Catal. 193, 1 (2000).

34. Huck, W.-R.; Mallat, T.; Baiker, A. “Transient behavior of the enantioselective hydrogenation of hydroxymethylpyrone,” Catal. Lett. 69, 129 (2000).

35. Borszeky, K.; Mallat, T.; Baiker, A. “Asymmetric hydrogenation of indene carboxylic acids: stereochemistry of hydrogen addition,” Tetrahedron Asymmetry 10, 4781 (1999).

36. Borszeky, K.; Mallat, T.; Baiker "Diastereoselective hydrogenation of indenols: evidence for sterically and electronically unfavorable adsorption on palladium," J. Catal. 188, 413 (1999).

37. Borszeky, K. Mallat, T; Baiker, A. "Enantioselective hydrogenation of 2-methyl-2-pentenoic acid over cinchonidine-modified Pd/alumina," Catal. Lett. 41, 199 (1996).

38. Huck, W.-R.; Mallat, T.; Baiker, A. "Entantioselective hydrogenation of a methoxypyrone with cinchona-modified palladium," Catal. Lett. 80, 87 (2002).

39. Casagrande, M; Franceschini, S.; Piccolo, O.; Vaccari, A "Cinchonidine doped Pd catalysts in the enantioselective hydrogenation of (E)-2-methyl-2-butenoic acid," J. Mol. Catal. A: Chem. 246, 263(2006).

40. Bisignani, R; Franceschini, S.; Lenarda, M.; Piccolo, O.; Vaccari, A "The solvent effect in the enantioselective hydrogenation of (E)-2-methyl-2-butenoic acid with cinchonidine doped Pd/Al2O3," J. Mol. Catal. A: Chem. 232, 161 (2005).

41. Solladie-Cavallo, A.; Hoernel, F.; Schmidt, M.; Garin, F. "Heterogeneous asymmetric hydrogenation and deuteration of 2-methyl-2-penenoic acid over Pd supported catalysts: proton/deuterium exchange," J. Mol. Catal. A: Chem. 195, 181 (2003).

42. Solladie-Cavallo, A.; Marsol, C.; Hoernel, F.; Garin, F. "Substrate-modifier but not catalystmodifier: heterogeneous hydrogenation of C=O and C=C using cinchonidine," Tetrahedron Letters 42, 4741 (2001).

43. Bhaduri, S.; Lahiri, G. K.; Munshi, P.; Mukesh, D. "Asymmetric hydrogenation of methyl pyruvate using platinum carbonyl cluster supported on an anion exchanger as the catalyst," Catal. Lett. 65, 61 (2000).

44. Kim, T.Y.; Uchida, T.; Ogawa, H.; Nitta, Y.; Okuyama, T.; Sugimura, T.; Hirayama, S.; Honma, T.; Sugiura, M.; Kubota, T.; Okamoto, Y. "Enantioselective hydrogenation of olefins using commercially acailable Pd/C. chiral heterogeneous catalyst applicable for high- throughput screening" Top Catal 53, 116 (2010).

45. Tungler, A.; Nitta, Y.; Fodor, K.; Farkas, G.; Mathe, T. "Comparison of chiral modifiers in the Pd catalysed hydrogenation of phenylcinnamic acid and isophorone" J Mol Catal a-Chem 149, 135 (1999).

46. Sugimura, T.; Uchida, T.; Watanabe, J.' Kubota, T.; Okamoto, Y.; Misaki, T.; Okuyama, T. "Structural requirements for substrate in highly enantioselective hydrogenation over the cinchonidine-modified Pd/C" J Catal 262, 57 (2009).

47. Misaki, T.; Otsuka, H.' Uchida, T.' Kubota, T.; Okamoto, Y.; Sugimura, T. "Substrate adsorption on the cinchonidine-modified Pd/C during the enantio-

differentiating hydrogenation as a vital stereocontrol factor" J Mol Catal a-Chem 312, 48 (2009).

48. Szollosi, G.; Varga, T.; Felfoldi, K.; Cserenyi, S.; Bartok, M. "Enantioselective hydrogenation of fluorinated unsaturated carboxylic acids over cinchona alkaloid modified palladium catalysts" Catal Commun 9, 421 (2008).

49. Szori, K.; Szollosi, G.; Bartok, M. "The enantioselective hydrogenation of 5, 6-dihydro-2H-pyran-3-carboxylic acid over a cinchona alkaloid-modified palladium catalyst: asymmetric synthesis of a cockroach attractant" New Journal of Chemistry 32, 1354 (2008).

50. Szollosi, G.; Herman, B.; Felfoldi, K.; Fulop, F.; Bartok, M. "Effect of the substituent position on the enantioselective hydrogenation of methoxy-substituted 2, 3-diphenylpropenoic acids over palladium catalyst" J Mol Catal a-Chem 290, 54 (2008).

51. Szollosi, G.; Herman, B.; Felfoldi, K.; Fulop, F.; Bartok, M. "Up to 96% Enantioselectivities in the Hydrogenation of Fluorine Substituted (E)-2,3-Diphenylpropenoic Acids over Cinchonidine-Modified Palladium Catalyst" Advanced Synthesis & Catalysis 350, 2804 (2008)

52. Dijkstra, G. D. H.; Kellogg, R. M.; Wynberg, H. "Conformational study of cinchona alkaloids. A combined NMR and molecular orbital approach" J Org Chem 55, 6121 (1990).

53. Aune, M.; Gogoll, A.; Matsson, O. "Solvent Dependence of Enantioselectivity for a Base-Catalyzed 1, 3-Hydron Transfer Reaction. A Kinetic Isotope Effect and NMR Spectroscopic Study" J Org Chem 60, 1356 (1995).

54. Dijkstra, G. D. H.; Kellogg, R. M.; Wynberg, H.;Svendsen. J.S.; Marko, I.; Sharpless, K.B. "Conformational study of cinchona alkaloids. A combined NMR, molecular mechanics and x-ray approach" J Am Chem Soc 111, 8069 (1989).

55. Schurch, M.; Schwalm, O.; Mallat, T.; Weber, J. Baiker, A. "Enantioselective Hydrogenation of Ketopantolactone" J Catal 169, 275 (1997).

56. Schurch, M.; Kunzel, N.; Mallat, T.; Baiker, A. "Enantioselective Hydrogenation of Ketopantolactone: Effect of Stereospecific Product Crystallization during Reaction" J Catal 176, 569 (1998).

57. Dijkstra, G.D.H.; Kellogg, R.M.;Wynberg, H. Recl Trav Chim Pay B 108, 195 (1989).

58. Oleksyn, B.J.; Suszkopurzcka, A.; Dive, G.; Lamottebrasseur, J. "Molecular properties of Cinchona alkaloids: A theoretical approach" Journal of Pharmaceutical Sciences 81, 122 (1992).

59. Caner, H. Biedermann, P.U.; Agranat, I. “Conformational spaces of Cinchona alkaloids” Chirality 15, 637 (2003).

60. Olsen, R.A.; Borchardt, D.; Mink, L.; Agarwal, A.; Mueller, L. J.; Zaera, F. “Effect of Protonation on the Conformation of Cinchonidine” J Am Chem Soc 128, 15594 (2006)

61. Burgi, T.; Baiker, A. “Conformational Behavior of Cinchonidine in Different Solvents: A Combined NMR and ab Initio Investigation” J Am Chem Soc 120, 12920 (1998).

62. Berg, U.; Aune, M.; Matsson, O. “Dihydroquinidine conformation revisited. Variable temperature NMR and CD spectroscopy, and molecular mechanics computations” Tetrahedron Lett 36, 2137 (1995).

63. Vayner, G.; Houk, K.N. Sun, Y.K. “Origins of Enantioselectivity in Reductions of Ketones on Cinchona Alkaloid Modified Platinum” J Am Chem Soc 126, 199 (2004).

64. Urakawa, A.; Meier, D.M.; Rugger, H.; Baiker, A. “Conformational Behavior of Cinchonidine Revisited: A Combined Theoretical and Experimental Study” J Phys Chem A 112, 7250 (2008).

65. Bartok, M. “Heterogeneous catalytic enantioselective hydrogenation of activated ketones” Curr Org Chem 10, 1533 (2006).

66. Kubota, J.; Zaera, F. “Adsorption Geometry of Modifiers as Key in Imparting Chirality to Platinum Catalysts” J Am Chem Soc 123, 11115 (2001).

67. Simons, K. E.; Meheux, P. A.; Griffiths, S. P.; Sutherland, I. M.; Johnston, P.; Wells, P. B. Carley, A. F.; Rajumon, M. K.l Roberts, M. W.; Ibbotson, A. Recl Trav Chem Pay B 113, 465 (1994).

68. Schwalm, O.; Weber, J.; Minder, B.; Baiker, A. “Theoretical investigation of the enantioselective hydrogenation of α-ketoesters over pt/alumina modified with cinchonidine” Int J Quantum Chem 52, 191 (1994).

69. Carley, A.F.; Rajumon, M.K. Roberts, M.W.; Wells, P.B. “XPS and LEED studies of 10, 11-dihydrocinchonidine adsorption at Pt(111). Implications for the role of cinchona alkaloids in enantioselective hydrogenation” Journal of the Chemical Society-Faraday Transactions 91, 2167 (1995).

70. Bond G.; Wells P. B. “Enantioselective Hydrogenation: IV. Hydrogen Isotope Exchange in 10, 11-Dihydrocinchonidine and in Quinoline Catalyzed by Platinum Group Metals” Journal of Catalysis 150, 329 (1994).

71. Evans, T.; Woodhead, A.P.; Gutierrez-Sosa, A.; Thornton, G.; Hall, T.J.; Davis A.A.; Young, N.A. etc. “Orientation of 10,11-dihydrocinchonidine on Pt(111)” Surf Sci 436, L691 (1999).

72. Schmidt, E.; Ferri, D.; Vargas, A.; Baiker, A. Chiral Modification of Rh and Pt Surfaces: Effect of Rotational Flexibility of Cinchona-Type Modifiers on Their Adsorption Behavior Journal of Physical Chemistry C 112, 3866 (2008).

73. Ferri, D.; Burgi, T.; Baiker,A. “Chiral modification of platinum catalysts by cinchonidine adsorption studied by in situ ATR-IR spectroscopy” Chem Commun 1172 (2001).

74. Ferri, D.; Brugi, T. “An in Situ Attenuated Total Reflection Infrared Study of a Chiral Catalytic Solid−Liquid Interface: Cinchonidine Adsorption on Pt” J Am Chem Soc 123, 12074 (2001).

75. Chu, W.; LeBlanc, R.J.; Williams, C.T.; Kubota, J.; Zaera, F. “Vibrational Band Assignments for the Chiral Modifier Cinchonidine: Implications for Surface Studies” J Phys Chem B 107, 14365 (2003).

76. Ferri, D.; Brugi, T.; Baiker, A. “The Fate of Ethyl Pyruvate during Adsorption on Platinum Chirally Modified by Cinchonidine Studied by ATR−IR Spectroscopy” J Phys Chem B 108, 14384 (2004).

77. Bonalumi, N.; Vargas, A.; Ferri, D.; Baiker, A. “Chirally Modified Platinum Generated by Adsorption of Cinchonidine Ether Derivatives: Towards Uncovering the Chiral Sites” Chemistry-a European Journal 13, 9236 (2007).

78. Chu, W.; LeBlanc, R.J.; Williams, C.T. “In-situ Raman investigation of cinchonidine adsorption on polycrystalline platinum in ethanol” Catal Commun 3, 547 (2002).

79. Xu, Q.M.; Wang, D.; Wan, L.J.; Bai, C.L.; Wang, Y. “Adsorption Mode of Cinchonidine on Cu (111) Surface” J Am Chem Soc 124, 14300 (2002).

80. Kim, T.Y.; Uchida, T.; etc. “Enantioselective Hydrogenation of Olefins using Commercially Available Pd/C. Chiral Heterogeneous Catalyst Applicable for High-Throughput Screening” Top Catal 53, 116 (2010).

81. Sun, X.; Williams, C. “In-situ ATR-IR investigation of methylcinnamic acid adsorption and hydrogenation on Pd/Al_2O_3” Catalysis Communications 17, 13 (2012).

82. IMSHealth, Top 15 global products 2008, 2008 Global Prescription Sales Information, Top-line Industry Data, Press Room, 22.04.2009, (2009).

83. A.M. Rouhi, Chiral chemistry, Chemical and Engineering News 82, 47 (2004).

84. AutoChem II 2920 Automated Catalyst Characterization System Operator's Manual V3.05.

85. a) Weaver, M. "Raman and infrared spectroscopies as in situ probes of catalytic adsorbate chemistry at electrochemical and related metal–gas interfaces: some perspectives and prospects" J. Top. Catal. 8, 65 (1999). b) Matyshak, V. A.; Krylov, O. V. "In situ IR spectroscopy of intermediates in heterogeneous oxidative catalysis" Catal. Today 25, 1 (1995). c) Sheppard, N.; Nguyen, T. T. Adv. Infrared Raman Spectrosc. 5, 67 (1978).

86. For review see: Weaver, M. J.; Zou, S. in Advances in Spectroscopy Vol 26, Eds. Clark, R.J.H.; Hester, R.E. Wiley, Chichester, UK, 219, (1998).

87. Ortiz-Hernandez I.; Williams C.T. "In Situ Investigation of Solid−Liquid Catalytic Interfaces by Attenuated Total Reflection Infrared Spectroscopy" Langmuir 19, 2956 (2003).

88. Ortiz-Hernandez I.; Williams C.T. "In Situ Studies of Butyronitrile Adsorption and Hydrogenation on Pt/Al_2O_3 Using Attenuated Total Reflection Infrared Spectroscopy" Langmuir 23, 3172 (2007).

89. Frisch, M. J.; Trucks, G. W.; Schlegel, H. B.; Scuseria, G. E.; Robb, M. A.; Cheeseman, J. R.; Montgomery, Jr., J. A.; Vreven, T.; Kudin, K. N.; Burant, J. C.; Millam, J. M.; Iyengar, S. S.; Tomasi, J.; Barone, V.; Mennucci, B.; Cossi, M.; Scalmani, G.; Rega, N.; Petersson, G. A.; Nakatsuji, H.; Hada, M.; Ehara, M.; Toyota, K.; Fukuda, R.; Hasegawa, J.; Ishida, M.; Nakajima, T.; Honda, Y.; Kitao, O.; Nakai, H.; Klene, M.; Li, X.; Knox, J. E.; Hratchian, H. P.; Cross, J. B.; Bakken, V.; Adamo, C.; Jaramillo, J.; Gomperts, R.; Stratmann, R. E.; Yazyev, O.; Austin, A. J.; Cammi, R.; Pomelli, C.; Ochterski, J.W.; Ayala, P. Y.;Morokuma, K.; Voth, G. A.; Salvador, P.; Dannenberg, J. J.; Zakrzewski,V.G.; Dapprich, S.; Daniels, A. D.; Strain, M. C.; Farkas, O.;Malick, D.K.; Rabuck, A. D.; Raghavachari, K.; Foresman, J. B.; Ortiz, J. V.; Cui, Q.; Baboul, A. G.; Clifford, S.; Cioslowski, J.; Stefanov, B. B.; Liu, G.; Liashenko, A.; Piskorz, P.; Komaromi, I.; Martin, R. L.; Fox, D. J.; Keith, T.; Al-Laham, M. A.; Peng, C. Y.; Nanayakkara, A.; Challacombe, M.; Gill, P. M. W.; Johnson, B.; Chen, W.; Wong, M.W.; Gonzalez, C.; and Pople, J. A.; Gaussian, Inc., Wallingford CT, (2004).

90. Perego C.; Villa P. "Catalyst preparation methods," Catalysis Today 34, 281 (1997).

91. Dobson K.; McQuillan A. "In situ infrared spectroscopic analysis of the adsorption of aromatic carboxylic acids to TiO_2, ZrO_2, Al_2O_3, and Ta_2O_5 from aqueous solutions" Spectrochimica Acta Part A 56, 557(2000).

92. van den Brand J.; Blajiev O.; Beentjes P.C.J.; Terryn H.; de Wit J.H.W. "Interaction of Anhydride and Carboxylic Acid Compounds with Aluminum Oxide Surfaces Studied Using Infrared Reflection Absorption Spectroscopy" Langmuir 20, 6308 (2004).

93. Tan, S.; Monnier, J.; Williams, C. “Kinetic study of asymmetric hydrogenation of α, β-unsaturated carboxylic acid over cinchona-modified Pd/Al_2O_3 catalyst”Top Catal 55, 512 (2012).

94. Meemken F.; Maeda N.; Hungerbühler K.; and Baiker A. “Heterogeneous Asymmetric Hydrogenation of Prochiral Alkenoic Acid: Origin of Rate and Enantioselectivity Enhancement by Amine Addition”ACS Catal 2, 464 (2012).

95. The 10 Biggest-selling Drugs that are about to lose their patent, Daily Finance.

96. Song, C.E. “Chaper 1 An Overview of Cinchona Alkaloids in Chemistry” Cinchona Alkaloids in Synthesis and Catalysis: Ligands, Immobilization and Organocatalysis (2009).

97. Ma, Z.; Zaera, F. “Role of the solvent in the adsorption-desorption equilibrium of cinchona alkaloids between solution and a platinum surface: correlations among solvent polarity, cinchona solubility, and catalytic performance” J. Phys. Chem. B 109, 406 (2005).

98. Ferri, D.; Burgi, T.; Baiker, A. “In situ ATR-IR study of the adsorption of cinchonidine on Pd/Al_2O_3: Differences and similarities with adsorption on Pt/Al_2O_3” Journal of Catalysis 210, 160 (2002).

99. Rebelli J.; Detwiler M.; Ma S.; Williams C.T.; Monnier J. R. “Synthesis and characterization of Au–Pd/SiO2 bimetallic catalysts prepared by electroless deposition” Journal of Catalysis 270, 224 (2010).

100. Mallat T.; Orglmeister E.; Baiker A., “Asymmetric Catalysis at Chiral Metal Surfaces” Chemical Reviews 107, 4863 (2007).

101. LeBlanc R. J.; Chu W.; Williams C. T. “Surface Raman Characterization of Cinchonidine-Modified Platinum in Ethanol: Effects of Liquid-Phase Concentration and Co-Adsorbed Hydrogen” J. Mol. Catal. A. 212, 277 (2004).

102. Chu W.; LeBlanc R. J.; Williams C. T.; Kubota J.; Zaera F. “Vibrational Band Assignments for the Chiral Modifier Cinchonidine: Implications for Surface Studies” J. Phys. Chem. B. 107, 14365 (2003).

103. LeBlanc R. J.; Williams C. T., “Surface Raman Characterization of Cinchonidine-Modified Polycrystalline Platinum in Ethanol: Effects of Temperature and Comparison with 10, 11-Dihydrocinchonidine” J. Mol. Catal. A 220(2), 207 (2004).